UNIVERSITÀ DEGLI STUDI DI CATANIA
FACOLTÀ DI SCIENZE MATEMATICHE FISICHE E NATURALI

Dottorato di Ricerca in Scienza dei Materiali
(Ph.D in Materials Science)
XXIV ciclo

Chemical Engineering of Silicon for Supramolecular Recognition

DOTT.SSA CRISTINA TUDISCO

Tutor:Chiar.mo Prof. G.G. Condorelli
Coordinatore: Chiar.mo Prof. A. Licciardello

Tesi di Dottorato di Ricerca

Contents

AIM OF THE WORK

This thesis discusses some strategies to anchor functional molecules on silicon-based substrates in order to introduce onto a solid surface specific functionalities. Two main typologies of silicon-based substrates both of technological interest have been functionalized through synthetic routes based on the hydrosilylation reaction. First typology consists of flat monocrystalline Si(100) which is the surface of election for the development of commercial microelectronic devices, while second substrate typology consists of porous silicon which represents an interesting candidate for novel devices due to its specific properties such as high surface area and luminescence. In particular, the attention is focused on the surface grafting of cavitand-based molecules, synthetic organic compounds with rigid cavities of molecular dimensions, which are interesting and versatile receptors. A key point of this thesis has been the study of the recognition properties of these receptors after surface anchoring. The obtained hybrid materials consisting of cavitand monolayer bonded to silicon surface combined the technological advantages of either Si(100) or porous silicon substrates with the recognition properties of cavitand, thus allowing various applications ranging from sensing to surface hierarchical nanoassembly.

Chapter 1

1.1 Introduction

1.1.1 Nanotechnology and nanomaterials

In 1959, Nobel award winner Richard Feynman first proposed the seminal idea of nanotechnology by suggesting the development of molecular machines. Ever since, the scientific community has investigated the role that nanotechnology can play in every aspect of society. Nanotechnology refers to the research and technology development at atomic, molecular, and macromolecular scales, which leads to the controlled manipulation and study of structures and devices with length scales in the range of 1-100 nanometers. One nanometer (nm) is one billionth of a metre; tens of thousands of times smaller than the width of a human hair (figure 1.1.1).

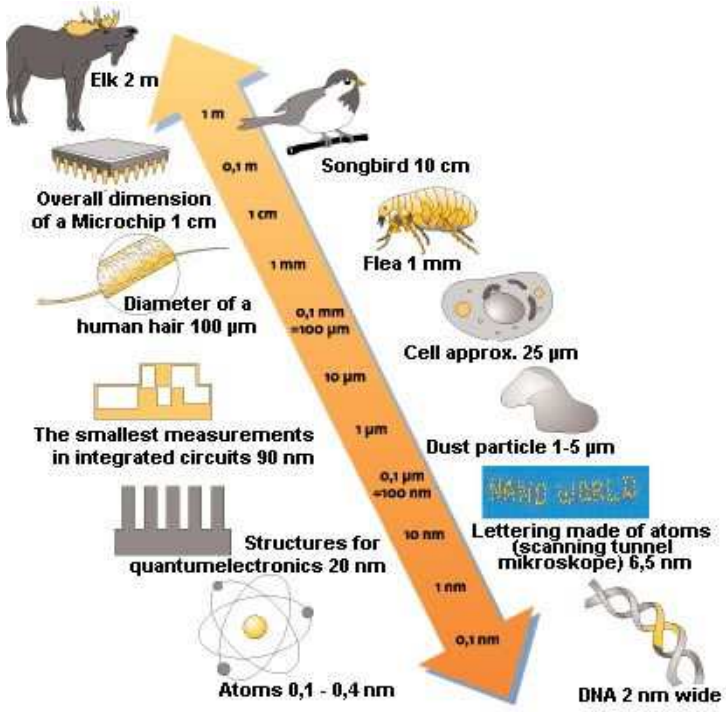

Figure 1.1.1: Objects of approximate size from 1 m to 10^{-10} m.

In the last two decades, the research of nanotechnology has grown explosively with over three hundred thousands publications in the field of nanoscience according to Web of Science[1].

The intrigue of nanotechnology comes from the ability to control material properties by assembling such materials at the nanoscale. The tunable material properties that nanotechnology can provide were stated in Norio Taniguchi's paper in 1974 where the term ''nanotechnology'' was first used in a scientific publication. Recently, nanomaterials, which are materials with basic structural units, grains, particles, fibers or other constituent components smaller than 100 nm in at least one dimension, have evoked a great amount of attention for improving disease prevention, diagnosis, and treatment.[2]

Nanostructured materials with tunable morphology have attracted exceptional interest over the past decades because of their unique architectures, tailored physicochemical properties, central roles in fabricating nanoelectronics, and potential applications in bionanotechnology. In recent years, a vast array of novel nanostructures have been manufactured and studied in the interdisciplinary fields of nanoscience, material science, biological science, etc. Thus far, lots of investigations with respect to inorganic nanomaterials have been reported and well documented, as summarized by recent review articles[3]. Compared with inorganic nanostructures, the organic counterparts have, in particular, fascinated scientists because of their multifunctionality, considerable variety and flexibility in molecular design, and solution processability. These advantages make the organic nanostructures promising candidates for electronics, including organic field-effect transistors, organic light emitting displays, nanosensors, etc. Thus, the exploration of the controlled synthesis of organic nanostructures is a significant issue.[4]

1.1.2 Self Assembled Monolayer

The term "self-assembling monolayer" was coined in 1983 in New Scientist[5] in an anonymous report describing the work of Lucy Netzer and Jacob Sagiv on the chemically controlled layer-by-layer self-assembly of multilayer films.[6] The self assembly of adsorbates on an appropriate surface has been known since 1946, when Zisman and co-workers reported the formation of monomolecular films of long-chain hydrocarbons carrying polar groups on a variety of polar surfaces.[7,8] Although these films are extremely thin (typically ca. 2 nm), they are able to completely change the surface properties.

However, the versatility of these adsorbed monolayers was not realized until 1978, when Polymeropoulos and Sagiv proposed their use for measuring electrical conduction between two metal surfaces.[9] In 1980, Sagiv published the first article

demonstrating the formation of well-defined organosilane monolayers on SiO_2 by direct adsorption (that is, self-assembly) from solution.[10,11]

Nowadays it is well know that Self-assembled monolayers (SAMs) provide a convenient, flexible, and simple system with which to tailor the interfacial properties of metals, metal oxides, and semiconductors. SAMs are organic assemblies formed by the adsorption of molecular constituents from solution or from gas phase onto the surface of solids or in regular arrays on the surface of liquids (in the case of mercury and probably other liquid metals and alloys); the adsorbates organize spontaneously (and sometimes epitaxially) into crystalline (or semicrystalline) structures.[12]

The method of self-assembled monolayers (SAMs) has witnessed exponential growth in synthetic sophistication and depth of characterisation over the last two decades. Figure 1.1.2 presents graphically the increasing number of articles/reports published per year in the fields of SAMs in the last two decades

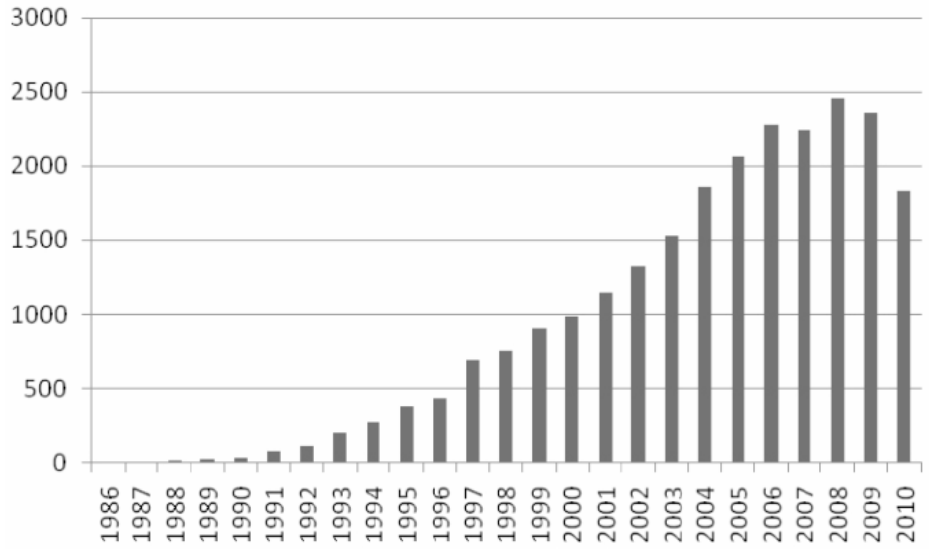

Figure 1.1.2: Numbers of published article addressing self-assembled monolayers.

The success of SAMs is due likely to their ability to create controlled surface chemistry with high molecular organization and defined stoichiometry over relatively large areas. SAMs have facilitated the study of molecular and cellular interactions with specific functional groups, surface energetic, surface charge, or other interface properties. SAMs can be used to include specific functionalities or ligands to study biological interactions such as cell signalling, cell adhesion,[13] and protein interactions.[14,15] SAMs have also been used for constructing molecular switches,[16] biosensors[17] and microarrays. SAMs offer a unique combination of physical properties that allow fundamental studies of interfacial chemistry, solvent-molecule interactions and self-organization.

1.1.3 Basics of SAMs

A schematic of an organic SAM is shown in Figure 1.1.3. Usually, SAMs are formed spontaneously by immersing Si substrates into an active solution, e.g. surfactant molecules $R(CH_2)_nSiX_3$ (X = Cl, OCH_3 or OC_2H_5) dissolved in alkane/carbon tetrachloride.

However, the SAMs can be deposited by other techniques as well, such as, vapor deposition. The self-assembling monolayer can be divided into three parts:

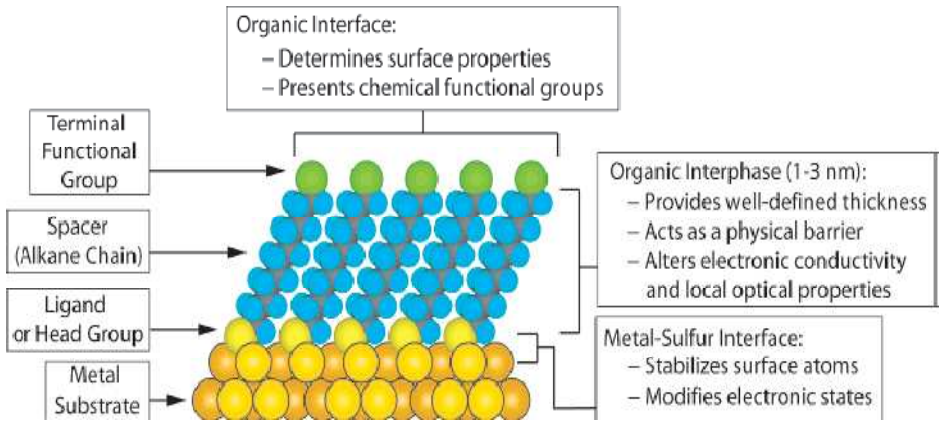

Figure 1.1.3: A schematic diagram showing different parts of a self-assembled monolayer on a metal surface.

(i) *Head group, i.e.* SiX_3. It forms the chemical bond with surface atoms of the substrate (exothermic: ~40-45 kcal/mol or ~1.7 eV) causing the pinning of surfactant molecule to the substrate.

(ii) *Alkyl chain, i.e.* $(CH_2)_n$. The inter-chain van der Waals interactions (exothermic <10 kcal/mol or <0.4 eV) could assist in formation of an ordered molecular structure. Of course, the possibility of obtaining ordered structures depends on the pinning density of the head groups.

(iii) *Surface group, i.e. R*. This is the terminal group which is replaced with or bonded to different functional groups to obtain specific applicative devices.

1.1.4 Characterization of SAMs

The quality of deposited SAMs is assessed by characterizing them for (i) thickness, (ii) molecular orientation and ordering, (iii) uniformity and coverage, (iv) chemical composition, and (v) thermal and chemical stability.

Various techniques are available for the characterization of monolayers[18]. The chemical composition of monolayers can be determined by Auger electron spectroscopy (AES), X-ray photoelectron spectroscopy (XPS) and secondary ion mass spectroscopy (SIMS). Only XPS can reliably characterize the chemical composition of organic ultrathin layers on metallic substrates With this method, which is possible only under UHV conditions, photoelectrons are released from the substrate by incoming X-rays and subsequently analyzed with respect to their kinetic energy. In this analysis, the core level binding energies of electrons can be determined, in turn allowing inferences about the chemical composition (elemental distribution and chemical state of the elements) of the examined sample.

1.1.5 SAMs on silicon surface

Although SAMs on gold have received more attention than the other typologies of SAMs, presumably because of their ease of preparation, monolayers on silicon surface possess some advantageous features. The covalent nature of the assembly process results in systems possessing superior stability, which allows extensive handling and further modification steps without deterioration of the monolayer.[11]
Silicon is the cornerstone of the microelectronics industry. In spite of uncertainties concerning looming limitations of feature sizes on chips within a decade, silicon will most likely remain a central material in computing technologies. The incredible degree of structural control over silicon, based on engineering and chemistry developed over the years by industry and academia, makes it practical to keep silicon as the platform on which complex molecular devices will be built. Research efforts to build hybrid silicon-organic structures are growing rapidly in both academia and industrial companies.[19] This approach to meeting future microelectronics demands by merging molecules with silicon is also critical for various applications that use silicon, but not necessarily for computing. For

instance, the integration of sensors with silicon, in-vivo drug delivery devices, microfluidics and labs-on-chips, bioanalysis, new catalytic materials, and many others, all based on silicon, are areas of intense interest. While the overall technological goals may be very different, all are related by the fact that surface properties of the silicon need to be tailored and controlled. For sensing, for instance, specificity must be introduced by attachment of recognition elements. For molecular electronics, on the other hand, molecules with specific electronic properties must be bound to the silicon surface in a way that is fluid or open to electrons and electronic information. Similar points can be made for most silicon-based applications for which the surface properties are critical.

While native oxide on silicon has proven extremely useful in the electric passivation of bulk silicon, much attention is being directed towards the synthesis of organic monolayers which can be modified upon demand for specific requirements. A wide variety of functionalities can be synthesized and incorporated which will allow for fine tailoring of surface characteristics for a broad range of applications. For the functionalization of silicon surface several different approaches have been taken to first understand its reactivity, and then to subsequently exploit the reactivity to prepare stable, sophisticated interfaces.

In addition to chemical properties of silicon surfaces, surface morphology must also be considered. A morphologically complex (i.e. rough) surface will have different characteristics from a flat surface. A surface that is not flat will have greater surface area that could be highly advantageous for sensing and analysis, for instance, since a much larger quantity of the recognition agent could be packed onto the exposed surface.

A very interesting variant of flat, single crystalline silicon is porous silicon.[20] This high surface area wafer formed from the same silicon wafers used in microelectronics has many advantages and attractions that result from its porosity[21].

Porous silicon can have surface areas of 500 m^2xcm^{-3} which is far greater than a sample of atomically flat silicon.

The approaches towards preparation of monolayers through Si-C bonds on both flat and photoluminescent porous silicon are described in the following paragraphs.

1.1.5.1 Flat, single crystal silicon

Single crystal silicon wafers of high purity are commercially available and relatively inexpensive due to their wide use in microelectronic applications. The most common surface orientations are Si(111) and Si(100) although other Si(*hkl*) orientations are known. Upon exposure to air, single crystal silicon becomes rapidly coated with a thin, native oxide that can be removed chemically with fluoride ion or thermally under UHV conditions. Depending upon the desired electronic properties, silicon wafers are doped in a controlled fashion with electron donating (P, As, Sb: *n*-type) or withdrawing (B: *p*- type) impurities to render the intrinsic material more highly conducting.

1.1.5.2 Porous Silicon

Porous silicon is a potentially revolutionary variant of crystalline silicon because of its tunable electro-, photo- and chemo-luminescent properties.[22] While bulk silicon is an extremely poor light emitter, porous silicon can achieve quantum efficiencies in excess of 10%, the earliest initial application envisaged for the material was optoelectronics, the integration of optical transduction with the electronics of silicon, but then was soon accompanied by sensing, bioanalysis and nanocrystalline silicon fundamentals, using the high surface area.

Because it is easily prepared through simple galvanostatic,[23] chemical (stain),[24] or photochemical[25] etches from silicon wafers (‘bucket’ chemistry),[22] porous silicon

could be readily integrated with silicon-based integrated circuit (IC) manufacturing processes.

The native surface of porous silicon, produced via electrochemical and chemical etches, is capped with hydrogen. In order to satisfy the tetravalency requirement of each silicon atom, the surface is capped with one, two or three hydrides. This surface is termed 'metastable' because this surface can be handled briefly in air for minutes or in some cases hours, but is reactive enough to use the Si-H groups as chemical handles through which further chemistry may be accomplished. Porous silicon has the added advantage of being transparent to infrared (IR) radiation, and combined with its high surface area, its surface terminations can be analysed directly by IR spectroscopy.

1.1.5.3 SAMs on native silicon oxide

The native oxide layer usually contains a high density of traps therefore, it is desirable to remove the native oxide layer and grow an ultra-thin (1-1.5 nm) thermal oxide layer of better electrical quality. On a silicon oxide surface, three classes of molecules, namely, silanes ($RSiX_3$, with X= Cl, OMe, OEt), organometallics (RLi or RMgX), and alcohols (ROH) are widely used for the formation of self assembled monolayers. Thorough cleaning of the substrate is a prerequisite for obtaining a clean oxide layer with high density of silanol groups (Si-OH) on the surface. These silanol groups, which provide a highly hydrophilic surface (allowing molecules to diffuse on the physisorbed ultra-thin water layer), are either used as anchoring sites for silanization reactions or converted into more reactive functions (i.e. Si-Cl or $Si-NEt_2$) suitable for alkylation or alkoxylation reactions.

1.1.5.4 SAMs directly on bare Si

For certain investigations pertaining to molecular electronics applications, the presence of native oxide layer between organic molecule and Si might cause some hindrance, e.g. to study an interface between the organics and Si. Thus, in order to deposit organic SAMs directly on the Si following two steps are necessary, (i) complete removal of the native oxide layer and obtain a reactive surface precursor and (ii) formation of organic SAMs on the freshly prepared reactive surface precursor by making Si-C or Si-O bonds.

There are three known strategies to obtain a reactive Si surface precursor namely, (i) hydrogen-terminated Si, (ii) halogenterminated Si and (iii) reconstructed Si surface. First reactive surface, obtained with Si-H passivation, is only metastable with respect to oxidation under ambient conditions, thus precluding long-term use in most cases. These surfaces can, however, be handled in air for tens of minutes with little degradation which renders them accessible to chemists and materials scientists wishing to use standard Schlenk and glove box techniques.[26] Silicon-hydride termination of commercial, native oxide capped flat crystal silicon wafers is carried out quickly and efficiently in less than10 min using commercially available fluoride sources. To obtain H-terminated flat silicon surfaces two etching process can be employed as shown in figure 1.1.4.

Dilute (1–2%) aqueous HF treatment of a Si(100) wafer yields the (100) dihydride =SiH2 capped surface, and 40% aqueous NH4F of a Si(111) wafer provides the atomically flat (111) monohydride ≡SiH terminated surface.[27] Porous silicon, when etched through standard procedures involving HF, is also hydride terminated but it is coated with $-SiH_3$, $=SiH_2$, ≡SiH groups in a variety of different local orientations and environments owing to the porous nature of the material. All the freshly etched silicon hydride terminated surfaces are chemically homogeneous (> 99% H termination) which is essential for clean reactions. The hydride terminated surfaces

are extremely useful surface precursors because the Si–H and Si–Si bonds can serve as chemical handles through which functionalization can be mediated.

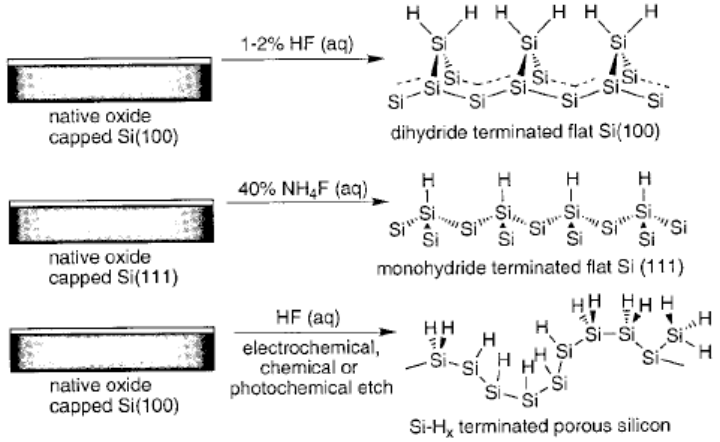

Figure 1.1.4: Fluoride-based etching conditions, leading to hydride-terminated flat and porous silicon surfaces.

Different methods employed to obtain halogen terminated Si surface are presented in figure 1.1.5.

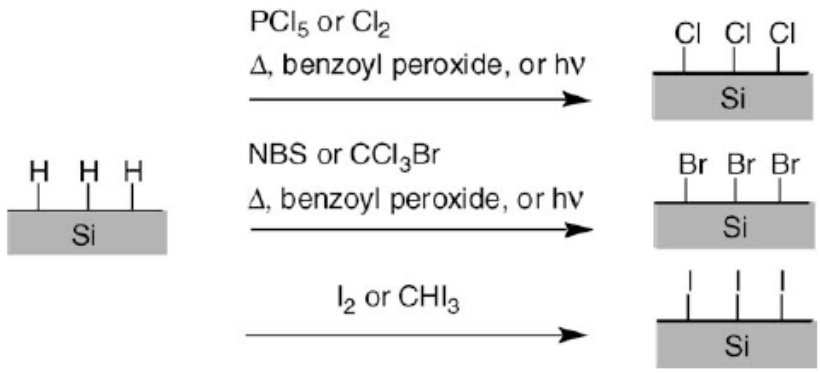

Figure 1.1.5: Common methods used for silicon halogenations.

The Chloro-terminated Si surfaces are prepared by treating the H-terminated Si (11 1) with PCl_5 at 80-100 °C using benzoyl peroxide as a radical initiator in chlorobenzene.[28,29] The other methods include (i) boiling Si wafer in chlorobenzene with PCl5 and UV irradiation, and (ii) heating H-terminated Si at 80 ℃ in the presence of chlorobenzene.[30] Recently, high quality of halogenated silicon surfaces has been produced using gas phase reactions of hydrogenated silicon with molecular chlorine or bromine at room temperature.[31] Bromo-terminated Si surfaces can also be obtained by treating the H-terminated Si surface with CCl_3Br at 80 °C under UV irradiation. Bromination of Si–H surface is also performed sometime using an etching mixture made of HF, HNO_3, CH_3CO_2H, Br_2 and KBr,[32] but this method causes morphology changes of silicon surface.[33] Iodine[34] or iodoforme[35] have also been used as iodinating agents to generate Si–I surface from hydrogenated silicon. The halogen-terminated surfaces are very reactive and thus need to be handled only under inert atmosphere.

Highly reactive bare silicon (100) and (111) surfaces can be obtained by heating Si wafers at temperatures >700 °C under ultra high-vacuum (UHV) conditions ($>10^{-10}$ Torr). Both the (100) and (111) Si surfaces undergo extensive reconstructions, i.e. their surface atomic geometry differs significantly from that of the bulk. However, the two surfaces have markedly different surface structures.

Treatment of a freshly etched hydride-terminated porous silicon surface with molecular chlorine, bromine, and iodine under nitrogen or argon results in efficient Si-X (X) Cl, Br, I) bond formation in 30 min at room temperature. In contrast to the preceding reactions on flat Si(111) surfaces, the hydrides remain intact and are not substituted by chloride; the weaker Si-Si bonds are cleaved and two new Si-X bonds are formed.

The surfaces of silicon have several different chemical reactive sites through which functionalization may be obtained. The general mechanistic trends, based on

hydrosilylation, for flat and porous silicon interfaces are very closely related and thus are discussed here interchangeably.

Hydrosilylation involves insertion of an unsaturated bond into a silicon–hydride group as shown in figure 1.1.6. Alkyne and alkene hydrosilylation on Si–H terminated surfaces yields alkenyl and alkyl termination, respectively. The first example of hydrosilylation of non-oxidized Si–H passivated silicon was carried out by Chidsey and coworkers in 1993 on flat crystal Si(111)

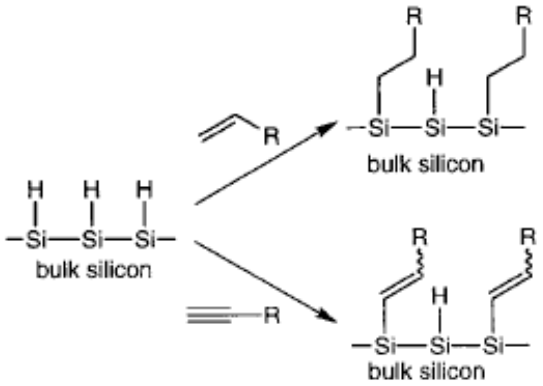

Figure 1.1.6: Hydrosilylation of alkenes or alkynes involves insertion of the carbon–carbon unsaturated bond into the silicon–hydride bond, yielding alkyl and alkenyl terminated surfaces, respectively.

Insertion of alkenes into surface bound Si–H groups, in the presence of a diacyl peroxide radical initiator, provided high quality alkyl monolayers at 100 °C. Monolayers prepared from octadecene, yielding octadecyl groups on the surface are densely packed and tilted approximately 30° from the surface normal. As a result of the good coverage provided by the film, the silicon surfaces demonstrate excellent stability and withstand extended boiling in aerated chloroform, water, acid (2.5 M H_2SO_4 in 90% dioxane, v/v) and base (10% aqueous 1 M NH_4OH), and

are resistant to fluoride (immersion in 48% aqueous HF). Under ambient conditions in air, little oxidation of the silicon surface is observed, indicating the usefulness of this approach for technological applications.[36]

A radical mechanism was proposed for monolayer formation under these conditions in figure 1.1.7. The initiator, the diacyl peroxide, undergoes homolytic cleavage to form two acyloxy radicals which decompose to carbon dioxide and an alkyl radical. The alkyl radical can then abstract H· from a surface Si-H group to produce a silicon radical. Because silyl radicals are known to react extremely rapidly with olefins, formation of a silicon carbon bond is the next probable step.[37] The carbon-based radical can then abstract a hydrogen atom either from a neighboring Si-H group or from the allylic position of an unreacted olefin. The majority of studies carried outinvolved perhydroalkenes but the ω-Cl terminated olefin, 11-chloroundec-1-ene, produced good quality monolayers with chloride termination. Further functionalization of the surface through the chloride is possible. Hydrosilylation of the alkyne, hexadecyne, produced a good quality monolayer and as noted in a footnote, may be bound to the silicon surface through a vinyl group as would be expected. The use of the bromide terminated olefin, 11-bromoundec-1-ene, however, produced a poorly organized monolayer, perhaps due to the incompatibility of the Br with the radical nature of the reaction.

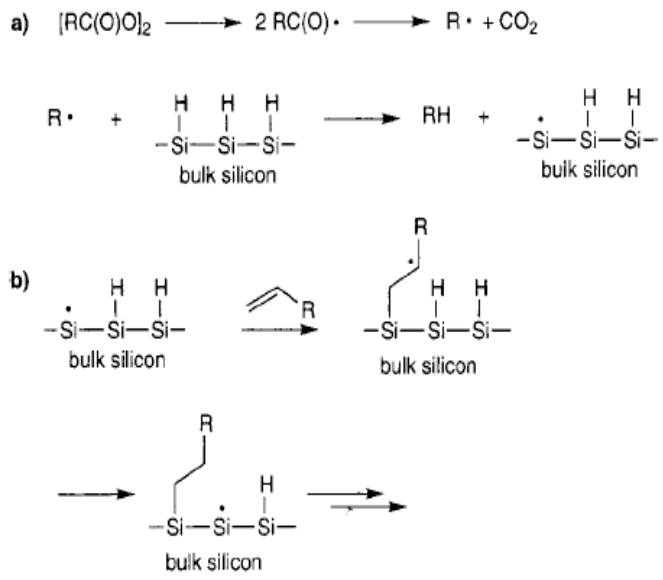

Figure 1.1.7: Mechanism for radical-based hydrosilylation.

Control experiments carried out by Chidsey and co-workers during their investigations of diacylperoxide initiated olefin hydrosilylation on Si(111) surfaces indicated that the reaction could occur in the absence of diacylperoxide initiator at higher temperatures (≥150 °C), almost certainly through homolytic Si–H cleavage, Si-H→Si· + H·. The silyl radical will then proceed to react with the olefin to form the silicon–carbon bond via the mechanism outlined in figure 1.1.7 b.

Hydride-terminated Si(100) was shown to react in a similar fashion.[38] Working at 200 °C, a number of different olefins were examined for their propensity to form stable monolayers. Examples of surface terminations accessible through the thermal hydrosilylation route are shown in Figure 1.1.8.

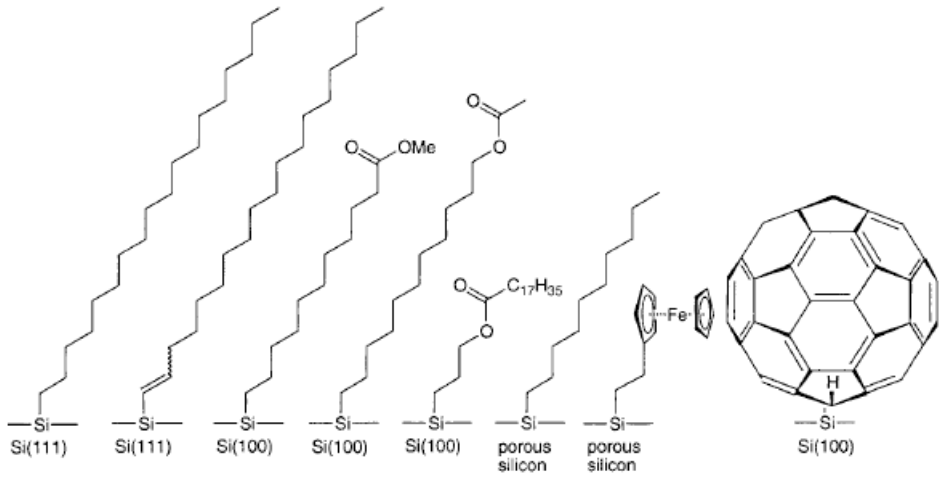

Figure 1.1.8: Examples of surface terminations produced by thermal hydrosilylation.

A 2 h contact time produced closely packed monolayers when long-chain aliphatic alkenes (12-18 carbons) were used as judged by X-ray reflectivity. A major limitation of the thermal hydrosilylation approach is the large excess of alkene required. For instance, up to several milliliters of neat alkene are required to modify the entire surface of a silicon parallelepiped (50x10x1 mm^3). While simple alkenes such as 1-hexadecene are not particularly expensive, for more exotic molecules and for those which are not commercially available and need to be synthesized this point is potential limitation. To circumscribe this restriction, a range of alkenes dissolved in inert, high-boiling hydrocarbons were examined. 1-Hexadecene (10%) in solvents such as *n*-decane, anisole, toluene, xylene, cumene, *tert*-butylbenzene, and mesitylene was compared with the results obtained with neat 1-hexadecene, the reference sample. The apparent advantage of mesitylene as opposed to the other high-boiling solvents tried is that the use of this molecule does not result in pinhole defects in the monolayer as a result of its large size, as

opposed to *n*-hexadecane which intercalates into the forming monolayer. This work is very useful because it reveals that even dilute solutions of alkene (2.5%) in mesitylene, a 40-fold reduction in absolute quantity, can result in ordered monolayers via thermal hydrosilylation; neat alkene is, therefore, not required. Thermally induced hydrosilylation of alkenes and alkynes has been applied to Si-H-terminated porous silicon surfaces.[39,40] Investigations of thermal hydrosilylation of 1-decene on porous silicon showed that before and after the thermal hydrosilylation the nanoscale structure of the porous silicon skeleton is not affected by the high temperatures and extended time of the reaction. The surfaces are chemically robust, as indicated by a range of chemically demanding conditions, including sonication and boiling in chlorinated solvents, boiling protic acid and base, long-term aqueous HF immersion, and steam treatment. Other mechanisms have been proposed as alternatives to a radical-based reaction, as outlined in figure 1.1.9.[41] The 'standard' radical mechanism is shown in Figure 1.1.9 b, which is initiated by Si-H bond homolysis or an adventitious radical remaining from the etching process. The first alternative mechanism proposed (path a) involves F^- catalysis, since residual fluoride from the etching is always present. Nucleophilic attack of a surface silicon atom by F^- results in a pentavalent intermediate which could transfer a hydride to the double bond to give the carbanion. This carbanion then attacks the polarized Si center ($^{\delta+}$Si-F$^{\delta-}$), releasing F^- and forming the Si-C bond. The second alternative mechanism (path b) is based on the ∂-electron-rich double bond attacking a surface silicon atom in a nucleophilic center to form a pentavalent silicon atom, followed by hydride transfer (a [1,3] shift) to the carbocation.

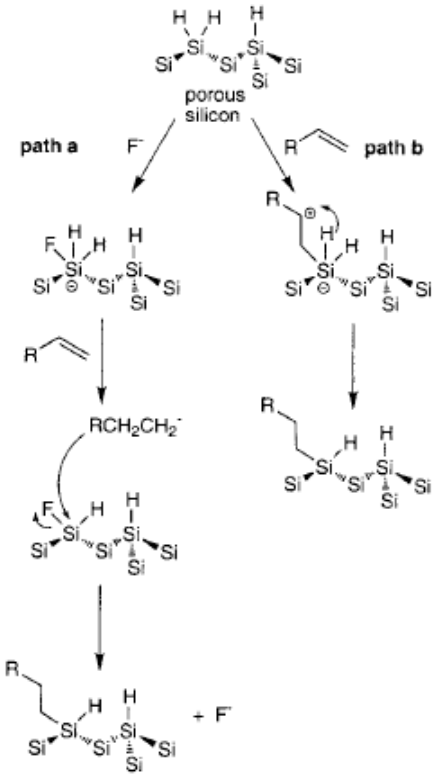

Figure 1.1.9: Two alternative mechanisms to the radical based mechanism proposed for thermal hydrosilylation.

It is known in the organic and organometallic literature that UV irradiation can promote hydrosilylation of unsaturated compounds[41] due to homolytic cleavage of Si-H bonds, as is the case with thermal induction. UV photoinduction, however, takes place at room temperature and thus provides a way to avoid thermal input that could be harmful to delicate or small features on a silicon chip. Minimal input of thermal energy would be preferable in any IC manufacturing process (thermal budget). Irradiation of a hydride-terminated Si(111) surface with UV light (185 and 253.7 nm) in the presence of an aliphatic alkene like 1-pentene or 1-octadecene

brings about hydrosilylation in 2 h at room temperature, as shown in figure 1.1.10.[42]

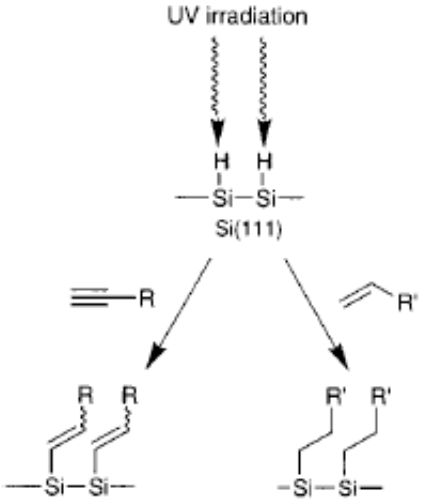

Figure 1.1.10: Schematic for UV-mediated alkene hydrosilylation on Si(111)-H.

A range of alkenes and alkynes were successfully tried, including 1-octene, 1-octadecene, 1-octyne, styrene, and phenylacetylene, with the alkenes yielding alkyl monolayers and the alkynes yielding alkenyl monolayers; examples of surfaces prepared are shown in Figure 1.1.11.

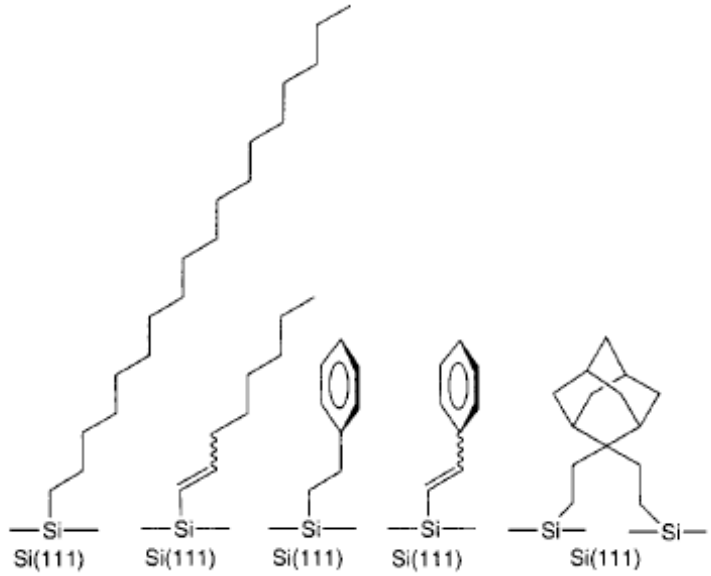

Figure 1.1.11: Examples of surfaces produced through UV mediated hydrosilylation on Si(111)-H.

The mechanism proposed is radical based, with homolytic Si-H bond cleavage initiating the reaction to form a silicon radical (dangling bond),[43] similar to that shown in Figure 1.1.7 b.[42] Because silicon radicals are known to react very rapidly with unsaturated carbon-carbon bonds,[44] Si-C bond formation is expected to be a facile step, forming the surface-bound carbon-based radical on the β-carbon. In contrast to flat, hydride-terminated silicon surfaces, simple reactions can induce hydrosilylation of alkenes and unconjugated alkynes on Si-H-terminated photoluminescent porous silicon surfaces at room temperature in minutes. Some examples of very efficient reactions starting from Si–H terminated porous surfaces are outlined in figure 1.1.12

.

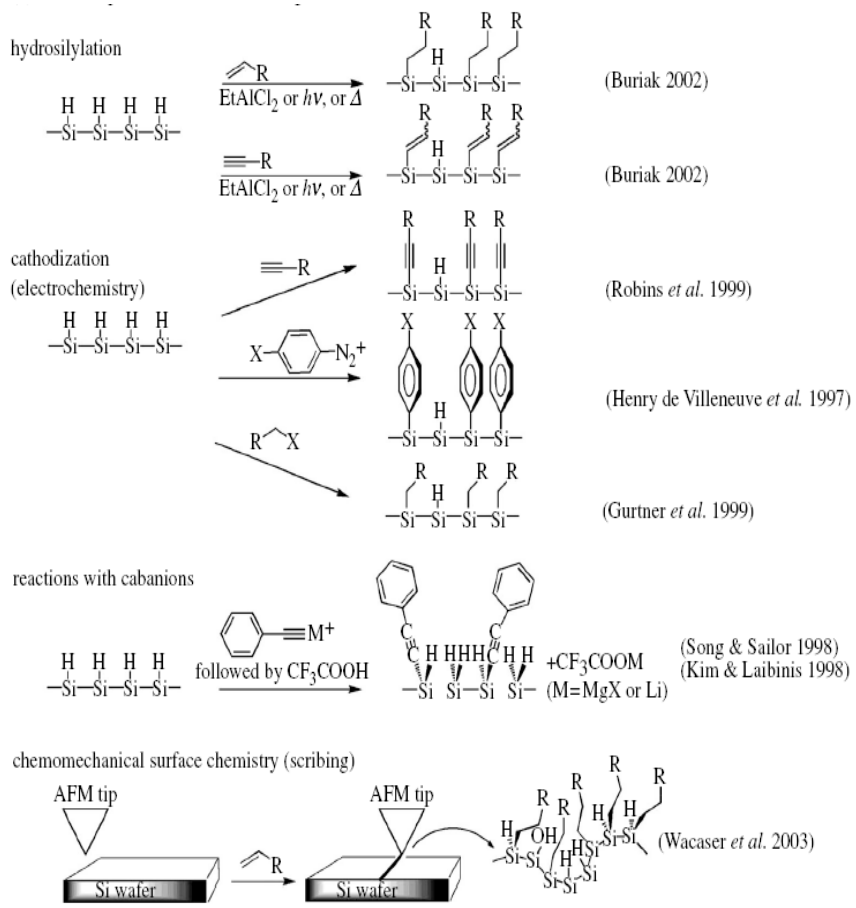

Figure 1.1.12: Some of the surface chemical reactivity of porous silicon.[19]

From this incredible body of research, many generalizations can now be made about the organometallic surface chemistry of silicon. The field is an extremely exciting one because of the close proximity between fundamental science and technological applications, and it is only a matter of time and circumstance before tailored organic interfaces reach their commercial potential.

1.2 Chemical Sensors

All over the world, billions of dollars are spent annually on chemical/biological detections related to medical diagnosis, environmental monitoring, public security and food safety because lab analysis using expensive equipment is usually cumbersome and time-consuming. Therefore, there has been a pressing societal need for the development of chemo/biosensors for the detection of various analytes in solution and atmosphere, which are both less expensive and simpler to construct and operate. Although considerable progress was made in the past several decades, the chemo/biosensor field remains underdeveloped and at a low level of commercialization because of the lack of alternative strategies and multidisciplinary approaches. Only a few chemo/biosensors for simple analytes have been able to meet commercial requirements with detection sensitivity, selectivity, accuracy and reliability approaching that of experimental equipment. However, the recent developments of novel chemosensory materials and fabrication technologies may provide many potential opportunities for the development of a new generation of chemo/biosensors. Thus, the explorations on chemo/biosensors based on novel sensing concept have attracted growing interest in recent years.[45]

A chemical sensor is a device that transforms chemical information, ranging from the concentration of a specific sample component to total composition analysis, into an analytically useful signal. The chemical information, mentioned above, may originate from a chemical reaction of the analyte or from a physical property of the system investigated.[46] The sensing material interacts with the chemical species present in the environment by changing some of its physicochemical properties, while the transducer transforms these variations into a readable signal.

The structure of a generic chemical sensor is shows in figure 1.2.1.

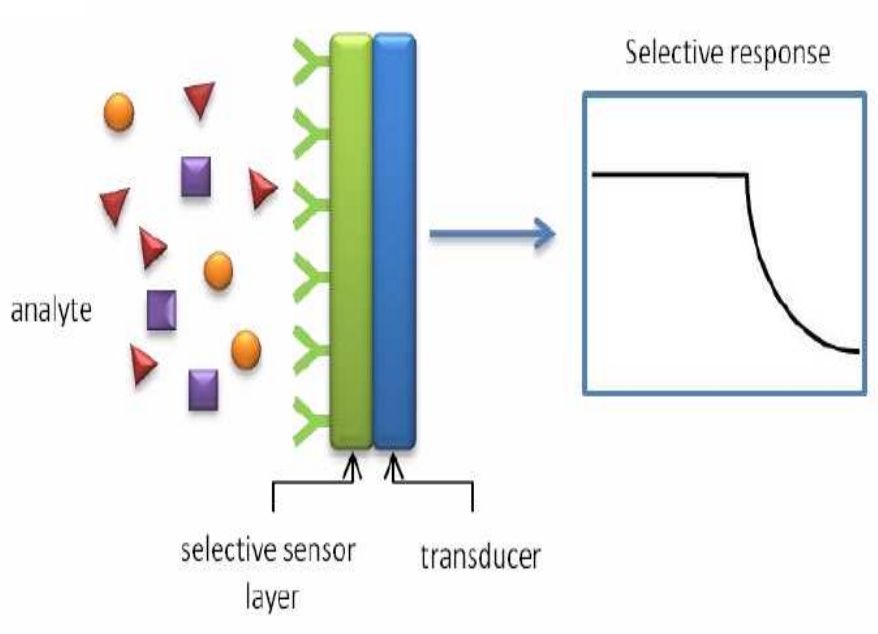

Figure 1.2.1: Working principle of supramolecular sensors.

Chemical sensors contain two basic functional units: a receptor part and a transducer part.

In the ***receptor*** part of a sensor the chemical information is transformed into a form of energy which may be measured by the transducer.

The ***transducer*** part is a device capable of transforming the energy carrying the chemical information about the sample into a useful analytical signal. The transducer as such does not show selectivity.

The receptor part of chemical sensors may be based upon various principles:

- physical, where no chemical reaction takes place. Typical examples are those based upon measurement of absorbance, refractive index, conductivity, temperature or mass change.

- chemical, in which a chemical reaction with participation of the analyte gives rise to the analytical signal.

- biochemical, in which a biochemical process is the source of the analytical signal. Typical examples are microbial potentiometric sensors or immunosensors. They may be regarded as a subgroup of the chemical ones. Such sensors are called ***biosensors.***

Chemical sensors may be classified according to the operating principle of the transducer.[47]

Optical devices transform changes of optical phenomena, which are the result of an interaction of the analyte with the receptor part. This group may be further subdivided according to the type of optical properties which have been applied in chemical sensors.

Electrochemical devices transform the effect of the electrochemical interaction analyte-electrode into a useful signal. Such effects may be stimulated electrically or may result in a spontaneous interaction at the zero-current condition.

Electrical devices based on measurements, where no electrochemical processes take place, but the signal arises from the change of electrical properties caused by the interaction of the analyte.

Mass sensitive devices transform the mass change at a specially modified surface into a change of a property of the support material. The mass change is caused by accumulation of the analyte.

Magnetic devices based on the change of paramagnetic properties of a gas being analysed. These are represented by certain types of oxygen monitors.

Thermometric devices based on the measurement of the heat effects of a specific chemical reaction or adsorption which involve the analyte. In this group the heat effects may be measured in various ways, for example in the so called catalytic sensors the heat of a combustion reaction or an enzymatic reaction is measured by use of a thermistor.

Sensors are typically characterized by three properties: *sensitivity*, *selectivity* and *reversibility*.

Sensitivity can be generally defined as the slope of the analytical calibration curve, that is correlated with the magnitude of the change in the sensor signal upon a certain change in the analyte concentration.[48] "Cross sensitivity" hence refers to the contributions of other than the desired compound to the overall sensor response.

Selectivity is instead the ability of a sensor to respond primarily to only one chemical species in the presence of other species (usually denoted interferents). The quest for better selectivity remains the cornerstone of the chemical sensing research:[49] it can be achieved by using biosensors (e.g. biologically derived selectivity by appropriate enzymes, structure-binding relationship in antibody-antigen complexes,) or by synthesizing materials containing specific binding sites.

Reversibility describes the sensor's ability to return to its initial state after it has been exposed to chemical species. The reversibility requires the involvement of weak interactions, since the formation of covalent or ionic bonds would result in an irreversible saturation of the layer.[50]

The conventional design of chemical sensors uses a "lock-and-key" approach (a steric fit concept enunciated for the first time by Emil Fischer in 1894),[51] wherein a specific receptor is synthesized to bind the analyte strongly and selectively.

This concept has been widely exploited by supramolecular chemists for the design and synthesis of molecular receptors which are useful to understand and mimic nature specific interactions. As for biological systems, the concepts of shape recognition and binding site complementarity are central for effective molecular recognition in artificial host-guest systems. The progress made in the designing synthetic receptors[52] allows sensor selectivity modulation towards different classes of compounds by mastering the weak interactions that occur between the sensing material and the analytes. The selective binding of a neutral substrate by a molecular receptor to form a complex (molecular recognition) is based besides on shape complementarity also on the presence of specific interactions such as hydrogen bonding,[53] π-π stacking,[54] and CH-π interactions.[55] The direct translation of the molecular recognition properties of a given receptor from solution to the solid-gas interface is not trivial, since non-specific interactions such as dispersion forces and material properties such as surface morphology and layer permeability come into play. Molecular recognition is a conceptually attractive and potentially powerful approach to engineering structures and devices at the molecular scale.[56] Organic monolayers hosted on inorganic surfaces[57-62] represent the best approach for harnessing the full potential of molecular recognition on surfaces.[63,64] Compared to both thin films and bulk materials containing molecular receptors, such hybrid organic-inorganic materials have the advantage of reducing or even eliminating non-specific interactions which often mask the recognition events.[65]

There are a wide choice of host-guest system, such as crown ethers, cavitands, cyclodextrins and calixarenes, very promising.

1.3 Cavitands

Interesting and versatile molecular receptors are cavitands, originally defined by Cram as "synthetic organic compounds with enforced concave cavities large enough to complex complementary organic molecules or ions"[66], whose complexation properties have been extensively studied in the solid state[67], in solution[68] and in the gas phase.

The concave surface permits the positioning of different functional groups on the substrate binding site that is usually located inside the cavity.[69]

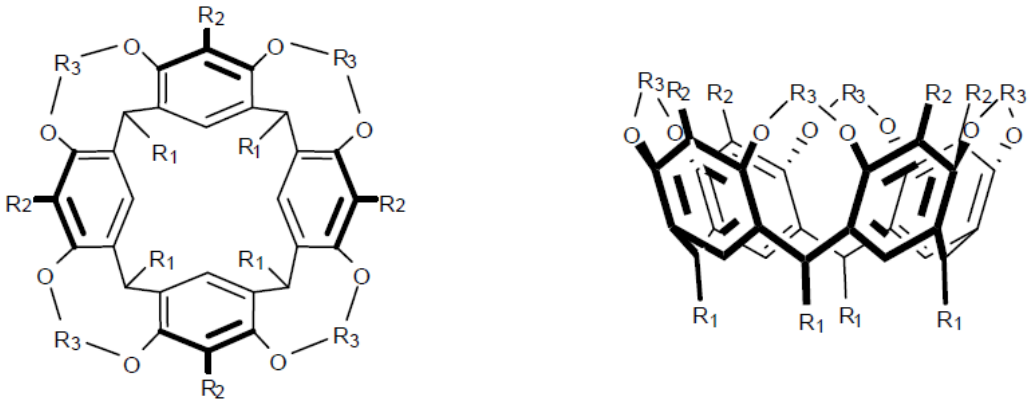

Figure 1.3.1: Structure of a cavitand top (left) and side(right) views.

Cavitands are generally synthesized by covalent linkage of neighboring phenolic hydroxyl groups in the corresponding octols. They are particularly attractive because the rim of the bowls can be varied by different R_2 substituent and bridging groups R_3 for deepening the bowl cavity and for introducing potentially cooperating functional groups to act as molecular receptors.[70] Moreover the R_1 substituent can be use for manipulating the solubility or the morphology in the solid state. The cavitands are designed to bind target molecules to form host-guest complexes with a variety of guest molecules and ions through their rigid, concave

π- basic cavity, which enables electrostatic interactions such as cation-π and CH-π and in addition, appropriate substitution at the upper-rim allows them to employ hydrogen bonding in the formation of complexes.

The most common bridging groups are alkylenedioxy, dialkylsilicon, heterophenylene and phosphoryl.

In this thesis we focalized the attention on three classes of cavitands for applications as sensors: phosphourus-bridged, quinoxaline-bridged and acid-bridged cavitands.

1.3.1 Quinoxaline-Salen-bridged cavitands

The cavity of resorcinarenes can be largely extended by bridging phenolic hydroxyl groups with aromatic spacers.[71]Tetraquinoxaline cavitands result from nucleophilic aromatic substitution with 2,3-dichloroquinoxaline on the phenolic oxydryl moieties of a resorcin[4]arene.

A particularly interesting properties of these systems is the reversible switching between a closed "vase" conformation with a deep cavity for guest complexation, and an open "kite" conformation with a flat extended surface.[72] Indeed the quinoxaline spacers can occupy either axial (a) or equatorial (e) positions (Figure 1.3.2). In the "vase" (aaaa) conformer, the spacers touch each other via their α-hydrogens while forming a box like cavity with C4V symmetry which is approximately 7 Å wide and 8 Å deep.[73]. The cavity is open at the top and closed at the bottom by the cavitand itself. In the "kite" (eeee) conformer, the spacers are more or less in the same plane (C_{2v} symmetry). Conformational switching can be reversibly induced by temperature or pH changes, with the "kite" conformation being preferred at low temperatures and low pH values, or by metal-ion addition.

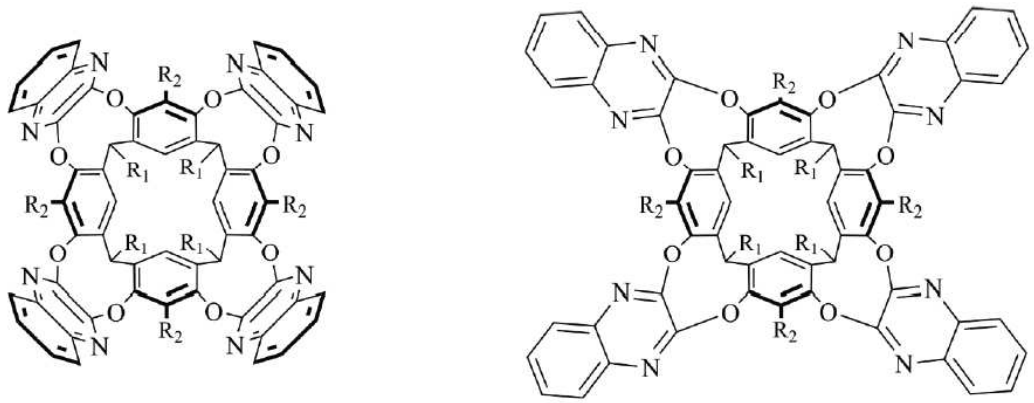

Figure 1.3.2: Structure of quinoxaline cavitand aaaa conformer (left) and eeee conformer (right).

In contrast, in mixed-bridged cavitands with one of the four quinoxaline wings displaced by a different bridge, the thermal vase-to-kite interconversion is switched off by substantially decreasing the solvation of the kite form. Mixed-bridged cavitands can only adopt the kite conformation by protonation of the quinoxaline nitrogen atoms with an acid such as TFA, as a result of the developing Coulombic repulsion in the vase geometry.

New mixed-bridged triquinoxaline (3QxCav) are proposed as receptor for the realization of materials to be used as trapping devices for nitroaromatic compounds.

The receptor discussed in this thesis consists of a 3QxCav compound functionalized with a, *N*,*N*-bis(salicylaldehyde) ethylenediimine (salen) functionality. In this receptor, in addition to CH-π interactions between the analytes and the cavity bottom and walls, the presence of the chiral salen allow a chiral discrimination. Chiral salen-metal complex act as a heteroditopic receptor in which the metal centre is able to coordinate the anion, whereas the π-rich

quinoxalinic cavity binds tetraalkylammonium cations by stabilizing them with CH···π and cation···π interactions.

1.3.2 Phosphorous bridged Cavitands

The first attempt to synthesize phosphorous-bridged cavitands was carried out in Cram's group in the 1980s by reacting a methyl-footed resorcin[4]arene with dichlorophenylphosphonate, obtaining a mixture of diastereomers difficult to isolate.[74]

In fact, the presence of four P^{V} stereogenic centers gives rise to six possible diastereomeric cavitands. The inward (i) and outward (o) configurations are defined relative to the different orientation of the P=O moieties (Figure 1.3.3)

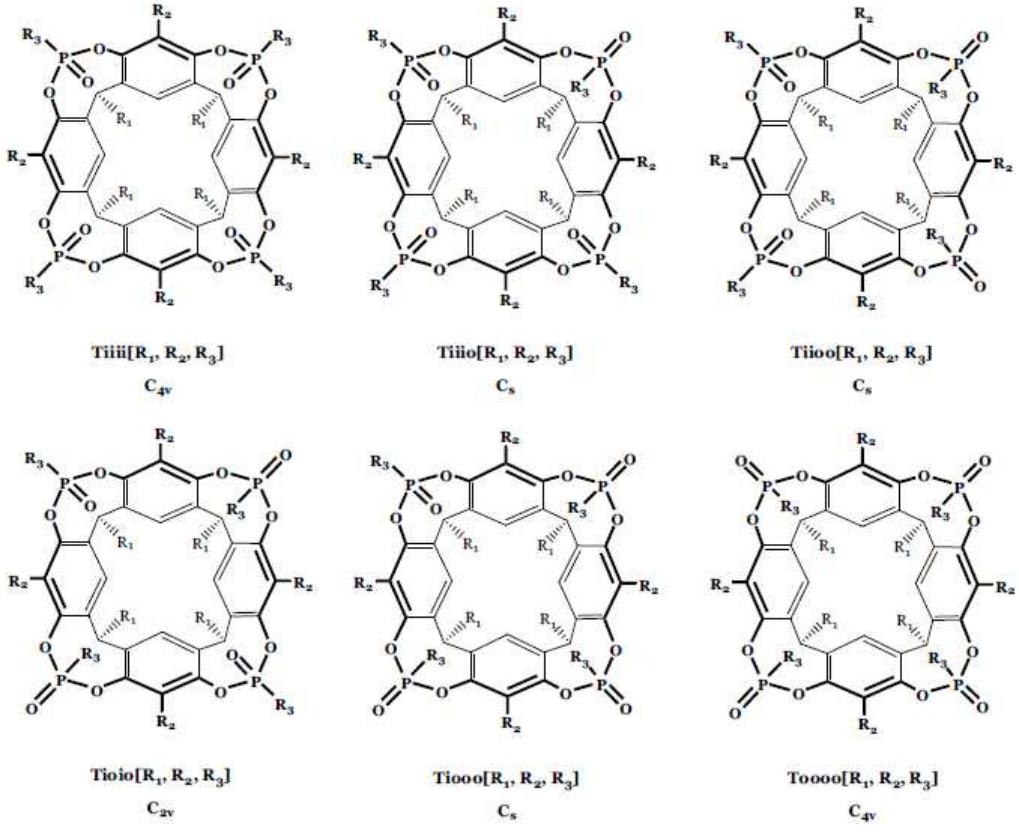

Figure 1.3.3: Isomers of tetraphosphonate bridged cavitands.

The tetraphosphonate cavitands nomenclature, reported in Figure 1.3.3, summarizes the number and relative positions of P^V bridges, their stereochemistry, and the type of substituents at the lower rim, at the apical positions, and on the phosphorus bridges, respectively, in a single term.

In particular, the capital letter, defines number and nature of bridges, the lower case letters define the in-out stereochemistry, and R_1, R_2 and R_3 in brackets define the substituents at the lower rim, in the apical positions and on the phosphorous stereocenters respectively.

Tetraphosphonate cavitand presents remarkable recognition properties toward N-methylammonium ($K_{ass} \sim 10^9$, Figure 1.3.4 a) and N-methylpyridinium ($K_{ass} \sim 10^7$ Figure 1.3.4 b) which can be attributed to three synergistic interaction modes:

(i) N+•••O=P cation-dipole interactions;

(ii) CH_3-π interactions of the acidic ^+N-CH_3 group with the π basic cavity;

(iii) two simultaneous hydrogen bonds between two adjacent P=O bridges and the two nitrogen protons,[75] in the case of protonated secondary amines;

The simultaneous hydrogen bonds are the reason for the higher affinity of the N-methylammonium toward the cavity.

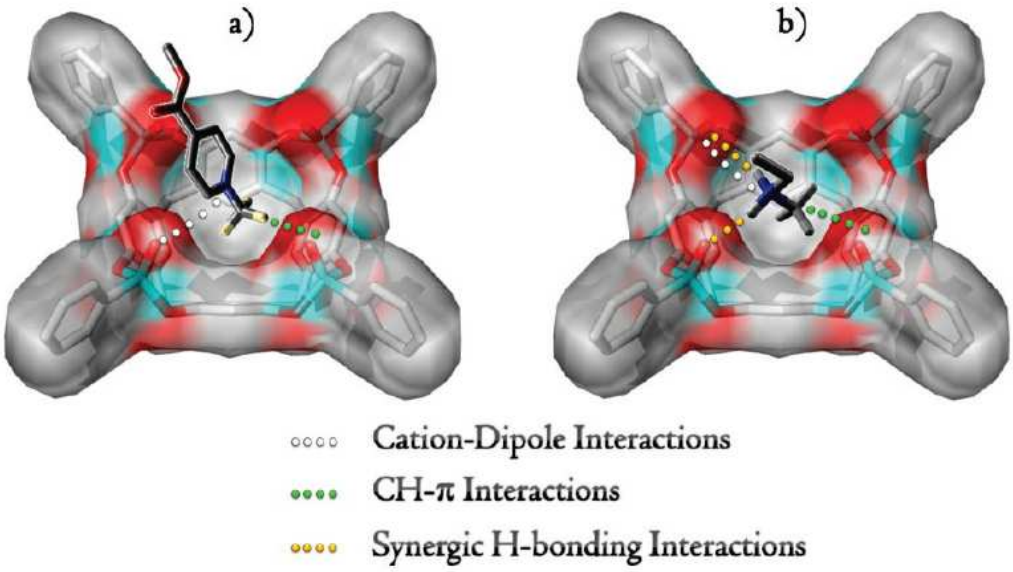

Figure 1.3.4: Interactions involved in the molecular recognition process.

Another class of cavitand (TS_{iiii}), structurally identical to the T_{iiii} receptor except for the presence of four P=S instead of four P=O has been synthesized via oxidation in situ of the tetraphosphonite cavitand with S_8.

This substitution strongly reduces the molecular recognition properties, because sulphur has lower electronic density with respect to the oxygen and consequently less affinity for H-bonding interactions.[22] In addition the cavity of TS_{iiii} is much smaller and less prone to guest inclusion because sulphur is larger (atomic radius=1 Å) than oxygen (atomic radius=0.6 Å). (Figure 1.3.5)

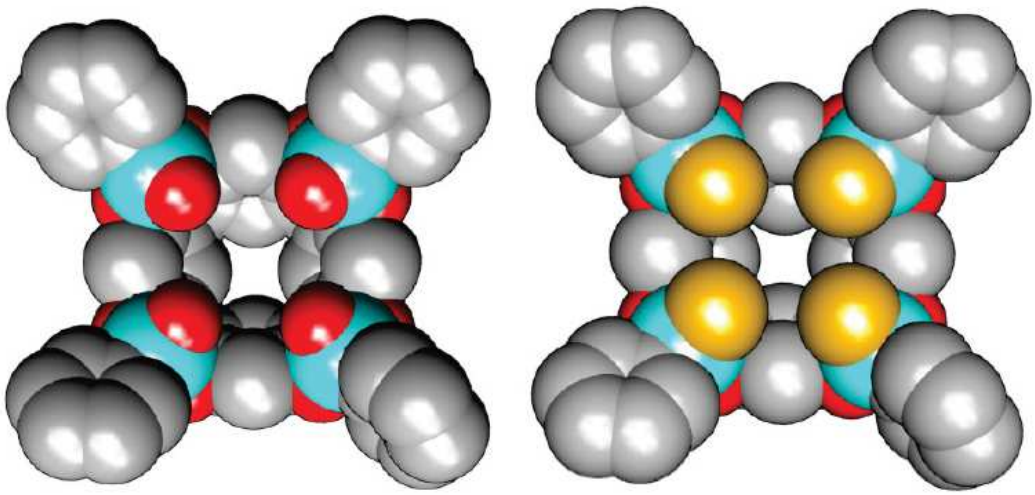

Figure 1.3.5: Comparison between tetraphosphonate and tetrathiophosphonate cavitands (top view).

1.4 References

[1] J. Gao, B. Xu, Nano Today, 2009, 4, 37-51.

[2] L. Zhang, T. J. Webster, Nano Today, 2009, 4, 66-80.

[3] a) C. Bae, H. Yoo, S. Kim, K. Lee, J. Kim, M. M. Sung, H. Shin, Chem. Mater. 2008, 20, 756–767. b) G. R. Patzke, F. Krumeich, R. Nesper, Angew. Chem., Int.Ed. 2002, 41, 2446–2461. c) S. J. Hurst, E. K. Payne, L. Qin, C. A. Mirkin, Angew. Chem., Int. Ed. 2006, 45, 2672–2692. d) B. Tian, T. J. Kempa, C. M. Lieber, Chem. Soc. Rev. 2009, 38, 16–24.

[4] Y. Qiu, P. Chen, M. Liu, J. Am. Chem. Soc., 2010, *132*, 9644-9652.

[5] New Scientist 1983, 98, 20.

[6] L. Netzer, J. Sagiv, J. Am. Chem. Soc. 1983, 105, 674.

[7] W. C. Bigelow, D. L. Pickett,W. A. Zisman, J. Colloid Sci. 1946, 1, 513.

[8] W. C. Bigelow, E. Glass, W. A. Zisman, J. Colloid Sci. 1947, 2, 563.

[9] E. E. Polymeropoulos, J. Sagiv, J. Chem. Phys. 1978, 69, 1836.

[10] J. Sagiv, J. Am. Chem. Soc. 1980, 102, 92.

[11] S. Onclin, B. J. Ravoo, D. N. Reinhoudt, Angew. Chem. Int. Ed. 2005, 44, 6282-6304.

[12] J. C. Love, L. A. Estroff, J. K. Kriebel, R. G. Nuzzo, G. M. Whitesides, Chem. Rev. 2005, 105, 1103-1169.

[13] C. Tidwell, S. Ertel, B. Ratner, B. Tarasevich, S. Atre, D. Allara, Langmuir 1997, 13, 3404-3414.

[14] R. E. Holmlin, X. Chen, R. G. Chapman, S. Takayama, G. M. Whitesides, Langmuir, 2001, 17, 2841-2850.

[15] E. Ostuni, R. G. Chapman, M. N. Liang, G. Meluleni, G. Pier, D. E. Ingber, G. M. Whitesides, Langmuir, 2001, 17, 6336-6343.

[16] C. Engtrakul, L.R. Sita, Nano Lett., 2001, 1, 541-549.

[17] J. J. Gooding, F. Mearns, W. Yang, J. Liu, Electroanal., 2003, 15, 81-96.

[18] M. Kind, C. Woll Progress in Surface Science, 2009, 84, 230–278.

[19] J. M. Buriak, Chem. Rev. 2002, 102, 5, 1271-1308.

[20] L. T. Canham, Properties of porous silicon. 1997, London: Inspec.

[21] M. J. Sailor, E. J. Lee, 1997 Adv. Mater. 9, 783.

[22] A. G. Cullis, L. T. Canham and P. D. J. Calcott, J. Appl. Phys., 1997, 82, 909.

[23] A. Halimaoui, in Properties of Porous Silicon, ed. L. T. Canham, INSPEC, London, 1997, p.12.

[24] M. T. Kelly, J. K. M. Chun, A. B. Bocarsly, Appl. Phys. Lett., 1994, 64, 1693.

[25] N. Noguchi, I. Suemune, Appl. Phys. Lett., 1994, 62, 1429; O. K. Anderson, T. Frello and E. Veje, J. Appl. Phys., 1995, 78, 6189.

[26] B. J. Tufts, A. Kumar, A. Bansal, N. S. Lewis, J. Phys. Chem., 1992, 96, 4581.

[27] G. S. Higashi, R. S. Becker, Y. J. Chabal, A. J. Becker, Appl. Phys. Lett., 1991, 58, 1656.

[28] A. Bansal, X. Li, I. Lauermann, N.S. Lewis, J. Am. Chem. Soc. 1996, 118, 7225.

[29] A. Bansal, X. Li, S.I. Yi, W.H. Weinberg, N.S. Lewis, J. Phys. Chem. B, 2001, 105, 10266.

[30] X.-Y. Zhu, V. Boiadjiev, J.A. Mulder, R.P. Hsung, R.C. Major, Langmuir, 2000, 16, 6766.

[31] B.J. Eves, G.P. Lopinski, Surf. Sci. 2005, 579, L89.

[32] D. Narducci, L. Pedemonte, G. Bracco, Appl. Surf. Sci. 2003, 212, 649.

[33] L. Pedemonte, G. Bracco, A. Relini, R. Rolandi, D. Narducci, Appl. Surf. Sci. 2003, 212, 595.

[34] J.M. Lauerhaas, M.J. Sailor, Science, 1993, 261, 1567.

[35] V.T. Joy, D. Mandler, Chem. Phys. Chem. 2002, 3, 973.

[36] J. M. Buriak, Chem. Commun., 1999, 1051-1060.

[37] C. Chatgilialoglu, Acc. Chem. Res., 1992, 25, 188.

[38] A. B. Sieval, A. L. Demirel, J. W. M. Nissink, M. R. Linford, J. H. van der Maas, W. H. de Jeu, H. Zuilhof, E. J. R. Sudhölter, Langmuir 1998, 14, 1759.

[39] R. Boukherroub, S. Morin, D. D. M. Wayner, F. Bensebaa, G. I. Sproule, J.-M. Baribeau, D. J. Lockwood, Chem. Mater. 2001, 13, 2002.

[40] J. E. Bateman, R. D. Eagling, B. R. Horrocks, A. Houlton, J. Phys. Chem. B 2000, 104, 5557.

[41] R. Boukherroub, S. Morin, D. D. M. Wayner, F. Bensebaa, G. I. Sproule, J.-M. Baribeau, D. J. Lockwood, Chem. Mater. 2001, 13, 2002.

[42] R. L. Cicero, M. R. Linford, C. E. D. Chidsey, Langmuir 2000, 16, 5688.

[43] C. A. Burkhard, R. H. Krieble, J. Am. Chem. Soc. 1947, 69, 2687.

[44] J. M. Kanabus-Kaminska, J. A. Hawari, D. Griller, C. Chatgilialoglu, J. Am. Chem. Soc. 1987, 109, 5267-5268.

[45] G. Guan, B. Liu, Z. Wang, Z. Zhang Sensors 2008, 8, 8291-8320.

[46] A. Hulanichì, S. Geab, F. Ingman, Pure&App. Chern., Vol. 63, No. 9, pp. 1247-1250, 1991.

[47] R. W. Cattrall, Chemical Sensors, Oxford Science Publications, 1997.

[48] A. D'Amico, C. Di Natale, IEEE Sensors Journal 2001, 1, 183.

[49] J. Janata, M. Josowicz, Anal. Chem. 1998, 70, 179.

[50] A. Hierlemann, A. J. Ricco, K. Bodenhöfer, W. Göpel, Anal. Chem. 1999, 71, 3022.

[51] E. Fischer, Ber. Dtsch. Chem. Ges. 1894, 27, 2985.

[52] J.-M. Lehn, Supramolecular Chemistry, Wiley-VCH, Wienheim, 1995.

[53] J. Rebek, Angew. Chem. Int. Ed., Engl., 1990, 29, 245-255.

[54] C. H. Hunter, K. R. Lawson, J. Perkins, C. J. Urch, J. Chem. Soc., Perkin Trans. 2001, 2, 651-699.

[55] M. Nishio, M. Hirota, Y. Umezawa, The CH-π Interactions, Wiley-VCH, New-York, 1998.

[56] G. M. Whitesides, B. Grzybowski, Science, 295, 2418.

[57] M. Dubey, S. L. Bernasek, J. Schwartz, J. Am. Chem. Soc. 2007, 129, 6980–6981.

[58] S. Zhang, C. M. Cardona, L. Echegoyen, Chem.Commun. 2006, 4461–4473.

[59] A. Facchetti, E. Annoni, L. Beverina, M. Morone, P. Zhu, T. J. Marks, G. A. Pagani, Nat. Mater. 2004, 3, 910–917.

[60] Z. Liu, A. A. Yasseri, J. S. Lindsey, D. F. Bocian, Science 2003, 302, 1543–1545.

[61] M. Altman, A. D. Shukla, T. Zubkov, G. Evmenenko, P. Dutta, M. E Van der Boom, J. Am. Chem.Soc. 2006, 128, 7374–7382.

[62] T. Gupta, M. E. Van der Boom, J. Am.Chem. Soc. 2006, 128, 8400–8401.

[63] A. B. Descalzo, R. Martìnez-Màòez, F. Sancenòn, K. Hoffmann, K. Rurack, Angew. Chem., Int. Ed. 2006, 45, 5924–5948.

[64] C. Lagrost, G. Alcaraz, J.-F. Bergamini, B. Fabre, I.Serbanescu, Chem. Commun. 2007, 1050–1052.

[65] M. Tonezzer, M. Melegari, G. Maggioni, R. Milan, G. DellaMea, E. Dalcanale, Chem. Mater. 2008, 20, 6535–6542.

[66] D. J. Cram, J. M. Cram, In Container Molecules and Their Guests (ED.: J. F. Stoddart), The Royal Society of Chemistry, Cambridge, 1994, Chapter 5.

[67] D. J. Cram, S. Karbach, H.-E. Kim, C. B. Knobler, E. F. Maverick, J. L. Ericson, R. C. Helgeson, J. Am. Chem. Soc. 1988, 110, 2229-2237.

[68] a) J. A. Tucker, C. B. Knobler, K. N. Trueblood, D. J. Cram, J. Am. Chem. Soc. 1989, 111, 3688-3699. b) P. Soncini, S. Bonsignore, E. Dalcanale, F. Ugozzoli, J. Org. Chem. 1992, 57, 4608-4612. c) T. Haino, D. M. Rudkevich, A. Shivanyuk, K. Rissanen, J. Rebek, Jr., Chem. Eur. J. 2000, 6, 3797-3805. d) K. Paek, J. Cho, Tetrahedron Lett. 2001, 42, 1927-1929.

[69] A. Friggeri, F.C.J.M. Van Veggel, D.N. Reinhoudt, Langmuir 1998, 14, 5457-5463.

[70] P. Timmerman, W. Verboom, D. N. Reinhoudt, Tetrahedron 1996, 52, 2663.

[71] a) J.R. Moran, S. Karbach, D.J. Cram J. Am. Chem. Soc. 1982, 104, 5826; b) J.A. Bryant, J.L Ericson, D.J. Cram J. Am. Chem. Soc. 1990, 112, 1255; c) D.J. Cram, H.–J. Choi, J.A. Bryant, C.B. Knobler, J. Am. Chem. Soc, 1992, 114, 7748.

[72] P. Roncucci, L. Pirondini, G. Paderni, C. Massera, E. Dalcanale, V.A. Azov, F. Diederich, Chem. Eur. J. 2006, 12, 4775.

[73] E. Dalcanale, P. Soncini, G. Bacchilega, F. Ugozzoli, J. Chem. Soc. Chem., Chem. Commun 1989, 500.

[74] K. D. Stewart, Ph.D. Dissertation, University of California, Los Angeles, 1984.

[75] J. J. Lundquist, T. E. Toone, The Cluster Glycoside Effect, Chem. Rev. 2002, 102, 555-578.

Chapter 2

Flat-Silicon grafting of Tetraphosphonate cavitand for molecular recognition: From Sensing to Nanoengineering of functional molecules.

2.1 Introduction

Among the several surface functions identified to be worth pursuing, molecular recognition is particularly noteworthy for its profound impact on biology and materials science. In living organisms, multiple recognition events trigger the immune system response through antibodies, and they promote the adhesion of viruses on cell surfaces.[1] A strong contribution to the development of molecular recognition themes was given by supramolecular chemistry. In the last decades, researchers active in this field have designed and prepared an amazing number of different synthetic receptors aimed either at the recognition of target molecules[2-4]

or at the fabrication of well-defined 2D and 3D molecular assemblies at interfaces,[5,6] through non-covalent interaction.

Tetraphosphonate cavitands are particularly versatile synthetic receptors: their complexation ability span from positively charged inorganic and organic species[7] to neutral molecules[8]. This diverse complexation ability is the result of three interaction modes, which can be activated either individually or in combination by the host according to the guest requirements: (a) multiple ion-dipole interactions between the inward facing P=O groups and the positively charged guests[9]; (b) single or dual H-bonding involving the P=O groups[9,10]; and (c) CH_3-π interactions between a methyl group present on the guest and the cavity of the host[11].

The complexation properties of tetraphosphonate cavitands anchored on silicon surface toward N-methyl pyridinium and N-methyl ammonium salts in organic solvents have been recently investigated[12]. In the present chapter I use the tetraphosphonate cavitands to distinguish between N-methylated amino acids and their non-methylad analogues and I explored the possibility to transfer their complexation properties to aqueous and biological environments. Moreover the combination of the molecular recognition properties of cavitands with the metal-coordination ability of specific guests allowed the development of a self-assembly protocol to build luminescent coordination structures on silicon.

2.1.1 Molecular recognition of N-methylated amino acids: sarcosine detection as tumoral marker

Prostate cancer is the most common cancer in men, with 913,000 new cases diagnosed and 258,000 related deaths worldwide in 2008[13]. Due to its large incidence, it is the second leading cause of cancer-related death among the male population in the United States[14] and in the European Union[15]. The traditional diagnosis, based on prostate specific antigen (PSA), does not distinguish between

aggressive and slow-growing cancer forms. In particular, it is important to differentiate the organ-confined disease from the aggressive metastatic one. This distinction is essential to guarantee the earliest treatment in the worse cases and to avoid unnecessary surgeries in the others. Early stage detection of aggressive prostate cancer has been recently linked to the presence of sarcosine in urine.[15] Sarcosine forms when the enzyme glycine-N-methyltransferase transfers a methyl group from S-adenosylmethionine to glycine. Being sarcosine one of the cancer biomarker candidates [16,17], effective diagnostic tools for the detection of sarcosine directly in urine are highly desirable. The basic methodology for sarcosine determination is gas chromatography-mass spectroscopy which, although highly sensitive and reliable, is hardly applicable for a widespread screening of this pathology. A different approach for sarcosine determination consists in the use of a fluorometric assay (BioVision Research Products, Mountain View, CA). However, it requires various reaction steps and it is prone to interference due to unspecific reactions with other (unknown) urinary analytes[16], making it unsuitable for sarcosine measurements directly in the urine. A diffuse screening of prostate cancer requires easy and fast methodologies which point to minimize sample manipulations, number of reagents and costs. An important step in this direction could be the development of an interactive surface akin to DNA chips, able to perform the recognition process directly in biological fluids.

In chemical terms, the preparation of a sarcosine detection chip requires: (i) the design of a receptor capable to bind exclusively N-methylated amino acids in the presence of overwhelming amounts of amino acids plus many other metabolites in urine (ii) the grafting of this receptor on a suitable solid surface, retaining the molecular recognition properties at the solid-liquid interface. In this context, in this thesis, I focused on a comprehensive investigation of the molecular recognition

properties of a phosphonate cavitand-functionalized silicon surface toward glycine and sarcosine in water and urine.

2.1.2 Hierarchical Self-Assembly of luminescent systems

The design and synthesis of functional material are of current interest in chemistry and nanoscience.[18,19] In particular, self-assembled hybrid materials[20-22], held together by different kinds of noncovalent interactions , are particularly intriguing because they lead to adaptive materials,[23] characterized by switchable functions. The resulting complexity of these hybrid materials requires implementing combinations of two or more different interaction modes, among which hydrogen bonding, host-guest complexation, and metal-ligand coordination.

The use of luminescence to investigate the properties and functions of supramolecular assemblies has been extensively employed due to its non-invasive nature, fast response time and high sensitivity.[24] Luminescence spectroscopy has been finding applications in fields of great impact from a social and economic point of view, such as medical diagnostics and imaging, environmental sciences, and molecular electronics. In this context, luminescence spectroscopy has proved to be a very powerful technique when it is necessary to monitor molecular recognition events in cells or on surfaces, because of its submicron visualization and submillisecond temporal resolution. Furthermore, one can take advantage of the variety of possible ways of modulating the photophysical properties of a chromophore. Starting from this premise, we designed a set of molecules (Figure 2.2.1) featuring one or two binding motifs, to use as “switching modules” to control the self-assembly process in the multistep growth of supramolecular structures on silicon.

2.2 General procedures

2.2.1 Synthesis of Tiiii, TSiiii, ammonium salts and lanthanide complexes

The synthesis of cavitands and methylated guests was carried out at University of Parma by the group of Professor Enrico Dalcanale and was synthesized following a published procedure (Figure 2.2.1).[12]

The Yttrium complex was purchased by Sigma-Aldrich and Europium complex was synthesized at University of Warszawa.

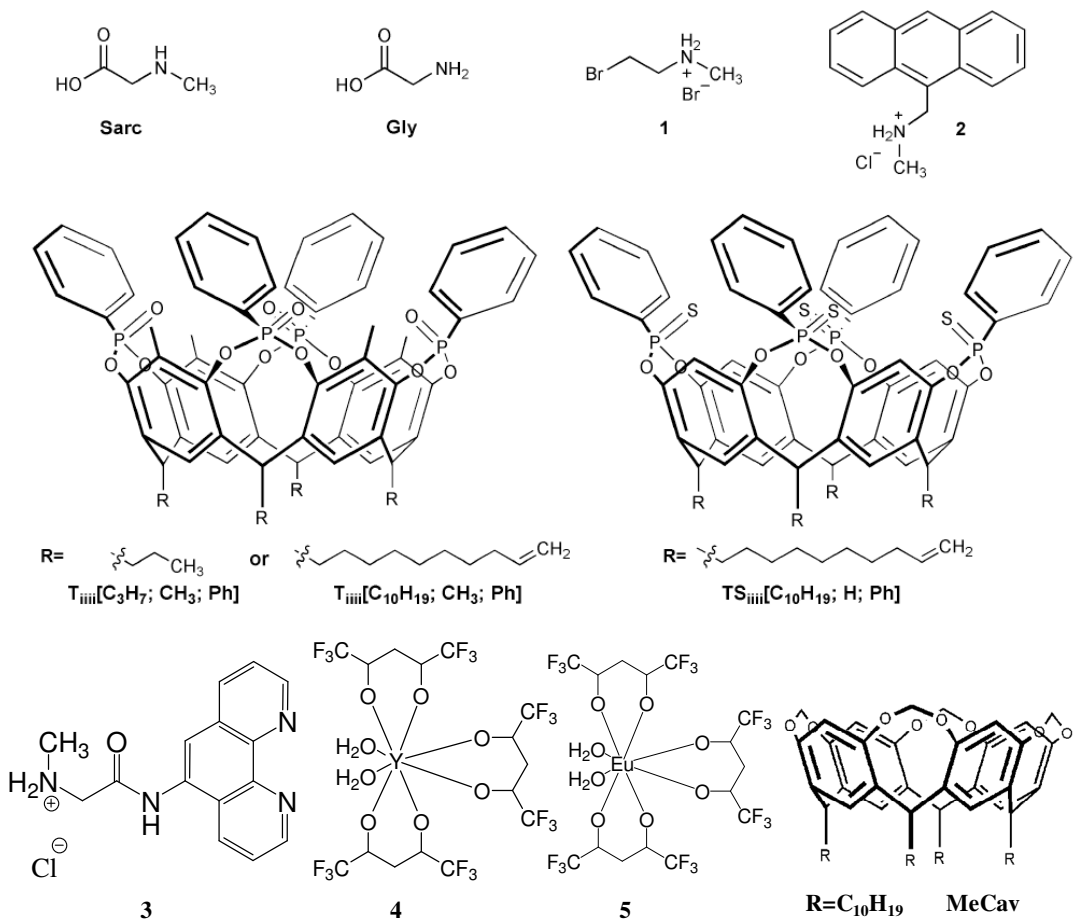

Figure 2.2.1: Chemical structure of guests and cavitands. The short chain footed **Tiiii[C_3H_7, CH_3, Ph**] cavitand was used for solid state and solution experiments. The double bond-terminated long chain footed **Tiiii[$C_{10}H_{19}$, CH_3, Ph] TSiiii[$C_{10}H_{19}$, H, Ph]** and **MeCav** cavitands were grafted on silicon wafers.

2.2.2 Synthesis of Tiiii

To a solution of resorcinarene[25] (1g, 0.91mmol) in freshly distilled pyridine (10 mL) dichlorophenylphosphine (0.504 mL, 3.72 mmol) was added slowly, at room temperature. After 3 hours of stirring at 80 °C, the solution was allowed to cool at

room temperature and 4mL of 35% H_2O_2 was added. The resulting mixture was stirred for 30 min at room temperature, then the solvent was removed under reduced pressure and water added. The precipitate obtained in this way was collected by vacuum filtration, and profusely rinsed with diethyl ether to give the product in a quantitative yield.

2.2.3 Preparation of Tiiii-grafted Si surface (Si-Tiiii)

For grafting monolayers, a Tiiii/1-octene mixture (χ_{cav} = 0.05) were dissolved in mesitylene (solution concentration = 50mM), the use of the 1-octene spacer improves the passivation of the silicon surface, thus minimizing the substrate oxidation after aging.[12] Cavitand solutions (2.0 mL) were placed in a quartz cell and deoxygenated by stirring in a dry box for at least 1 h. A Si(100) substrate was dipped in H_2SO_4/H_2O_2 (3:1) solution for 12 min to remove organic contaminants, then it was etched in a hydrofluoric acid solution (1% v/v) for 90 s and quickly rinsed with water. The resulting hydrogenated silicon substrate was immediately placed in the mesitylene solution. The cell remained under UV irradiation (254 nm) for two hours. The sample was then removed from the solution and sonicated in dichloromethane for 10 min to remove residual physisorbed material.

2.2.4 Monolayer Characterization

XPS spectra were run with a PHI 5600 multi-technique ESCA-Auger spectrometer equipped with a monochromated Al *K*α X-ray source. Analyses were carried out with a photoelectron angle of 45° (relative to the sample surface) with an acceptance angle of ± 7°. The XPS binding energy (B.E) scale was calibrated by centering the C 1s peak due to hydrocarbon moieties and “adventitious” carbon at 285.0 eV.[26]

2.3 Molecular recognition of sarcosine in urine

In this paragraph it is reported a comprehensive investigation of the molecular recognition properties of a silicon surface decorated with phosphonate cavitands (Figure 2.2.1) toward glycine and sarcosine in water and urine. The entire complexation process has been investigated in the solid state, in solution and at the solid-liquid interface in order to determine and weight all the factors responsible of the observed specificity. The final outcome is a Si-based active surface capable of binding exclusively sarcosine and other N-methylated amino acids in a biological fluid like urine.

2.3.1 Sarcosine complexation in the solid state

At first, the crystal structures of the complexes formed by tetraphosphonate cavitand **Tiiii[C_3H_7, CH_3, Ph]**[27,28], with glycine and sarcosine hydrochlorides were solved to define and compare type, number and geometry of host-guest interactions present in the solid state in the two cases. Suitable crystals of both complexes were obtained under the same conditions, i.e. via slow evaporation of a methanol/water solution containing the host in the presence of an excess of guest. The complex **Tiiii•glycine methyl ester hydrochloride** (the use of glycine hydrochloride led to non-diffracting crystals) features a molecule of methanol into the cavity and the protonated amino acid methyl ester perching on top of the cavity (Figure 2.3.1 a). The affinity of this class of cavitands towards methanol has been previously reported,[11] and also in this case the alcohol is stabilized within the cavity by an hydrogen bond with one P=O group at the upper rim and by two CH_3-π interactions between two methyl hydrogens of the guest and two aromatic rings of the host.[11] The methanol results thus preferred by the cavitand with respect to glycine methyl

ester hydrochloride, which could be expected to interact through dipolar interactions between the P=O groups and the positively charged nitrogen atom. But, while the methanol can exploit the synergistic effect of both CH-π interactions and hydrogen bonding, this is not the case for glycine methyl ester hydrochloride**,** whose interaction with the cavity is mediated by the solvent. The NH_3^+ group of the amino acid forms a network of hydrogen bonds both with the methanol hosted inside the cavity and with the three lattice water molecules.

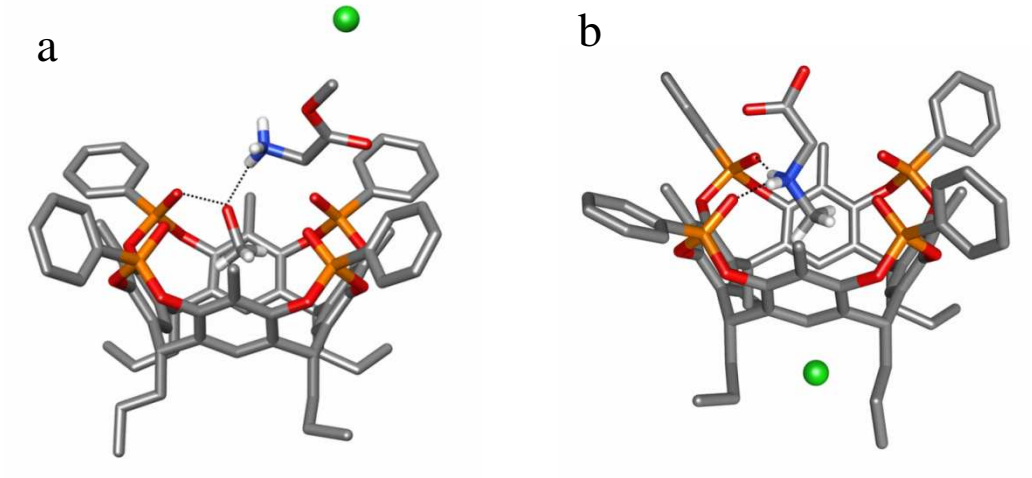

Figure 2.3.1: Crystal structures of complexes Tiiii•glycine methyl ester hydrochloride (a) and Tiiii•sarcosine hydrochloride (b). Grey, C; red, O; orange, P; blue, N; green, Cl; white, H. For clarity, the H atoms of the cavitand and those not involved in complexation of the guests have been omitted.

The situation is completely different for the complex **Tiiii•sarcosine hydrochloride** (Figure 2.3.1 b): In this case, all three interaction modes with the guest described in the introduction are activated. Sarcosine enters the cavity with its methyl group forming two CH-π interactions with two aromatic rings of the host. The complex is further stabilized by two hydrogen bonds involving the

positively charged NH_2 moiety and two adjacent P=O groups. Methanol does not interact with the cavity even if it is present in the crystal lattice. The chloride ion is located among the four alkyl chains at the lower rim of the cavitand, separated by a distance of 7.136Å[29] from the positive nitrogen atom, forming C-H···Cl^- interactions with the four α CH_2 residues.

The different behaviour of the two guests towards the cavitand can be attributed to the presence of the methyl residue on the nitrogen in the sarcosine. Its interaction with the cavity triggers the formation of the two H-bonds and the inset of cation-dipole interactions, which further stabilize the complex. Therefore, sarcosine is preferred over methanol for cavity inclusion.

DFT calculations have been performed to estimate the energetic differences between **Tiiii•sarcosine** and **Tiiii•glycine** complexes, since the theoretical model allows to exclude the effects due to the presence of specific solvents. The stabilization introduced by the additional CH_3-π interaction has been evaluated in 3.8 kcal mol^{-1}. In both cases, the formation of H-bonds between NH_2 groups and P=O apical fragments is pointed out by the elongations of the P=O bonds with respects to the non interacting $\mathbf{T_{iiii}}$ (Δ= +0.02 Å) and the parallel elongation of the N-H bond with respect to the non interacting guest (Δ= +0.02 Å). Regarding the ***T*$_{iiii}$ •sarcosine** adduct, the distance between the C atom of the sarcosine N-methyl group and one benzene centroid ($Be_{centroid}$) of the cavitand (3.65 Å) as well as the C-H•••$Be_{centroid}$ angle (138.5°) are compatible with a CH-π interaction.[30] Being this interaction absent in the ***T*$_{iiii}$ •glycine** adduct, the difference in energy stabilization between $\mathbf{T_{iiii}}$ **•glycine** and $\mathbf{T_{iiii}}$ **•sarcosine** complexes arises mainly from the CH-π interaction.

2.3.2 Sarcosine complexation in solution

Next, we examined the complexation properties of **Tiiii** in solution. The K_{ass} of **Tiiii** and sarcosine methyl ester hydrochloride was determined in methanol at 303 K via Isothermal Titration Calorimetry (ITC). The direct comparison between glycine and sarcosine was not possible since glycine is insoluble in methanol. The determination of the thermodynamic data from the ITC curves requires the knowledge of the binding stoichiometry of the formed complexes. In our case, the Job's plot provided clear evidence of 1:1 binding in methanol solution. For sarcosine methyl ester hydrochloride a K_{ass} of $6.8\pm0.5 \times 10^4$ M^{-1} was obtained. Interestingly, the thermodynamic profile showed that the enthalpic (-14.5 KJ mol^{-1}) and entropic contributions (13.5 KJ mol^{-1} at 303 K) to the binding are comparable. This large, positive entropic component underlines the importance of desolvation of both host and guest in the binding process. By comparison, the interaction of glycine methyl ester hydrochloride with **Tiiii** in methanol was too low to be measured by ITC. Therefore the ITC measurements reinforce the crystal structure determinations in supporting the preferential cavity inclusion of sarcosine in polar solvents.

The ability of **Tiiii** to extract the two amino acids from water was studied via ^{31}P and ^{1}H NMR in a water/chloroform biphasic system in collaboration with Parma University. The downfield shift of P=O signals is a clear indication of the participation of phosphonates in the guest complexation, while the upfield shift of the methyl residue is diagnostic of N-CH_3 inclusion into the cavity[9]. An aqueous solution of glycine or sarcosine was added to a NMR tube containing the biphasic system, in which the water insoluble **Tiiii** is confined in the organic phase. In water both amino acids are in their zwitterionic form. In the case of sarcosine the ^{31}P resonance of the four P=O groups moved downfield of 3.5 ppm (from 67.6 to 10.1 ppm, Figure 2.3.2 a) and the ^{1}H resonance of the N-CH_3 moiety moved upfield to -

0.5 ppm. Under the same conditions glycine produced no detectable variation in the P=O chemical shift (Figure 2.3.2 b). This experiment proves that water does not hamper the ability of **Tiiii** to bind sarcosine, while it completely shuts down glycine uptake. This result can be rationalized by recalling that CH-π interactions, like the ones present between sarcosine and **Tiiii**, are dispersive in nature, therefore unaffected by the presence of water[31]. On the contrary, glycine complexation is suppressed in water, being water a competitive solvent in exohedral **Tiiii** H-bonding[32]. The final outcome of these two offbeat trends is a boost to sarcosine versus glycine selectivity in water.

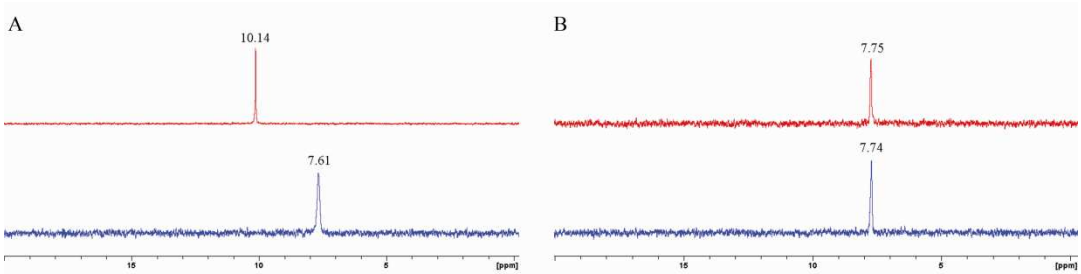

Figure 2.3.2: Sarcosine versus glycine complexation at the chloroform-water interface. A ^{31}P NMR spectrum of **Tiiii** before (below) and after (above) addition of sarcosine to the water phase. **B** ^{31}P NMR spectrum of **Tiiii** before (below) and after (above) addition of glycine to the water phase.

In a separate experiment, addition of solid sarcosine to a chloroform solution of **Tiiii,** where sarcosine is insoluble and not zwitterionic if taken into solution, did not lead to complexation. When, instead, solid sarcosine hydrochloride was added, **Tiiii** was able to complex it efficiently and dissolve it. Therefore, **Tiiii** is capable of binding sarcosine both in the protonated and zwitterionic forms, through interaction with the $^{+}NH_2$-CH_3 moiety. The acid component does not interfere with complexation either in the anionic or protonated form. This set of experiments

qualifies **Tiiii** as promising receptor for the diagnostics of sarcosine in biological fluids.

2.3.3 Sarcosine complexation at the solid-water interface

Silicon wafers grafted respectively with **Tiiii[$C_{10}H_{19}$, CH_3, Ph]** and its complexation inactive but structurally related thiophosphonate analogue **TSiiii[$C_{10}H_{19}$, H, Ph]** were prepared via photochemical hydrosilylation of the double bonds on H-terminated Si(100) surfaces.[11] The reaction leads to the formation of strong, hydrolytically stable Si-C bonds, capable to withstand the exposure to water and biological fluids in a wide range of pH. To maximize surface passivation, mixed monolayers constituted by **Tiiii**/1-octene and **TSiiii**/1-octene were prepared. The use of cavitand/1-octene mixture allows the anchoring of a denser layer in which the octyl chains cover the voids left under the cavitand heads and between cavitands, thus preventing silicon oxidation.[33] The four methyl groups in the apical position of **Tiiii[$C_{10}H_{19}$, CH_3, Ph]** were introduced to enhance CH_3-π interactions with the guests with respect to its protio analogue **Tiiii[$C_{10}H_{19}$, H, Ph]**[12,34], as indicated by DFT calculations (0.5 Kcal/mole energy gain by DFT calculations).

Initially the complexation properties of **Tiiii-Si** surface were tested in water adopting the bromine-marked methyl-ammonium guest **1** (see Figure 2.2.1) as probe. As control experiment to rule out physisorption phenomena, the complexation-inactive **TSiiii-Si** surface was similarly treated with guest **1** in water. In particular **Tiiii-Si** surface was dipped in a 1 mM aqueous solution of guests **1** for 30 min and then the wafer was sonicated in CH_3CN for 10 min to remove any physisorbed material. Sarcosine recognition was carried out dipping **Tiiii-Si•1** wafers in a 1 mM sarcosine solution in water at pH = 0.7 for 10 min. As blank experiment, **Tiiii-Si•1** wafers were dipped in a 1 mM glycine solution in water at

pH = 0.7 for 10 min. All experiments have been repeated three times for consistency, without significant differences.

Initially, the complexation properties of the **Tiiii-Si** surface were tested in water XPS analysis shows that the Br atoms were detected only on the active **Tiiii-Si** surface, whereas the XPS spectra of the inactive **TSiiii-Si** surface did not show any Br signal. Since the atomic ratio between Br and P for a 1:1 complex is 1/4 the yield of the complexation can be calculated as follows:

$$\text{Yield of complexation } \% = \frac{\%Br}{\%P} \Big/ \frac{1}{4} \times 100 \qquad (1)$$

The complexation yield was estimated in the range 50- 60%.

Since sarcosine is bound by **Tiiii** in its N-protonated form, the stability of the **Tiiii-Si•1** surface complexes in water was studied as function of pH (Table 2.3.1). No Br signal was evident in the Br 3d XPS region of **Tiiii-Si•1** surface after dipping it for 10 min in water in the pH range 1-7, thus indicating the removal of **1** upon deprotonation. Below pH=1, the XPS Br 3d signal retain a comparable intensity before and after water dipping, proving the **Tiiii-Si•1** stability at that pH. The unexpected need to acidify the solution at very low pH to avoid guest deprotonation can be rationalized by recalling two surface effects: i) the apparent pKa of surface groups,[35] and in particular of surface bound amines (pKa ~ 4)[36] are much lower than their intrinsic value in solution (pKa~10); ii) the protonation/deprotonation equilibrium is strongly driven towards deprotonation since the free amines diffuse from the surface to the solution, while the protonated ones remain bound to the surface receptors.

Table 2.3.1: Br/P atomic concentration ratio from XPS data and complexation yield calculated from eq. 1 as a function of pH.

	Br/P	Yield of complexation (%)
Before water dipping		
as-prepared	0.13	54
After water Dipping		
pH 7-1	<0.02	-
pH 0.7	0.14	56
pH 0	0.13	54

Then, the exchange reaction between sarcosine/glycine and **Tiiii-Si•1** was monitored by XPS to test the selectivity of **Tiiii-Si** surface toward N-methylated amino acids. Two **Tiiii-Si•1** wafers were exposed to water solutions of sarcosine and glycine respectively. Both solutions were at the same concentration (1 mM) and pH (0.7). XPS analyses performed on the two surfaces after the treatment showed that the Br signal disappeared only in the wafer dipped in the sarcosine solution (Figure 2.3.3). Sarcosine completely replaced guest **1** on the **Tiiii-Si** surface, while glycine was totally ineffective. Therefore, the behaviour of **Tiiii** at the silicon-water interface is consistent with its conduct at the organic-water interface.

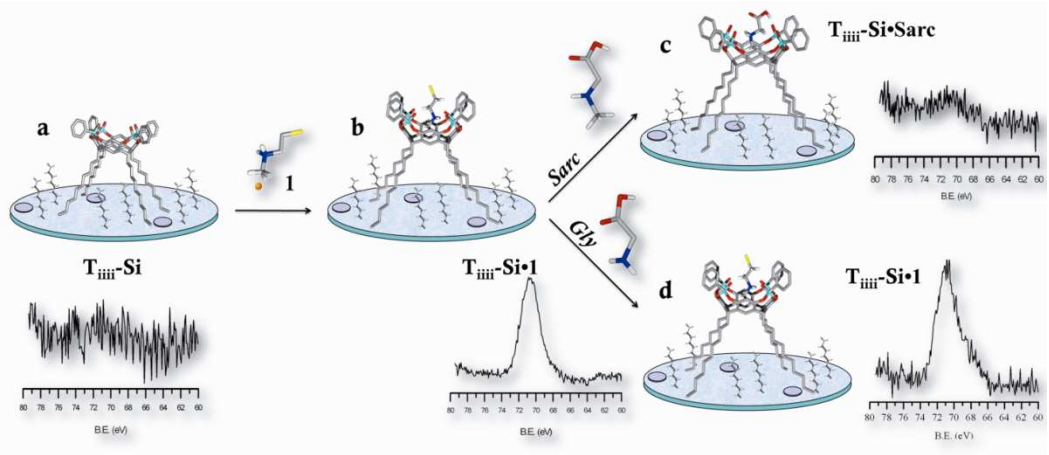

Figure 2.3.3: XPS analysis of Br 3d region along all steps of the sarcosine recognition protocol in water. a, pristine **Tiiii-Si** wafer and its XPS spectrum. **b**, **Tiiii-Si•1** and its XPS spectrum after exposure of the wafer to a water solution of **1**. **c**, **Tiiii-Si•Sarc** and its XPS spectrum after exposure to a water solution of sarcosine. **d**, **Tiiii-Si•1** and its XPS spectrum after exposure of the wafer to a water solution of glycine.

2.3.4 Sarcosine detection in urine

The procedure based on the surface exchange reaction was adopted to identify sarcosine directly in urine. In particular individual human urine samples (15 mL) were loaded onto 15-ml Vivaspin filters with a molecular weight cutoff of 3,000 DA and centrifuged at 8,000 x *g* at 15°C and then the urine was acidified at pH 0.7. For XPS detection, the urine sample was divided in two portions and to one of them solid sarcosine was added up simulate its biological occurrence due to prostatic cancer. **Tiiii-Si•1** wafers were dipped in both urine samples for 10 min, washed in water at pH = 0.7 for 1 min and analyzed by XPS. Addition of sarcosine to urine before filtration led to the same results.

The **Tiiii-Si•1** wafers were exposed to the two urine samples and then analyzed via XPS to verify the presence of complexed guest **1** on the surface through its diagnostic Br 3d signal (Figure 2.3.4). The sarcosine laced urine removed **1** from the surface, while the untreated one did not. None of the potential ionic interferents present in urine (protonated amino acids, NH_4^+, Na^+, K^+, Mg^{2+} and Ca^{2+} just to mention the major ones) has sufficient affinity for the cavity to replace N-methyl ammonium salts. The resulting exquisite selectivity demonstrate by **Tiiii-Si** is unprecedented for a synthetic receptor operating at interfaces.

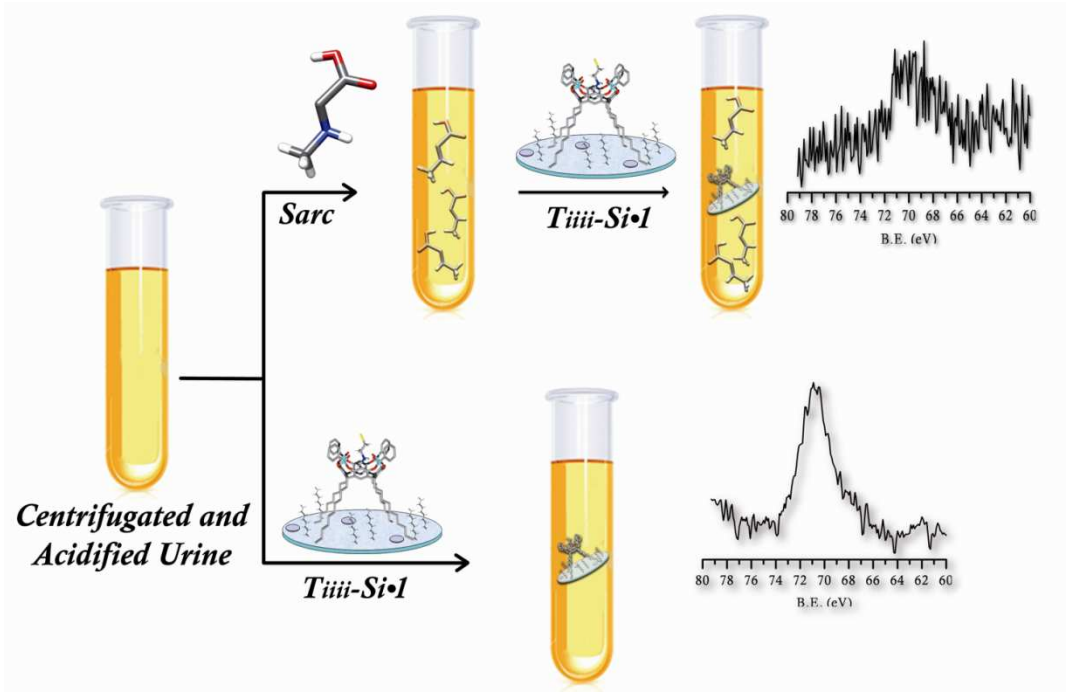

Figure 2.3.4: Scheme of the detection procedure of sarcosine in human urine: after filtration, centrifugation and acidification, the urine sample was divided into two portions. One portion (control sample) was tested with **Si-Tiiii-1** (lower scheme), the other portion was added with sarcosine before testing with **Si-Tiiii-1** (upper scheme)**.** The XPS P 2p spectra of **Si-Tiiii-1** slides dipped in the control sample and the in sarcosine-added sample are reported sideways.

A fluorescence-based detection mode was then developed to prove the potential of **Tiiii-Si** as active surface for sarcosine detection with optical devices. Sarcosine presence in urine was monitored via fluorescence dye displacement[37], using (9-anthrylmethyl)methyl ammonium chloride **2** as indicator dye[38]. **Tiiii-Si** wafers complexed with guest **2 (Tiiii-Si•2)** were prepared by dipping of **Tiiii- Si** surface in a 5 mM ethanol solution of guests **2** for 1h min. Then the wafer was sonicated in water at pH = 0.7 for 5 min. **2** binds efficiently to **Tiiii-Si** retaining its fluorescence, and it can be replaced only by molecules with comparable affinity for the cavity (sarcosine in our case). **Tiiii-Si•2** wafers were exposed to three portions of human urine sample treated as above described, two of them laced with sarcosine (1 mM and 0.1 mM respectively). The wafers were then analyzed via fluorescence spectroscopy to detect the presence of residual complexed guest **2** on the surface through its diagnostic fluorescence signal (Figure 2.3.5). The fluorescence results confirmed the XPS experiments since both sarcosine added samples displaced fluorescence guest (traces c and d) while the untreated one did not (trace b). Results also indicated that guest **2** displacement depends on sarcosine concentration since a residual fluorescence signal was observed for sample exposed to the urine with lower sarcosine content (0.1 mM).

All experiments have been repeated three times for consistency, without significant differences.

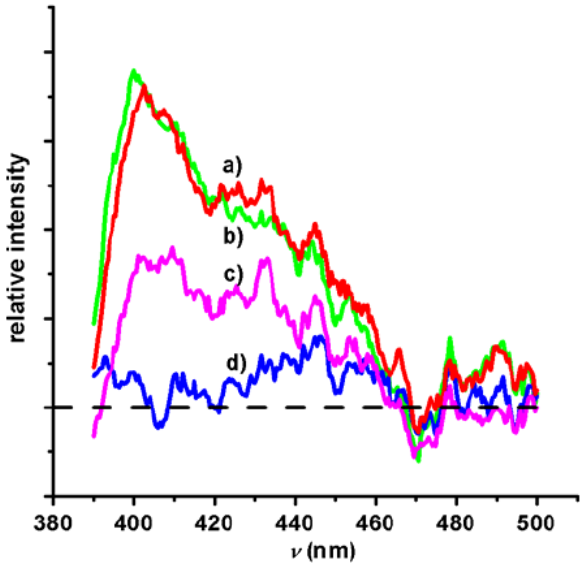

Figure 2.3.5: Luminescence spectra of **Tiiii-Si•2**: (a) before urine exposure (red line). (b) after dipping for 5 min in urine (green line). (c) after dipping in 0.1 mM sarcosine-added urine (magenta line). (d) after dipping in 1 mM sarcosine added urine (blue line). **Tiiii-Si** spectrum was subtracted to all signals. Excitation wavelength λ_{ex} = 340 nm.

2.3.5 Conclusions

In conclusion a new, highly innovative active surface for the specific recognition of sarcosine in water and urine using tetraphosphonate cavitand **Tiiii** as receptor has been prepared. At the molecular level, the recognition process has been dissected in its three interaction modes and investigated in the solid state, in solution and at the solid-liquid interface. In aqueous environment, the enhanced role played by the CH_3-π interactions leads to complete selectivity toward sarcosine versus glycine. The energy stabilization due to the CH_3-π interactions of sarcosine with the cavity has been estimated in 3.8 kcal/mole from DFT calculations.

The complexation properties of **Tiiii** have been transferred to Si wafers with high fidelity and the exquisite ability of **Tiiii-Si** to specifically detect sarcosine has been extended to urine, where several potential interferents are present. Complementary XPS and fluorescence guest displacements tests have demonstrated the selectivity of **Tiiii-Si** under these stringent conditions. In particular, the fluorescence detection mode represents a fundamental requirement for the prospective application of these materials in devices for biomedical diagnostics. These results allow us to envision the use of the **Tiiii-Si** surface for the specific detection of sarcosine as a marker of the aggressive forms of prostate tumor. Although the present fluorescence dye displacement approach is not yet suitable for sensing sarcosine at the low biological concentrations ($1\text{-}4x10^{-5}$ M)[16], obtained result indicate that this approach can lead to important steps in this direction. Moreover, given the wide variety of biologically relevant compounds presenting *N-CH3* groups (drugs, neurotransmitters, painkillers, antidepressants, etc.), the use of **Tiiii** cavitands can be extended to the detection of such compounds.

2.4 Hierarchical assembly of Lanthanide Complex through molecular recognition

In this chapter we report a precise and reversible hierarchical assembly on silicon functionalized with phosphonate cavitands (Tiiii), using a sequence of host-guest interactions and metal-ligand coordination. As a guest, it was synthesized compound **3**, which has a sarcosine (N-methylammonium) unit as recognition moiety connected to a phenanthroline ligand, able to antenna effect, via an amino linkage. As luminescent probe, an europium diketonate complex (**5)** was used. To

demonstrate the luminescence properties of surface, an yttrium compound (**4**), with a same structure of the europium complex was used.

In particular, the Tiiii molecular recognition properties toward phenanthroline ligand and the formation of a self-assembly between Europium (or Yttrium) complex and a sensitizing antenna (Figure 2.2.1) were demonstrated. The analogous not-active methyl-bridged cavitand (MeCav) has been grafted on silicon as not-active reference monolayer (Figure 2.2.1).

The entire process has been fully tested and characterized in solution, and then successfully transferred to the solid state and the protocol of complexation was monitoring via XPS spectroscopy and fluorescence spectroscopy.

2.4.1 XPS characterization

Hierarchical silicon anchoring of metal complexes was performed through a three step approach consisting on i) grafting of mixed Tiiii/octene (χ=0.05) monolayers by photochemical hydrosilylation, ii) guest **3** binding in the Tiiii cavity and finally, iii) **4** or **5** β-diketonate complexation with phenanthroline moiety of guest **3**. The anchoring sequence is summarized in the figure 2.4.1.

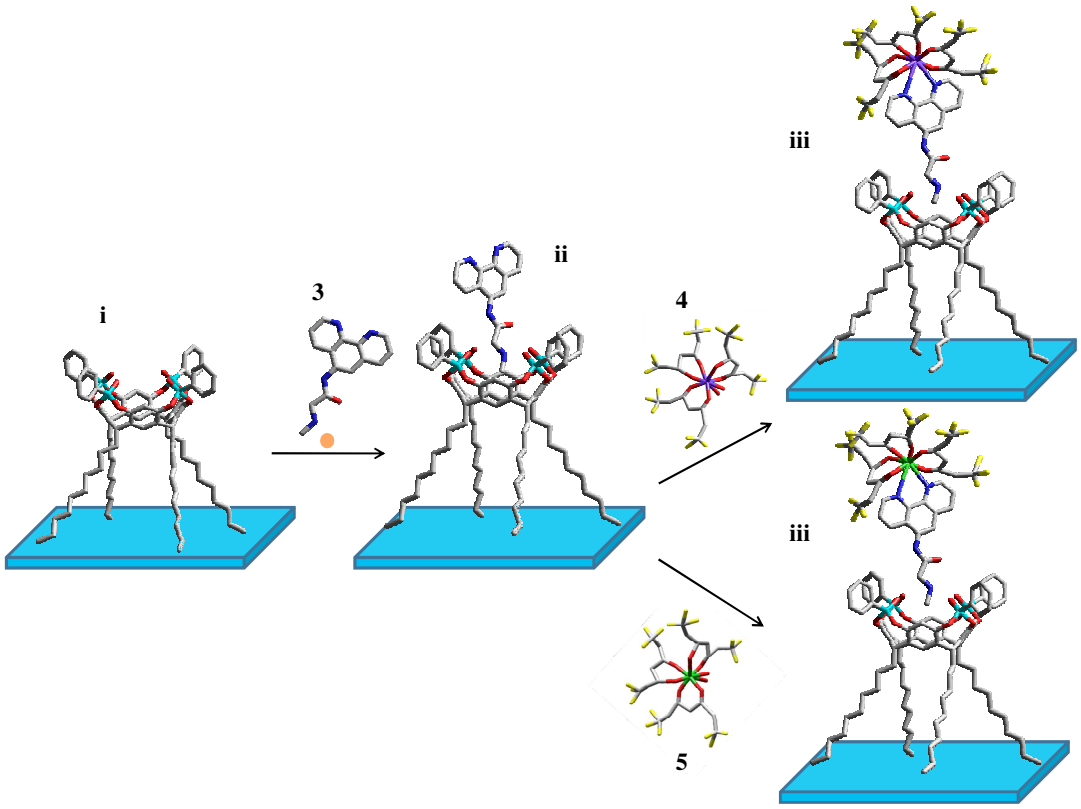

Figure 2.4.1: Hierarchical silicon anchoring of metal complexes through a three step approach consisting on i) grafting of mixed Tiiii/octene (χ=0.05) monolayers by photochemical hydrosilylation, ii) guest **3** binding in the Tiiii cavity and iii) **4** or **5** β-diketonate complexation with phenanthroline moiety of guest **3**.

Each step of the hierarchical β-diketonate assembly has been evaluated by XPS measurements.

Table 2.4.1 compares XPS determined elemental composition of (a) mixed (χ=0.05) **Tiiii/Oct** monolayer (**Si-Tiiii**) (b) **Si-Tiiii** complexed with guest **3** (**Tiiii-Si•3**) (c) **Tiiii-Si•3** self assembly with complex **4** (**Tiiii-Si•3•4**) (d) **Tiiii-Si•3** self

assembly with complex **5** (**Tiiii-Si•3•5**) (e) **Si-Tiiii** capped with complex **4** (**Tiiii-Si•4**) (f) **Si-Tiiii** capped with complex **5** (**Tiiii-Si•5**) (g) decomplexation test of **Tiiii-Si•4** with guest **1**.

	P 2p	P 2s	Si 2p	O 1s	C 1s	N 1s	F 1s	Eu 3d	Y 3d	Br 3d
Tiiii-Si	1.15	-	16.26	31.02	49.98	0.8	0.8	-	-	-
Tiiii-Si•1	1.17	-	13.31	22.44	61.32	0.9	0.8	-	-	-
Tiiii-Si•1•2	1.1	-	7.89	29.52	51.03	0.76	9.5	-	0.6	-
Tiiii-Si•1•3	-	1.12	14.47	28.12	46.5	0.75	5.2	0.4	-	-
Tiiii-Si•2	1.03	-	10.24	19.96	66.2	0.59	1.3	-	0.3	-
Tiiii-Si•3	-	1.09	12.87	29.13	53.84	0.6	1.2	0.2	-	-
Tiiii-Si•2•4	1.1	-	12.78	23.55	61.03	0.54	0.27	-	-	0.1

Table 2.4.1: (a) mixed (χ=0.05) **Tiiii/Oct** monolayer (**Si-Tiiii**) (b) **Si-Tiiii** complexed with guest **3** (**Tiiii-Si•3**) (c) **Tiiii-Si•3** self assembly with complex **4** (**Tiiii-Si•3•4**) (d) **Tiiii-Si•3** self assembly with complex **5** (**Tiiii-Si•3•5**) (e) **Si-Tiiii** capped with complex **4** (**Tiiii-Si•4**) (f) **Si-Tiiii** capped with complex **5** (**Tiiii-Si•5**) (g) decomplexation test of **Tiiii-Si•4** with guest **1** (**Tiiii-Si•1**).

The complexation of **Tiiii-Si** with guest **3** was performed in a solution 10^{-3} M of guest **3** in CH_3OH for 60 min and after sonicated in CH_3OH for 5 minutes. Table 2.4.1 show a slight increases of N 1s quantity in **Tiiii-Si•3** samples compared to **Si-Tiiii** surface. However this increment is low due to the presence of adventicious ammonia groups inside the cavity before **3** treatment. However, the indication of the success of complexation can be obtained by considering the high resolution band of N 1s XPS region (figure 2.4.2). In fact, the band consists of two components: i) a main component at 400.0 eV assigned to phenanthroline nitrogens and aminic nitrogen (N_{lig}), and ii) a less intense component at 402.0 eV assigned to

the protonated nitrogen of sarcosine(N_{sar}). The observed intensity ratio N_{lig} /N_{sar} is about 3:1 as expected from molecular structure.

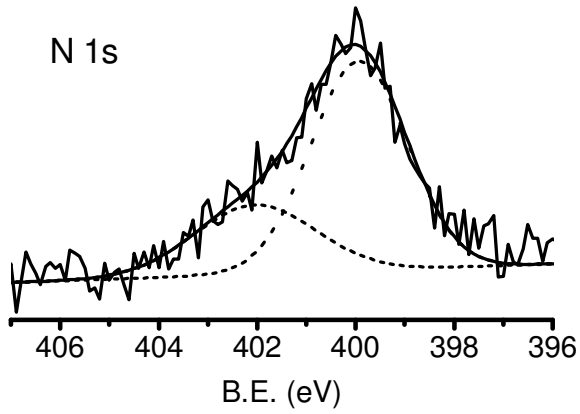

Figure 2.4.2: N 1s XPS region of **Tiiii-Si•3**.

The **Tiiii-Si•3** surface was processed respectively with **4** and **5** complexes.

The metal-coordination reactions was performed by dipping cavitand decorated surfaces (**Si-Tiiii**) in solutions of complexes **4** and **5** respectively, 10^{-3} M in THF for 30 min and after sonicated in THF for 5 minutes. Complexation of guest **1** was performed in solution 10^{-3} M in CH_3CN for 30 min and after sonicated in CH_3CN for 5 min.

The presence of metal XPS bands (Figure 2.4.3) together with an evident enhancement of the F 1s signal demonstrates metal-coordination by guest **3**. The Eu 3d XPS region shows the characteristic doublet of Eu $3d_{5/2}$- Eu $3d_{3/2}$ centered respectively at 1164.8 eV and 1135.1 eV, consistent with the presence of EuIII in the coordination environment with phenanthroline. In addition a low intensity doublet is observed at 1155.1eV and 1121.1eV, suggesting the presence of Eu in a reduced oxidation state. The relative intensity of these bands (with respect to the main doublet) is low after short acquisition time and it increases for longer

acquisitions. These bands are due to the reduction of europium ion induced by X-rays exposure. Therefore long acquisitions (hence prolonged exposure to X-rays) determines the appearance of two new bands, as shown in figure 2.4.3 a.

The Y $3d_{5/2}$ – Y $3d_{3/2}$ peaks (2.4.3 b) appear respectively at 158.8 eV and 160.6 eV, consistent with the presence of Y(III) coordinated with guest **3**.

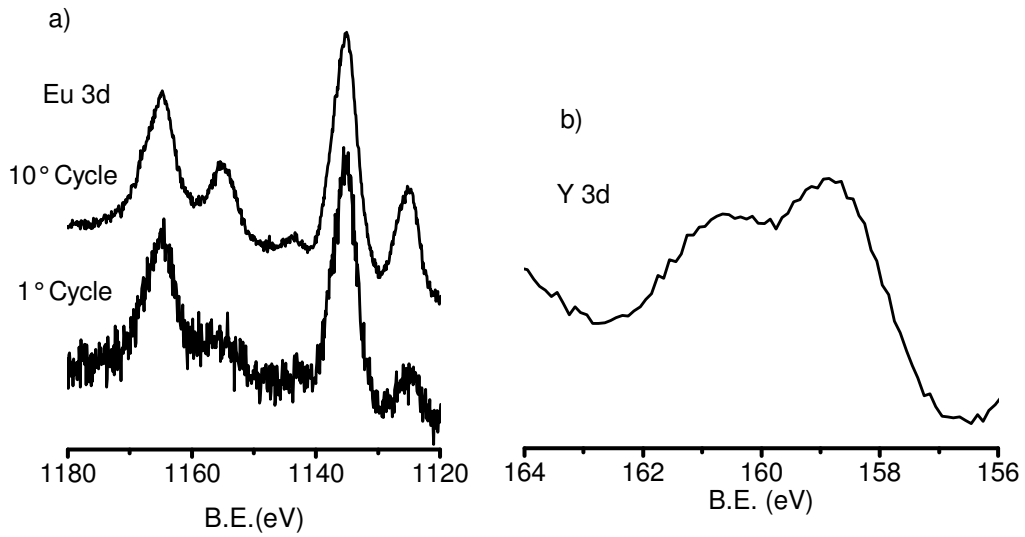

Figure 2.4.3: a) Eu 3d XPS region for **Tiiii-Si•3•5** and b) Y 3d XPS region for **Tiiii-Si•3•4**.

Note, however, that the atomic ratio (Eu/N/F) is richer in fluorine and Europium than the expected value from theoretical formula. This behavior can be explained assuming that the coordination with metal complexes occurs directly with some cavities without phenanthroline. In this case, the complexes could lose one or more β-diketonate ligands leading to a different coordinated environment for EuIII and YIII. To investigate this possible side reaction pathways, some experiments have been performed in which **Tiiii-Si** surfaces without guest **3** were treated with complexes **4** and **5**. The data shown in table 2.4.1, indicate that the Tiiii cavity interacts with complex **4** or **5** also in absence of guest **3**, even though the fluorine

and metals amounts are much lower than in the case of **Tiiii-Si•3•4** and **Tiiii-Si•3•5**.

To demonstrate that the complexation of metal diketonates on **Tiiii-Si** surface occurs in the Tiiii cavity a set of experiments have been specifically designed. First to ruled out the possibility of physisorption, a control surface with the structurally related, but complexation inactive MeCav, have been prepared and treated with **3** guest or **4** and **5** complexes. After treatment, XPS analysis of the surface did not show the presence of nitrogen, europium or yttrium, thus indicating that physisorption does not occur.

Moreover, it was proved the reversibility of the complexation process between **Tiiii•Si** and metal diketonates **4** and **5** by performing cyclic guest exchange between **4** and guest **3**. XPS measurements were used to monitor the cyclic exchange, by tracking the presence of the yttrium complex **4** and the bromine marked guest **1**.

Tiiii-Si•4 surface, which was taken as the starting point of the cycle; shows a signal in the Y 3d region (as described above) and, obviously, no signal in the Br 3d region (Figure 2.4.4 a). After treatment of **Tiiiii-Si•4** with a solution of guest **1** (10^{-3} M in CH_3CN), a negligible signal is present in the Y 3d region, while the Br 3d region presents an evident Br 3d signal (Figure 2.4.4 b).

Treatment of the **Tiiii-Si•1** surface with a hindered Brønsted base (such as 1,8-diazabicyclo[5.4.0]undec-7-ene, DBU; 10^{-3} M in CH_3CN), led to complete removal of guest **1** from the surface, as demonstrated by the absence of both elements signatures in Y 3d and Br 3d regions (Figure 2.4.4 c).

DBU, by extracting a proton from guest **1**, induces the dissociation of the **Tiiii-Si•1** complex, restoring the pristine **Tiiii-Si** surface. The finding that the surface bonding is reversible.

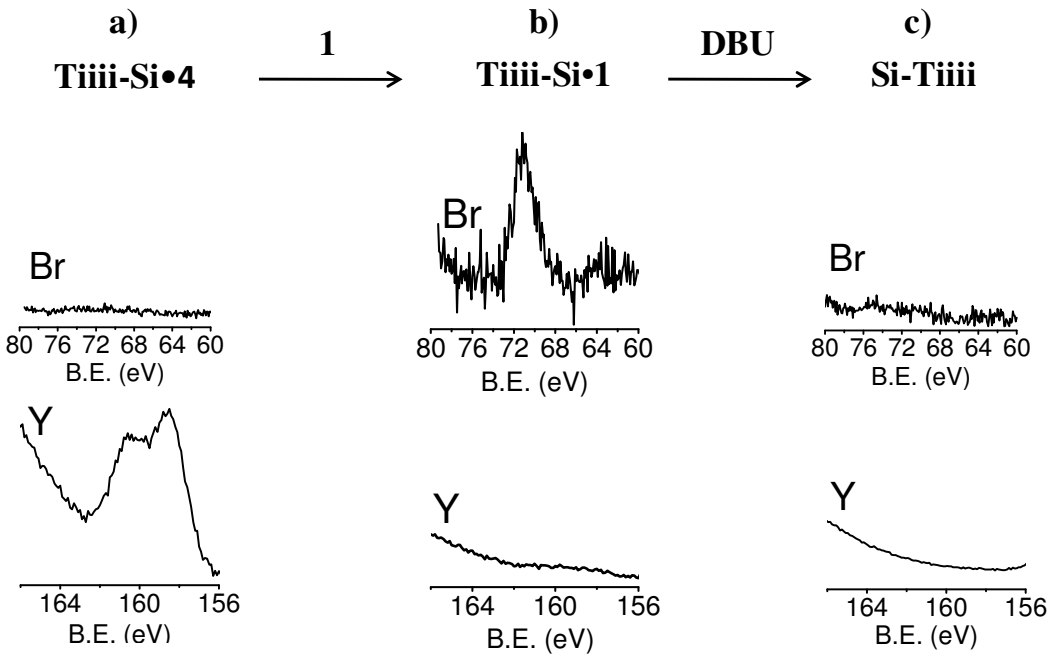

Figure 2.4.4: Y 3d and Br 3d XPS region after treatment of the Tiiii surface with a) a solution of guest **4**, b) a solution of guest **1**, c) a solution of DBU.

Control experiments with the structurally related, but complexation inactive MeCav, ruled out the possibility of physisorption. After treatment with **1** and with, **4** or **5**, the surface did not show the presence of nitrogen, europium or yttrium, thus indicating no complex physisorption.

2.4.2 Fluorescence Characterization

It is well known that luminescence effects in rare earth complexes are due to f–f transitions. In the case of EuIII β-diketonate complexes, the emission spectra consist of $^5D_0 \rightarrow {}^7F_J$ transitions (J = 0–4) mainly dominated by the $^5D_0 \rightarrow {}^7F_1$ and $^5D_0 \rightarrow {}^7F_2$ emissions at 590 and 613 nm, respectively.[39] In general, luminescence properties of EuIII complexes depend on the energy transfer properties of ligands

since excited organic ligands act as light harvesting groups that, in turn, promote intramolecular energy transfer from the triplet state to an excited state of Eu^{3+}. Therefore, emission occurs from the lowest excited state ($^5D_0$) to the ground state (^7F_J) of Eu^{3+} and the presence of organic ligands, namely β-diketonates and phenanthroline, whose triplet states are higher in energy than the emissive $^5D_0$ excited state determines an efficient energy transfer process.[40] However, intensities of the emission spectra related to Eu^{3+} intra-4f6 transitions between the $^5D_0$ and $^7F_{0-4}$ levels do not depend on the energy transfer mechanisms but on the excitation wavelength[40a] and on the local environment around the europium ion.[40,41]

Fluorescence measurement has been performed at CNR-ISOF of Bologna by the group of Dr. Nicola Armaroli. The emission spectra of **Tiiii-Si•5** and **Tiiii-Si•3•5** (Figure 2.4.5) in the 540–750 nm range, at λ_{ex}=340 nm, corresponding to the π-π* transition of the β-diketonate,[42] consist of the characteristic sharp emission peaks at 578 ($^5D_0 \rightarrow {}^7F_0$), 590 ($^5D_0 \rightarrow {}^7F_1$) and 611 nm ($^5D_0 \rightarrow {}^7F_2$).

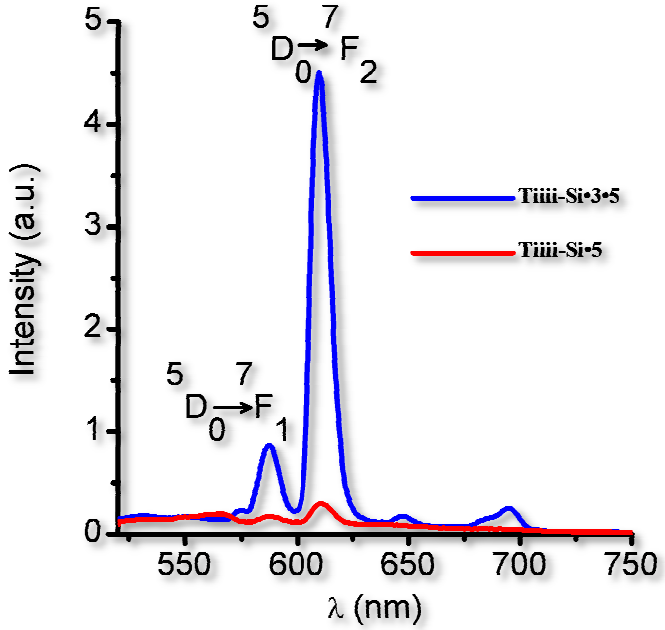

Figure 2.4.5: Emission spectra at λ_{ex}=340 nm of **Tiiii-Si•5** (red line) and **Tiiii-Si•3•5** (blue line).

A good overlap between the two spectra is evident, however, the relative intensities of the $^5D_0 \rightarrow {}^7F_1$ and $^5D_0 \rightarrow {}^7F_2$ transitions are different for the two complexed surfaces **Tiiii-Si•3•5** and **Tiiii-Si•5** and this difference can be related to different chemical environments around Europium in the two cases. In fact, the $^5D_0 \rightarrow {}^7F_1$ transition does not depend on the chemical environment around the Eu^{3+} ion due to its magnetic dipole nature. By contrast, the $^5D_0 \rightarrow {}^7F_2$ transition is influenced by the perturbing field of the ligand arrangement. The intensity ratio between the $^5D_0 \rightarrow {}^7F_2$ and $^5D_0 \rightarrow {}^7F_1$ transitions (4:1) is similar to that observed for **Tiiii-Si•3•5** in solution (5:1), but higher than that observed in **Tiiii-Si•5** spectra (2:1). These results suggest that the complexation of **5** inside Tiiii cavity, in presence of **3,** occurs without significant degradation of the Eu coordination environment. By contrast, the direct complexation of **5** on Tiiii cavity leads to some modification of

the original Eu environment. According to the XPS results (vide supra), these changes can be related to the absence of the phenanthroline ligand and the lose of β-diketonate ligands.

To demonstrate the presence of **3** in surface, and to confirm XPS results, emission spectra of the different surfaces has been carried out. Figure 2.4.6 reports the spectra in the 350–600 nm range, at λ_{ex}=270 nm, corresponding to the absorption of the phenanthroline ligand for various surfaces.[42]

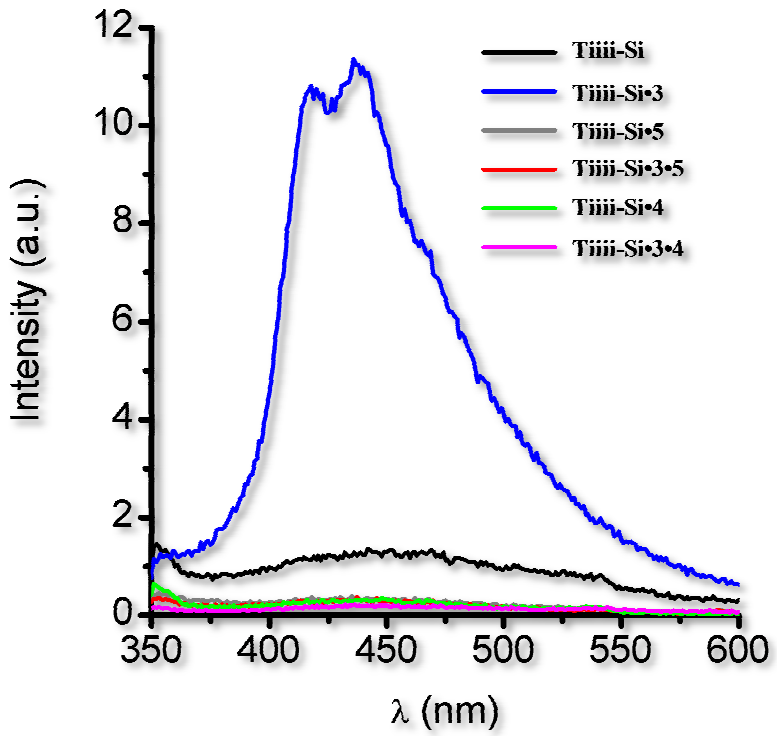

Figure 2.4.6: Emission spectra at λ_{ex}=270 nm of **Tiiii-Si** (black line), **Tiiii-Si•3** (blue line), **Tiiii-Si•5** (gray line), **Tiiii-Si•3•5** (red line), **Tiiii-Si•4** (green line) and **Tiiii-Si•3•4** (magenta line).

Only **Tiiii-Si•3** spectra show the transitions typical of phenanthroline, while in all other samples no phenanthroline signals are evident. This result is clearly expected

for **Tiiii-Si**, **Tiiii-Si•5** and **Tiiii-Si•4** samples since phenanthroline is not present. In the case of **Tiiii-Si•3•5** and **Tiiii-Si•3•4** samples the absence of phenanthroline emission is due to the energy transfer properties of this ligand since excited phenanthroline act as light harvesting groups and, its emission is quenched by the intramolecular energy transfer from its triplet state to an excited state of Eu^{3+} and Y^{3+}. (vedi supra).

2.4.3 Conclusions

In summary, the results demonstrated the affinity of tetraphosphonate cavitand **Tiiii** towards N-methylated group and the possibility to build 3D nanostructures through self-assembly. The multistep growth of such supramolecular structures on the surface resulted from the combined use of host-guest interaction and metal coordination between the guest inside the cavity and the metal of lanthanide complex.

The surface complexation experiments were monitored with two different techniques, namely XPS and fluorescence spectroscopy.

XPS results show evidence of supramolecular interaction between the guest and the Tiiii cavity and the subsequent interaction with metal complex.

Fluorescence measurements provided indications of the integrity of Eu(III) chemical environment. In particular, photoluminescence analysis showed that luminescence properties are retained in the monolayer thus suggesting that this material is suitable for application in the photonic field. Moreover, control experiments with the structurally similar, but complexation inactive, MeCav surface excluded the possibility of nonspecific interactions between the substrate and the guests. The sequence complexation-guest exchange-decomplexation demonstrated that the process is reversible.

2.5 References

[1] M. Mammen, S.-K. Choi, G. M. Whitesides, Angew. Chem. Int. Edit. 1998, 37, 2754.

[2] J. L. Atwood, J. E. D. Davies, D. D. MacNicol, F. Vogtle, Comprehensive Supramolecular Chemistry, Pergamon, Oxford 1996,Vol. 2.

[3] S. Richeter and J. Rebek, Jr., J. Am. Chem. Soc. 2004, 126, 16280.

[4] F. Lupo, C. Capici, G. Gattuso, A. Notti, M. F. Parisi, A. Pappalardo, S. Pappalardo, A. Gulino, Chem. Mater. 2010, 22, 2829.

[5] A. Gonzalez-Campo, S.-H. Hsu, L. Puig, J. Huskens, D. N.Reinhoudt, and A. H. Velders, J. Am. Chem. Soc. 2010, 132, 11434.

[6] E. Menozzi, R. Pinalli, E. A. Speets, B. J. Ravoo, E. Dalcanale, D. N. Reinhoudt, Chem. Eur. J., 2004, 10, 2199.

[7] J.-P. Dutasta, Top. Curr. Chem. 2004, 232, 55-91.

[8] L. Pirondini, E. Dalcanale, Chem. Soc. Rev. 2007, 36, 695-706.

[9] P. Delangle, J.-C. Mulatier, B. Tinant, J.-P. Declercq, J.-P. Dutasta, Eur J Org Chem. 2001, 3695-3704.

[10] E. Kalenius, D. Moiani, E. Dalcanale, P. Vainiotalo, Chem. Commun. 2007, 3865-3867.

[11] M. Melegari, M. Suman, L. Pirondini, D. Moiani, C. Massera, F. Ugozzoli, E. Kalenius, P. Vainiotalo, J.-C. Mulatier, J.-P. Dutasta, E. Dalcanale, Chem. Eur. J. 2008, 14, 5772-5779.

[12] E. Biavardi, M. Favazza, A. Motta, I. L. Fragalà, C. Massera, L. Prodi, M. Montalti, M. Melegari, G. G. Condorelli, E. Dalcanale, J. Am. Chem. Soc. 2009, 131, 7447-7455.

[13] Cancer research UK; see http://info.cancerresearchuk.org/cancerstats/types/prostate/ incidence/#geog

[14] E. Marshall, Science 2011, 331, 1540-1541.

[15] A. Sreekumar, L. M. Poisson, T. M. Rajendiran, A. P. Khan, Q. Cao, J. Yu, B. Laxman, R. Mehra, R. J. Lonigro, Y. Li, M. K. Nyati, A. Ahsan, S. Kalyana-Sundaram, B. Han, X. Cao, J. Byun, G. S. Omenn, D. Ghosh, S. Pennathur, D. C. Alexander, A. Berger, J. R. Shuster, J. T. Wei, S. Varambally, C. Beecher, A. M. Chinnaiyan, Nature 2009, 457, 910-914.

[16] J. A. Schalken, Eur. Urol. 2010, 58, 19-21

[17] D. L. Cao, D. W. Ye, Y. Zhu, H. L. Zhang, Y. X. Wang, X. D. Yao, Prostate Cancer and Prostatic Diseases 2011, 14, 166–172,

[18] a) V. Serreli, C. F. Lee, E. R. Kay and D. A. Leigh, Nature, 2007, 445, 523. b) E. R. Kay, D. A. Leigh and F. Zerbetto, Angew. Chem., Int. Ed., 2007, 46, 72. c) C. D. Meyer, C. S. Joiner and J. F. Stoddart, Chem. Soc. Rev., 2007, 36, 1705.

[19] P. Ghosh, G. Han, M. De, C. K. Kim and V. M. Rotello, Adv. Drug Delivery Rev., 2008, 60, 1307; N. L. Rosi and C. A. Mirkin, Chem. Rev., 2005, 105, 1547.

[20] V. Balzani, A. Credi, M. Venturi, Molecular Devices and Machines, Wiley-VCH, Weinheim, 2nd edn, 2008.

[21] a) U. Pischel, Angew. Chem., Int. Ed., 2007, 46, 4026. b) A. P. de Silva, Y. Leydet, C. Lincheneau N. D. McClenaghan, J. Phys.: Condens. Matter, 2006, 18, S1847.

[22] a) C. S. Bonnet, T. Gunnlaugsson, New J. Chem., 2009, 33, 1025. b)A. P. de Silva and S. Uchiyama, Nat. Nanotechnol., 2007, 2, 399. c) A. P. de Silva, S. Uchiyama, T. P. Vance, B. Wannalerse, Coord. Chem. Rev., 2007, 251, 1623.

[23] J. M. Lehn, Chem.s Eur. J. 1999, *5*, 2455–2463.

[24] N. S. Murrayab, S. P. Jarvisbc, T. Gunnlaugsson, Chem. Commun., 2009, 4959–4961.

[25] E. U. Thoden van Velzen, J. F. J. Engbersen, D. N. Reinhoudt, Synthesis 1995, 989-997.

[26] a) I. L. Swift, Surf. Interface Anal. 1982, 4, 47–51. b) D. Briggs, G. Beamson, Anal. Chem. 1992, 64, 1729–1736.

[27] E. Biavardi, G. Battistini, M. Montalti, R. M. Yebeutchou, L. Prodi, E. Dalcanale, Chem. Commun. 2008, 44, 1638–1640.

[28] For the nomenclature adopted for phosphonate cavitands see: R. Pinalli, M. Suman, E. Dalcanale, Eur. J. Org. Chem. 2004, 451-462.

[29] Cram DJ & Cram JM (1994) Container Molecules and their Guests. Monographs in Supramolecular Chemistry, Vol 4, ed JF. Stoddart (Royal Society of Chemistry, Cambridge).

[30] R. Chandra Dey, P. Seal, S. Chakrabartl, J. Phys. Chem A 2009, 113, 10113-10118.

[31] M. Nishio, Y. Umezawa, M .Hirota, Y. Takeuchi, Tetrahedron 1995, 51, 8665-8701.

[32] C. Massera, M. Melegari, E. Kalenius, F. Ugozzoli, E. Dalcanale, Chem. Eur. J. 2011, 17, 3064-3068.

[33] G.G. Condorelli, A. Motta, M. Favazza, I. L. Fragalà, M. Busi, E. Menozzi, E. Dalcanale, L. Cristofolini, Langmuir 2006, 22, 11126-11133.

[34] D. Menozzi, E. Biavardi, C. Massera, F.-P. Schmidtchen, A. Cornia, E. Dalcanale, Supramol. Chem. 2010, 22, 768-775.

[35] E. J. Faber, W. Sparreboom, W. Groeneveld, L. de Smet, J. Bomer, W. Olthuis, H. Zuilhof, E. J. R. Sudholter, P. Bergveld, A. van den Berg, ChemPhysChem 2007, 8, 101112.

[36] Y. Tong, E. Tyrode, M. Osawa, N. Yoshida, T. Watanabe, A. Nakajima, S. Ye, Langmuir 2011, 27, 5420-5426.

[37] S. L. Wiskur, H. Ait-Haddou J. J. Lavigne, E. V. Anslyn, Acc. Chem. Res. 2001, 34, 963-972.

[38] M. Montalti, L. Prodi, Chem. Commun., 1998, 1461–1462.

[39] G. G. Condorelli, C. Tudisco, A. Motta, A. Di Mauro, F. Lupo, A. Gulino, I. L. Fragalà, Eur. J. Inorg. Chem. 2010, 4121–4129.

[40] a) L. D. Carlos, R. A. S. Ferreira, V. De Zea Bermudes, S. J. L. Ribeiro, Adv. Mater. 2009, 21, 509–534; b) A. M. Kłonkowski, S. Lis, M. Pietraszkiewicz, Z. Hnatejko, K. Czarnobaj, M. Elbanowski, Chem. Mater. 2003, 15, 656–663.

[41] a) D.-J. Qian, K.-Z. Yang, H. Nakahara, K. Fukuda, Langmuir 1997, 13, 5925–5932. b) R. F. Silva, M. E. D. Zaniquelli, O. A. Serra, I. L. Torrioni, S. G. C. de Castro, Thin Solid Films 1998, 324, 245–252.

[42] a) A. Bellusci, G. Barberio, A. Crispini, M. Ghedini, M. La Deda, D. Pucci, Inorg. Chem. 2005, 44, 1818–1825. b) M. O. Ahmed, J.-L. Liao, X. Chen, S.-A. Chen, J. H. Kaldis, Acta Crystallogr., Sect. E 2003, 59, m29–m32. c) J. Peng, N. Takada, N. Minami, Thin Solid Films 2002, 405, 224–227.

Chapter 3

Fictionalization of porous silicon with cavitand-based receptors

3.1 Introduction

An interesting approach for harnessing the full potential of molecular receptors consists in their arrangement in monolayers hosted on the silicon surface[1,2] which, compared to both thin films and bulk materials, have the advantages of improving miniaturization and integration and of reducing nonspecific interactions which often mask the recognition events.[3] One of the limitations of monolayers on flat surfaces is related to the low surface area and, in turn, to the low amount of material involved in the recognition task thus requiring high sensitivity

techniques[4,5] or nanoscale devices[6-9] to detect analyte signals. To overcome this limitation, sensing devices can be fabricated adopting high surface area substrates[10,11] like porous silicon (**PSi**) Therefore, functionalization of **PSi** substrates with organic monolayers represents a theme of great interest for the synthesis of new functional materials in various applicative fields[12-14] and, in particular, for gas sensing in which high surface areas represent a significative advantage.[10,15]

In this chapter systems based on porous silicon (**PSi**) technology for liquid and vapour detection are presented. **PSi** based sensors for chemical contaminants can adopt a spectroscopic method (usually in the IR region where gas absorption spectra have specific signatures), or measure the changes in some physical properties (colour, refractive index, photoluminescence, fluorescence and so on) due to the interaction between the substances under investigation and the sensor itself. From this point of view, **PSi** is a very interesting material due to its large specific surface area (on the order of 500 m^2/cm^3) which is a great advantage in gas sensing applications, so that this technology has been extensively studied in this field. A key feature for a recognition transducer is a large surface area: so that it can be very sensitive to the presence of different analytes which penetrate inside the pores.

This chapter reports on the covalent anchoring onto silicon of a quinoxalinic cavitand modified with *N*,*N*-bis(salicylaldehyde) ethylenediimine (salen), receptor **1**, and of a methyl bridged cavitand having one acid group at the upper rim which make it suited for organophosphours vapours detection. The processes of covalent anchoring of the salen-modified cavitand has been investigated onto both monocrystalline Si(100) and porous silicon (**PSi**) since both of these substrates are of technological interest[12a,16].

3.2 General Procedures

3.2.1 Synthesis of 1

The **1** molecules were synthesized at the University of Catania by the research group of Professor Ballistreri according to reference.[13]

A cavitand-modified salen suited for silicon anchoring (**1**) was synthesized (according to Figure 3.2.1) from the monoformyl cavitand **2.** The reaction of 3-hydroxysalicylaldehyde with 11-bromo-1-undecene leads to compound **3**. Condensation of **3** with (1*R*,2*R*)-(+)-diphenylethylenediamine chloride affords the monoimine ammonium chloride derivative **4**. Monoformyl cavitand **2** was finally converted into the enantiopure receptor **1** by treatment with compound **4** in the presence of triethylamine.

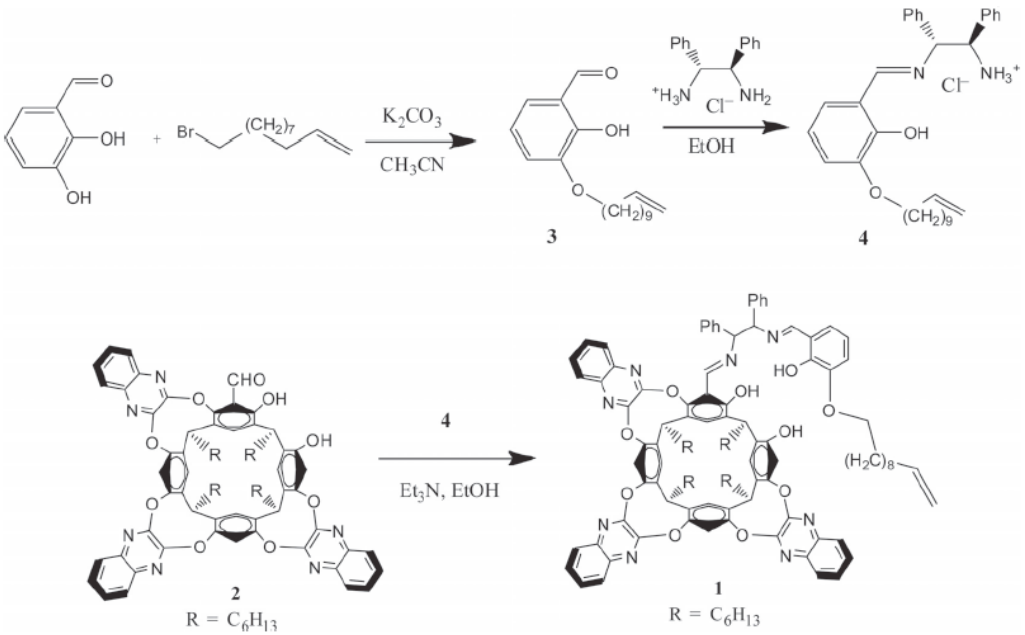

Figure 3.2.1: Synthesis of cavitand-salen **1** receptor.

3.2.2 Synthesis of methyl esters of AcIN, AcOUT cavitands, and MeCav cavitand

AcIN and **AcOUT** cavitands (Figure 3.2.2) suited for silicon anchoring and with the acid functions protected as methyl esters were synthesized according to a modified previously reported procedure.[17] Note that carboxylic groups in **PSi-AcOUT** and **PSi-AcIN** were methyl protected to avoid interaction between the upper cavity and the surface.[18] The hydrolysis of the ester group was done directly on **PSi** after grafting. **MeCav** (Figure 3.2.2) with ω-decenyl feet was prepared according to a published procedure.[19]

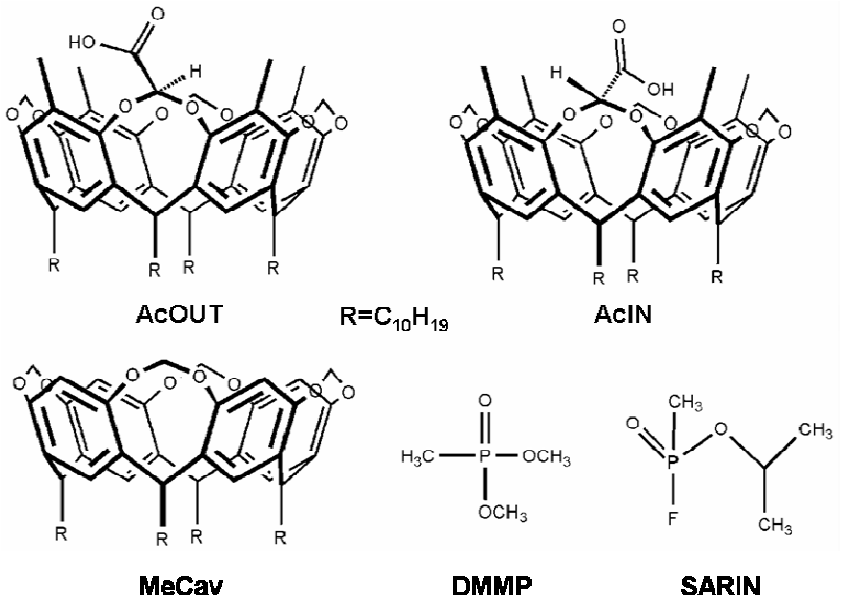

Figure 3.2.2: Chemical structure of cavitands and guests.

3.2.3 Porous Silicon preparation.

Porous silicon (**PSi**) has been obtained by wet metal assisted chemical etching according to the procedure reported by Chartier et al.[20] Briefly, Si(100) slides were dipped for 5 minutes in an aqueous solution of HF (0.14M) and $AgNO_3$ (5×10^{-4}M) to deposit Ag particles. The slides were then etched in aqueous solutions containing HF, H_2O_2 and ultra-pure H_2O (40% HF: 30% H_2O_2 :H_2O 25:10:4 V/V) for 1

minute and after etching, samples were rinsed with ultra-pure water and dried with prepurified N_2. Thickness and morphology of the etched layer, checked by SEM cross section are consistent with those reported in literature for Ag-assisted chemical etching.[13,20]

3.2.4 Monolayer Preparation.

For grafting on porous substrates, **PSi** was etched in 10% HF solution for 1h, washed with ultra-pure water for 20s, dried with N_2, and immediately placed in the methyl ester protected cavitand solution in mesitylene. The solution was then refluxed at 200°C for 5 h, under slow N_2 bubbling to prevent bumping. After grafting, the sample was removed from the solution (after cooling at room temperature) and cleaned by two rinsing cycles of ultrasonic cleaner (5 min each) in dichloromethane. Note that SEM cross section analysis of samples after grafting shows a morphology similar to that observed before grafting, indicating that the anchoring route does not degrade the structure of porous silicon, as previously reported.[13] The procedure used for the grafting of cavitands **1** and on flat Si surface is the same used and described in chapter 2 section 2.2.3.

3.2.5 Monolayer Characterization.

XPS spectra were run with a PHI 5600 multi-technique ESCA-Auger spectrometer equipped with a monochromated Al *K*α X-ray source. Analyses were carried out with a photoelectron angle of 45° (relative to the sample surface) with an acceptance angle of ± 7°. The XPS binding energy (B.E) scale was calibrated by centering the C 1s peak due to hydrocarbon moieties and "adventitious" carbon at 285.0 eV.[21] SEM analysis was performing with a LEO SUPRA 55VP equipped with a field emission gun. Transmission FTIR measurements were recorded on a JASCO FTIR 430, with 100 scans collected per spectrum (scan range 560-4000

cm^{-1}, resolution 4 cm^{-1}). Thermal desorption experiments have been performed in an UHV chamber (10^{-9} Torr) equipped with a resistive heated sample holder (Vacuum Science, Italy) and a quadrupole mass spectrometer Smart-IQ^{+TM} (Thermo Electron Corporation). During experiments holder was heated with a ramp of 10 °C/min from 30 to 130°C and quadrupole spectrometer operated with electron filament ion source and a multiplier detector (mass range 1-300).
AFM images were obtained in high amplitude mode (tapping mode) by a NT-MTD Solver P47 instrument. The noise level before and after each measurement was 0.01 nm.

3.2.6 Computational Details.

DFT calculations used the Gaussian and plane wave mixed-basis method (GPW), as implemented in the QUICKSTEP module[22] within the CP2K simulation package.[23] A triple quality TZVP Gaussian basis set was employed for all the atoms. The Goedecker-Teter-Hutterpseudopotentials[24] together with a 320 Ry plane wave cutoff were used to expand the densities obtained with the Perdew-Burke-Ernzerhof (PBE)[25] exchange-correlation density functional. Molecular geometry optimization of stationary points used the Broyden–Fletcher–Goldfarb–Shanno (BFGS) method. For the non periodic calculation of the system the wavelet method[26] was adopted as cell decoupling procedure. Van der Walls contribution is taken in account with the Grimme 2D Method.[27] Vibrational analysis was carried out to obtain IR information within the harmonic approximation approach. Anharmonic effects are taken in account by adding an anharmonic constant term of 80 cm^{-1}.[28] Ethyl groups replace the decyl chains in the bottom side of the cavitand. Natural Bond Orbital (NBO) analysis was performed by Gaussian code (6-311G**/PBE)[29] to obtain information regarding charge distribution.

3.3 Covalent Functionalization of Silicon Surfaces with a Cavitand-Modified Salen

This paragraph reports on the covalent anchoring onto silicon of a quinoxalinic cavitand modified with *N*,*N*-bis(salicylaldehyde) ethylenediimine (salen), receptor **1,** which has been functionalized with an undecylenic group for Si anchoring (Figure 3.2.1).

The first site is a quinoxalinic cavity that is active for tetraalkylammonium ions binding, and the second site is a salen-derived moiety based on a bis(salicylidene)-1,2-diphenylethylenediimine group that is active for the complexation of metallic cations such as Mn(III) and UO_2 (VI).

Cavitand-salen **1** was grafted onto H-terminated Si(100) surfaces via photochemical hydrosilylation of the double bonds, while thermal- driven hydrosilylation was adopted for grafting of **1** onto **PSi**. The functionality of the hybrid **Si-1** surface was tested by reacting **Si-1** with uranyl acetate solution. In this way a salen uranyl complex was obtained directly on the **Si-1** surface via a 2D surface synthetic route.

The synthesis of the uranyl-salen complex on **Si-1** was performed with a double purpose: (i) to evaluate possible surface routes towards metal-salen complexes, and (ii) to prove that after silicon anchoring the salen molecules are intact and keep their specific molecular properties. To validate the complexation results, control experiments on native silicon oxide and alkyl-functionalized surfaces were also performed. Moreover the chiral uranyl-salen complexes act as receptors for enantioselective molecular recognition, due to the fact that they are able to recognize anions by exploiting the Lewis acidity of the uranyl centre that equatorially coordinates with anions. The uranyl-salen complex derived from receptor **1** behaves as a heteroditopic receptor in which the metal centre is able to coordinate

the anion, whereas the π- rich quinoxalinic cavity binds tetraalkylammonium cations by stabilizing them with CH···π and cation···π interactions.

3.3.1. XPS Characterization

Table 3.3.1 compares the elemental compositions of two reference samples, namely HF-etched silicon (a) and HFetched **PSi** (b), with freshly prepared **Si-1** (c), aged **Si-1** (d)and freshly prepared **PSi-1** (e).

	Atomic Concentration			
	Si 2p	**O 1s**	**C 1s**	**N 1s**
a) HF-etched Si	77.0	7.8	15.2	-
b) HFetched **PSi**[a]	76.7	7.6	15.7	-
c) Fresh **Si-1**	58.5	17.8	23.0	0.7
d) Aged **Si-1**	48.6	29.7	22.0	0.7
e) **PSi-1**	28.4	22.0	47.7	1.8

[a] A small amount of residual Ag (Ag < 0.2%) was found in the **PSi** substrates.

Table 3.3.1: XPS determined atomic concentrations for (a) HF-etched Si; (b) HF-etched **PSi**; (c) fresh **Si-1** (d) aged **Si-1** and (e) **PSi-1**.

XPS data show that C 1s signals are observed for both reference samples due to the ubiquitous presence of "adventitious" contaminant species.[30] However, both the **Si-1** and **PSi-1** surfaces show a significant enhancement of C 1s related signals compared to both the HF-etched Si and **PSi** samples. This enhancement, and especially the presence of N 1s signals due to the quinoxaline and salen moieties, is an indication of the grafting of **1** onto the substrate surfaces. The Si 2p spectra of

the freshly etched Si and **PSi** surfaces show bands due to a doublet (at 99.2 and 99.8 eV, respectively) associated with elemental silicon (Si^0). After grafting **1** onto the surfaces, the Si 2p spectra of both **Si-1** and **PSi-1** show, besides the Si^0 2p3/2-1/2 doublet, broad bands at 103.0 eV[31] that are consistent with the presence of oxidized silicon in the samples (Figure 3.3.1). The intensity of this band in the spectrum of thermal grafted **PSi** is slightly higher than the intensity of the same band in the spectrum of UV grafted **Si-1**, but after aging (1 week) the oxidation levels of the two samples became comparable. The presence of surface oxidation indicates that the monolayers are not densely packed, which is in accordance with the low surface coverage estimated from the XPS data in Table 3.3.1. This result is not unexpected since the larger size of the cavitand moiety compared to the alkyl foot precludes a close packing arrangement.

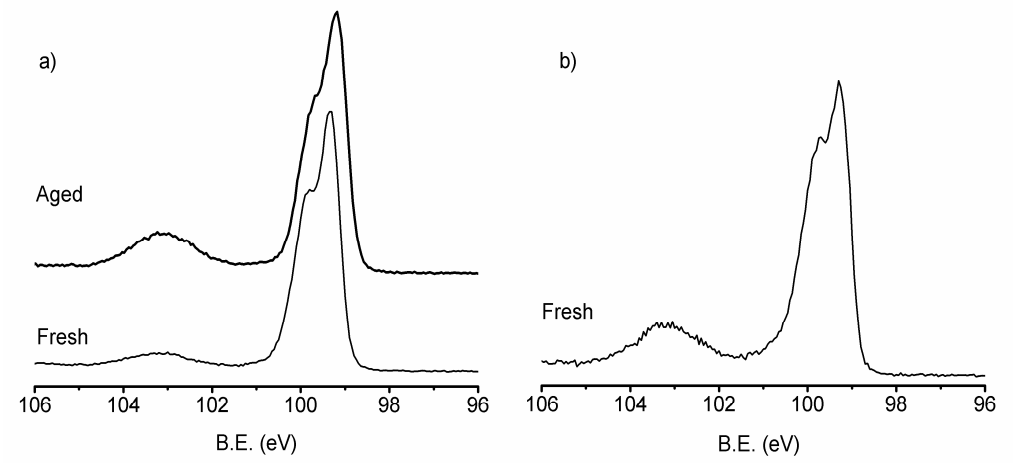

Figure 3.3.1: High resolution Si 2p XPS spectra of (a) fresh **Si-1** and 1 week aged **Si-1**, and (b) fresh **PSi-1**. The Si 2p spectrum of **PSi** does not change after aging.

The high resolution C 1s spectra (Figure 3.3.2) of **Si-1** and **PSi-1** are similar, and consist of three main peaks: (i) a component at 285.0 eV (C^0) due to the aliphatic and aromatic hydrocarbon backbone of **1** and "adventitious" carbon; (ii) a component at 286.3 eV (C^{+1}) due to oxidized carbon bonded to one oxygen atom (or double bonded to nitrogen) in the cavitand phenyl rings,[1] salen moiety,[32] as well as in the Si–O–C frameworks of "adventitious" contaminants, [1,33,34] and (iii) a third component at 287.7 eV due to the quinoxalinic carbons that bond to oxygen and nitrogen atoms.[1] The broad band detectable in the spectrum of **PSi-1** at approximately 291.5 eV can be assigned to the π-π* shake-up of aromatic rings.[35] The same band in the **Si-1** spectrum cannot be discerned from the background due to the much lower absolute amount of **1** on the flat surface of Si compared to number of molecules of **1** on the porous surface of **PSi**. No relevant change in the C 1s band shape occurs after aging of the samples.

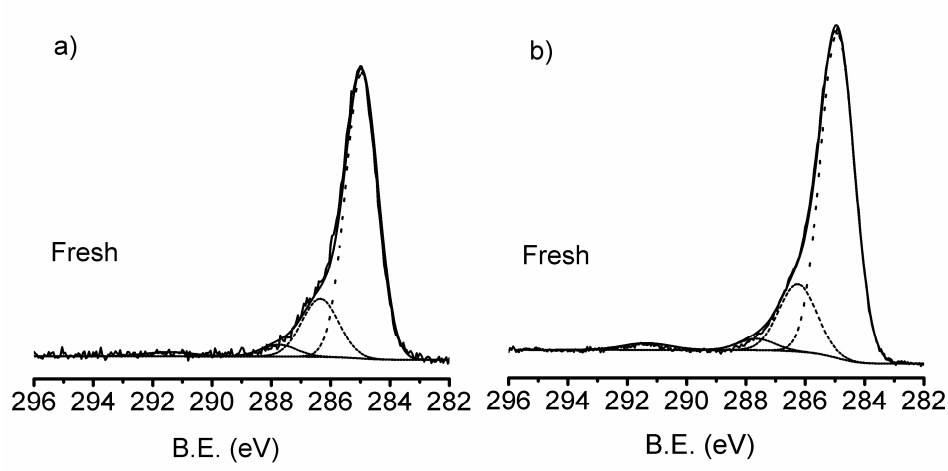

Figure 3.3.2: High resolution C 1s XPS spectra of (a) fresh **Si-1** and (b) fresh **PSi-1**. C 1s spectra of **Si-1** and **PSi-1** do not change after sample aging.

High resolution data for the N1s region of the XPS spectra of fresh and aged **Si-1** samples and of **PSi-1** samples are shown in Figure 3.3.3. The signals in the N 1s

spectral regions give a clear indication of the surface anchoring of **1** in these samples. The N1s band in the spectrum of freshly prepared **Si-1** consists of two components: (i) a main component at 399.8 eV (N_{qx}) that is assigned to the quinoxaline nitrogen atoms,[1,32] and (ii) a less intense component at 398.0 eV (N_{sal}) that is assigned to the iminic nitrogen atoms[36] of the salen. The observed intensity ratio N_{qx}/N_{sal} is about 3, which is as expected from the molecular structure. After one week of sample aging, the N 1s band shape changes (Figure 3.3.3) even though the total amount of nitrogen remains constant (Table 3.3.1). The N 1s spectrum of the aged **Si-1** samples consists of the same main components; the N_{qx} band is at 399.8 eV whilst the N_{sal} component (denoted as N_{salH}) is shifted to a higher binding energy (N_{salH} at 401.7 eV) than the signal in the spectrum of the freshly prepared sample. This energy shift can be explained either by the formation of hydrogen bonds or by the protonation[37] of the salen nitrogen atoms due to the presence of acidic O_xSi–OH groups on the oxidized surface (p*K*a ≈ 4.5).[38] Moreover, the N_{qx}/N_{salH} intensity ratio is about 3, which is consistent with the atomic ratio between the quinoxalinic and salen nitrogen atoms. The N 1s band in the high resolution XPS spectrum of **PSi-1** is similar to that observed in the spectrum of aged **Si-1**. It consists of a N_{qx} component at 399.8 eV and a component at 401.8 eV that is due to protonated or H-bonded salen nitrogen atoms (N_{salH}). The intensity ratio N_{qx}/N_{salH} is equal to 3, which is equivalent to the ratio observed in the spectrum of aged **Si-1**. Note that the surface oxidation (Figure 3.3.1), and hence the availability of acidic O_xSi–OH groups on **PSi-1**, is comparable to the aged **Si-1** surface; this explains why there are similar interactions (H-bonding or protonation) involving the salen nitrogen atoms in **PSi-1** as in aged **Si-1 s**amples.

To rule out any possible physisorption and to demonstrate the covalent anchoring of **1** on both flat and porous silicon, **blank-Si** and **blank-PSi** samples have been obtained by processing the Si and **PSi** surfaces with the same treatment adopted for

Si-1 and **PSi-1**, but in the absence of UV irradiation and heating, respectively. The N 1s regions in the XPS spectra of these samples are reported in Figure 3.3.3. The spectra do not show any significant signal in the N 1s region, which indicates the absence of physisorbed **1** in these samples.

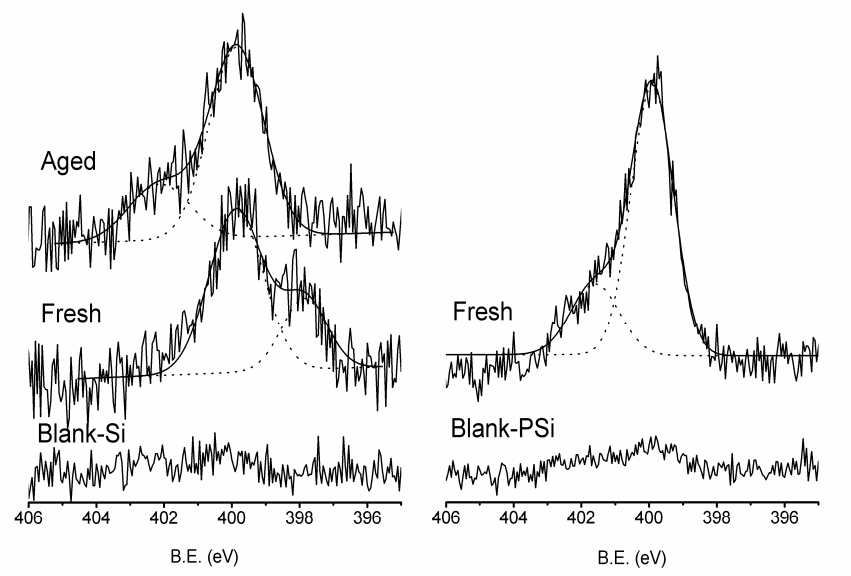

Figure 3.3.3: (a) High resolution N 1s XPS spectra of aged **Si-1** (upper), fresh **Si-1** (middle) and **blank-Si** (bottom); (b) High resolution N 1s XPS spectra of fresh **PSi-1** (upper) and **blank-PSi** (bottom). The N 1s spectrum of **PSi-1** does not change after sample aging.

3.3.2 FTIR characterization of PSi-1

FT-IR measurements provided useful information for monitoring the grafting reaction of **1** onto **PSi** substrates by taking advantage of the high surface area of the porous samples. FTIR spectra of HF-etched **PSi**, **blank-PSi** and **PSi-1** samples are compared in Figure 3.3.4. In particular, three spectral regions are reported: (a) the

C-H stretching region between 3200 and 2600 cm^{-1}, (b) the Si-H stretching region between 2300 and 1900 cm^{-1} and (c) the region between 1300 and 600 cm^{-1} in which SiO_x stretching vibrations and some bending modes are present. The presence in the **PSi-1** spectrum (Figure 3.3.4 a) of intense bands due to the CH_2 symmetric ($\nu s(CH_2)$) and antisymmetric ($\nu a(CH_2)$) stretches at 2858 cm^{-1} and 2926 cm^{-1}, respectively, and of a shoulder at 2956 cm^{-1} due to the CH_3 antisymmetric stretch ($\nu a(CH_3)$), combined with the absence of the homologous stretches in the spectrum of HF-etched **PSi** and with the negligible intensity of these signals in the **blank-PSi** spectrum, is consistent with the thermal anchoring of **1** onto the **PSi** surface. These results are supported by the evolution of Si-H features in the spectra as the grafting reaction progresses. The spectrum of HFetched **PSi** (Figure 3.3.4 b) shows intense bands at 2087 cm^{-1}, 2106 cm^{-1} and 2142 cm^{-1} due to SiH, SiH_2 and SiH_3 stretches of H-terminated **PSi**, respectively.[39] After grafting **1** onto the **PSi** surface, the intensities of the SiH_x bands clearly decrease (Figure 3.3.4, b, **PSi-1**) due to the hydrosilylation reaction between Si–H terminations and the double bonds of **1**. Note that a new broad feature appears at 2260 cm^{-1} due to oxygen back-bonded SiH groups (mainly O_3SiH),[39] which are formed because of silicon oxidation. On the other hand, the **blank-Si** spectrum shows an intense band due to SiH_x stretches (2150-2080 cm^{-1}), indicating that no hydrosilylation reaction occurred with this sample. In addition, two new features are observed (Figure 3.3.4, b, **blank-Si**) at 2260 cm^{-1} and 2200 cm^{-1}, which can be assigned to Si-H stretches of the O_3SiH and O_2SiH species of the oxidized surface, respectively.[39,40]

The 1300-600 cm^{-1} region of the FTIR spectrum of HFetched **PSi** (Figure 3.3.4, c) shows two intense bands at 660 cm^{-1} and 625 cm^{-1} that are due to the wagging vibration modes of SiH_2 and SiH, respectively, and the spectrum also shows the SiH_2 bending vibrations (δSiH_2) at 910 cm^{-1}.[39c] In the **PSi-1** spectrum, the intensity of these features strongly decrease, analogously to the Si–H stretching signals, due

to the hydrosilylation reaction. The 1300-600 region of the **PSi-1** FTIR spectrum is dominated by a broad band centred at 1040 cm^{-1} that is assigned to the vibrational modes of SiO_2.[41] In the spectrum of the **blank-PSi** sample, Si-H wagging modes are intense even though silicon oxide vibrations centred at 1110 cm^{-1} are also present.[41]

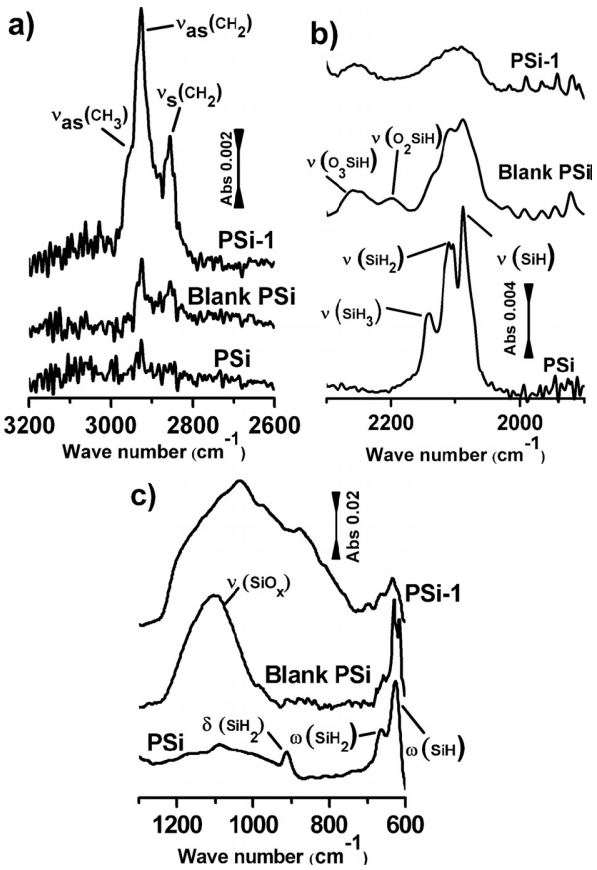

Figure 3.3.4: FTIR spectral regions between (a) 3200-2600 cm^{-1} (C–H stretching region), (b) 2300-1900 cm^{-1} (Si-H stretching region) and (c) 1300-600 cm^{-1} (SiO_x stetching and bending modes) of HFetched **PSi**, **blank-PSi** and **PSi-1**. The transmission spectrum of Si(100) has been subtracted from these spectra as the background.

3.3.3 AFM lithography on Si-1

AFM studies were carried out on HF-etched Si and flat **Si-1** samples. AFM topographic images of **Si-1** show a uniform surface with measured statistical parameters (mean height *R*mean = 1.1 nm and roughness *RMS* = 0.21 nm) that are slightly higher than measured for HF-etched Si (*R*mean = 0.3 nm and *RMS* = 0.11 nm). Since AFM images do not have enough resolution to discern single molecules, AFL (contact mode)[42] has been used to evaluate the structure of the functionalized surface.[13] Thus, grafted molecules of **1** were removed by rastering different surface areas (0.5-1.5 μm^2) with the AFM tip under a suitable constant force (0.24 μN). The thus obtained scratches have an average depth of 1.1-0.2 nm (Figure 3.3.5). Such a value is lower than that expected for **1** with an extended configuration. DFT geometry optimization was performed on **1** with a linear configuration and gave a molecular length of 2.6 nm (Figure 3.3.5, c). These differences can be explained by either assuming a folded configuration for the molecules or by considering a model, previously proposed, of a low density monolayer with silicon oxidation of the surface.[43]

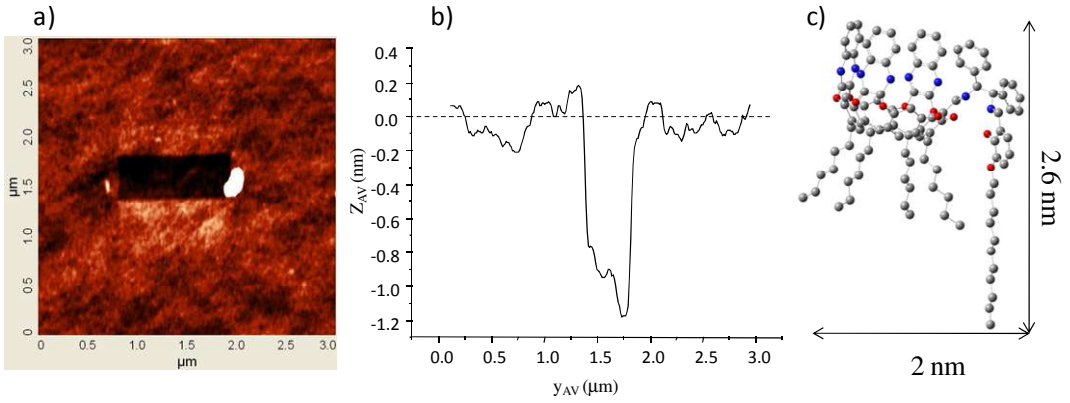

Figure 3.3.5: (a) AFM image of **Si-1** after AFL, (b) average cross-section profile of **Si-1** surface scratch and (c) DFT estimated height of **1**. The large feature on the scratch edge is due to the material removed from the scratch.

3.3.4 Surface synthesis of uranyl complexes

Si-1 surface reactions have been performed to test 2D surface routes for the preparation of metal-salen complexes and to demonstrate that salen maintains its molecular functionalities after grafting onto the Si surface. Surface reaction experiments were performed by dipping **Si-1**, **SiO*x*/Si** and **Si- decyl** surfaces into a solution of uranyl acetate (10^{-3} M) in ethanol for 1 h at 20 °C. Samples were then repeatedly rinsed with EtOH and water, and then dried under a nitrogen gas stream. Reactivity towards uranyl ions has been evaluated for different functionalized surfaces, the active **Si-1** and, as control experiments, native silicon oxide **SiO*x*/Si** and decyl-functionalized Si (**Si-decyl**), by treating samples with ethanol solutions of uranyl acetate.

Figure 3.3.6 compares high resolution U 4f regions of the XPS spectra of **Si-1** and the reference samples (**SiO*x*/Si** and **Si-decyl**) after uranyl treatment. Peaks associated with U 4f7/2 and U 4f5/2 at 382.1 eV and 392.7 eV, respectively, are

evident in the spectrum of uranyl treated **Si-1**, which indicates the presence of U^{VI} species in this sample.[44,45] No significant signals are detected in the spectra of uranyl-treated **SiO*x*/Si** and **decyl-Si**, proving that salen is required for uranyl coordination. The theoretical atomic ratio between U and N in the uranyl complex is 1/8, hence the complexation yield can be estimated from the measured U/N atomic ratio (ca. 1/15) as follows:

$$\text{Complexation Yield (\%)} = \frac{\%U}{\%N} \times \frac{8}{1} \times 100$$

The thus obtained complexation yield was found to be in the 50-60% range.

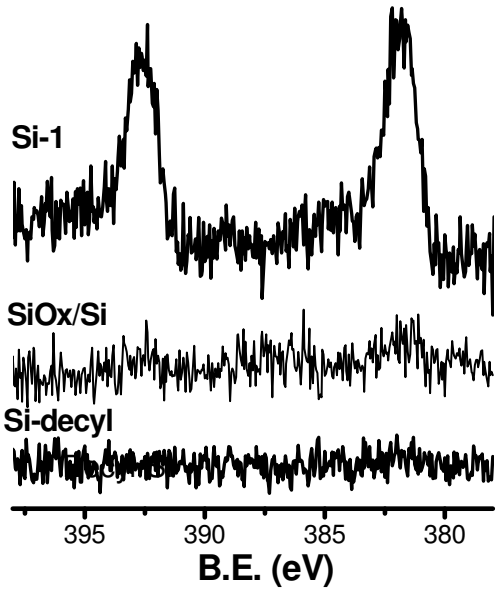

Figure 3.3.6: High resolution U 4f XPS spectra of various surfaces treated with uranyl solutions: **Si-1** (upper spectrum), **SiO*x*/Si** (middle spectrum) and **Si-decyl** (bottom spectrum).

3.3.5 Conclusions

New hybrid organic-inorganic materials consisting of quinoxaline cavitand-salen monolayers covalently bonded to flat and porous silicon have been synthesized. The success of the grafting protocol has been demonstrated by combining different analytic techniques (XPS, FTIR and AFM) with control experiments performed in the absence of UV or thermal activation. The results from this work indicate that molecules of **1** are covalently grafted to the silicon surface through a hydrosilylation reaction, but after anchoring further interactions occur between the salen nitrogen atoms and the Si-OH termination groups of the oxidized surfaces through nitrogen protonation or H-bonding. In addition, a surface-based synthetic route has been developed for the preparation of metal-salen complexes directly on a functionalized surface. This synthetic route is based on the reaction between the **Si-1** surface and uranyl acetate solution. The results from this experiment proved that the preparation of a system with different recognition properties was achieved, and it also showed that the salen reactivity, and hence its structural integrity, are kept after it is covalently anchored to the Si surface. The functional materials described in this paragraph represent a useful addition to the available pool of hybrid systems that are suited for silicon integration and, in particular, the use of porous substrates which allows simple I.R. characterization represents a strategy with interesting potentialities.

3.4 Detection of DMMP by cavitand functionalized PSi

3.4.1 Sensing of organophosphorus vapors

Organophosphonates (OPs) are a family of organic compounds bearing phosphorous–oxygen bonds that are often highly toxic since they can inhibit the activity of the critical enzyme acetylcholinesterase.[46] In the last years, OPs have aroused interest in environmental and security fields due to their use in pesticides and as chemical welfare agents, thus spurring a great effort on the detection, monitoring and decontamination of environments containing toxic OPs.

Many studies have been reported on the detection of these OPs adopting a wide range of transduction signals based on electric[47,48] or optical[49,50] changes, surface acoustic waves,[51] quartz crystal microbalances,[52,53] smectic liquid crystals,[54] microcantilever,[55] and using various organic and inorganic sorbents as active[47,49] or preconcentration[56] materials such as various metal oxides,[48,53] polysiloxanes[57-59] organic polimer,[49] functionalized carbon nanotubes[60,61,9] , SAM,[62] and MOFs.[63] Although all these schemes allow possible routes to detect OPs in the parts-per-million (ppm) range or lower, most surface-based techniques suffer from low selectivity and, in some cases, lack of reversibility.[56,64] In most of the mentioned sorbents, OP complexation is mainly driven by the H bonding between –OH sorbent groups and the P=O moiety in OPs, but this interaction is strongly affected by the presence of H_2O,[65] which reduces selectivity and sensitivity. Recently, cavitands have been used as efficient recognition films deposited on a Surface Plasmon Resonance transducer to detect dimethyl methylphosphonate (DMMP)[17] a nontoxic homologue of the nerve agents, which is used as a model compound to mimic their reactivity. In that study, the proposed combined effects due to the

cavity and the H-bond interaction improved the complexation efficiency and reduced water interferences compared to commercial sorbents.

In this chapter, is reported a strategy for the detection of organophosphorous vapors which combines the supramolecular recognition properties of two cavitand receptors with the potentialities of **PSi**.

The two adopted isomeric receptors, denoted **AcOUT** and **AcIN** (Figure 3.2.2), differ only for the orientation of the acid groups at the upper rim, since both cavitands contain one acid group at the upper rim, pointing respectively outward or inward the cavity. The capacity of thin films of these receptors to detect DMMP has been previously demonstrated.[17]

Each of these cavitands was functionalized in the lower rim with four undecylenic feet for surface anchoring and then grafted on H-terminated **PSi** surfaces via thermal hydrosilylation of the double bonds. In addition, control samples, inactive towards organophosphorous gas sensing, were prepared by grafting on **PSi** the methyl-bridged cavitand MeCav (Figure 3.2.2) which is structural similar to both **AcOUT** and **AcIN**, but it is inactive towards DMMP complexation. X-ray Photoelectron Spectroscopy (XPS), and Fourier transform infrared spectroscopy (FTIR) were adopted to probe the cavitand-grafting route on **PSi** and to evaluate the sensing properties of the functionalized **PSi** surfaces. Mass spectroscopy coupled with thermal desorption was also used to monitor the products desorbing from the surface. Host-guest interactions and energetic differences among DMMP complexes with active and inactive cavitands have been explored by DFT calculation. Theoretical modeling also allowed to extend experimental results to sarin molecule, an effective nerve gas agent used during the terroristic attack of Tokyo subway in 1995.

3.4.2 Characterization of Cavitand functionalized PSi

Since FTIR spectra of **PSi-AcOUT** and **PSi-AcIN** are almost identical, only **PSi-AcIN** spectra are reported. FT-IR spectra of HF-etched **PSi, PSi-AcIN** and **PSi-MeCav** samples are compared in Figure 3.4.1. In particular, three spectral regions are reported: a) the C-H stretching region between 3100 and 2750 cm^{-1}, b) the Si-H stretching region between 2300 and 1900 cm^{-1} and c) the region between 1350 and 600 cm^{-1} which contains SiOx stretching vibrations and SiHx bending modes.

The appearance in **PSi-AcIN** and **PSi-MeCav** spectra of intense bands due to the CH_2 symmetric ($\nu_s(CH_2)$) and antisymmetric ($\nu_a(CH_2)$) stretches at 2858 cm^{-1} and 2926 cm^{-1} and a characteristic smaller band at 3005 cm^{-1} assigned from Friggeri et al.[66] to the stretches of aromatic C-H (ν(CH)) in cavitands (Figure 3.4.1 a), combined with the absence of the homologous stretches in the spectrum of HF-etched **PSi,** confirms the covalent grafting of the cavitands onto the porous silicon surface. In the region between 2300 and 1900 cm^{-1}, three absorption peaks at 2140 cm^{-1}, 2114 cm^{-1} and 2087 cm^{-1} due to $Si–H_3$, $Si–H_2$ and Si–H stretching modes, respectively,[67] are present in the spectrum of HF-etched **PSi** (Figure 3.4.1 b, bottom). In all cavitand-grafted samples SiHx peaks are significantly reduced (Figure 3.4.1 b, upper and middle curves), due to the hydrosilylation reaction which determines the replacement of several Si–H bonds by Si–C bonds. A low broad band at 2251 cm^{-1} corresponding to OSi–Hx stretches was, however, observed due to a partial silicon oxidation.

The 1350–600 cm^{-1} region of the FTIR spectrum of HF-etched **PSi** (Figure 3.4.1 c, bottom curve) shows two intense bands at 660 cm^{-1} and 625 cm^{-1} that are due to the wagging vibration modes of SiH_2 and SiH, respectively, and the SiH_2 bending vibrations (δSiH_2) at 910 cm^{-1}.[68] In the spectrum of grafted samples (Figure 3.4.1.c, middle and upper curves), the intensity of these features decreases, analogously to the Si–H stretching signals, due to the hydrosilylation reaction. The

1350– 600 cm^{-1} region of the **PSi-AcIN** spectrum is dominated by a broad band around 1100 cm^{-1} that is assigned to the vibrational modes of SiO_2[13].

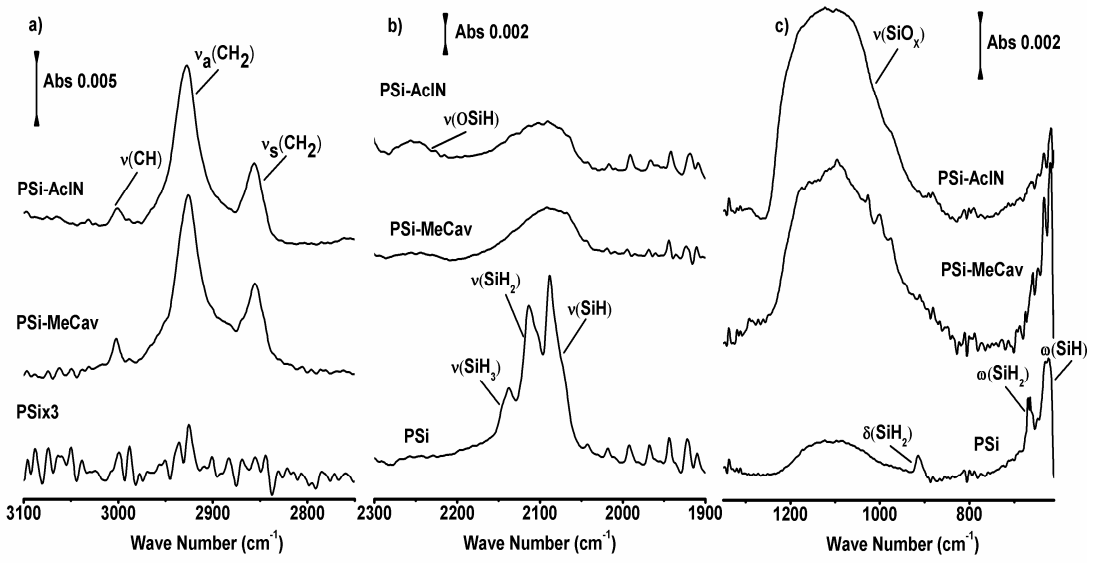

Figure 3.4.1: FTIR spectral regions between (a) 3200–2750 cm^{-1} (C–H stretching region), (b) 2300–1900 cm^{-1} (Si–H stretching region) and (c) 1350–600 cm^{-1}(SiOx stretching and bending modes) of HF-etched **PSi**, **PSi-MeCav** and **PSi-AcIN**. The transmission spectrum of Si(100) has been subtracted from these spectra as background.

Cavitand-functionalized **PSi** based materials (**PSi-AcIN, PSi-AcOUT** and **PSi-MeCav**) were also characterized by XPS. Elemental composition of as-grafted samples and of HF-etched **PSi** substrates are reported in Table 3.4.1.

	Atomic concentration		
	Si 2p	**O 1s**	**C 1s**
HF-etched **PSi**[a]	76.7	7.6	15.7
PSi-AcIN	25.4	27.8	46.8
PSi-AcOUT	21.7	28.1	50.2
Psi-MeCav	29.0	21.2	49.8

[a]A small amount of residual Ag (Ag< 0.2%) was found in the **PSi** substrates.

Table 3.4.1: Elemental composition of porous silicon samples before and after the grafting of AcIN, AcOUT and MeCav cavitands.

XPS data show that C 1s signals in cavitand decorated surfaces increase significantly compared to C 1s related signal of the HF-etched **PSi** sample, as expected after the grafting of a cavitand monolayer.[5,13]

High resolution C1s and O1s photoelectron spectral regions of HF-etched **PSi**, as-grafted **PSi-AcIN** and **PSi-MeCav** are compared in Figures 3.4.2 and 3.4.3. Analogous XPS spectra of as-grafted **PSi-AcOUT** are similar to those of **PSi-AcIN**.

C1s region of as-prepared **PSi** sample (Figure 3.4.2 a) consists of two components. The first component is centered at 285.0 eV and it represents aliphatic and aromatic hydrocarbons.[34a] The second component is centered at 286.5 eV and it is attributed to carbon bonded to one oxygen. The latter component of this "adventitious" carbonaceous layer was attributed to the formation of Si-O-C groups due to the reaction between Si-H and Si-OH groups on the silicon surface with oxidized carbon species.[1]

The C 1s spectra of both **PSi-MeCav** and **PSi-AcIN** (Figures 3.4.2 b and 3.4.2 c, respectively) consist of three main components. First two components at 285.0 eV

and 286.3 eV are analogues to those observed in **PSi**, even though they have higher intensity.

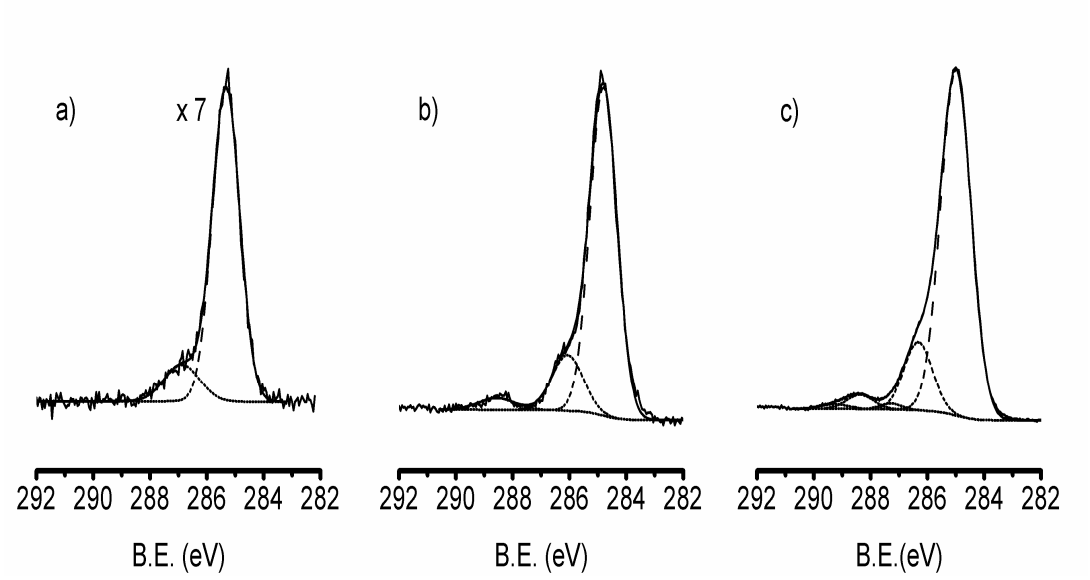

Figure 3.4.2: High-resolution C 1s XPS spectra (takeoff angle 45°) of a) HF-etched **PSi**, b) **PSi-MeCav** and c) **PSi-AcIN**.

The first component is due to the aliphatic and aromatic hydrocarbon backbone of cavitands, while the component at 286.3 eV is due to oxidized carbons in the resorcinarene phenyl rings bonded to one oxygen atom.[32] A third component at 288.4 eV, only observed in cavitand decorated surfaces, can be used as fingerprint of the presence of cavitand molecules and it represents the four methylene groups bridging the oxygen atoms at the upper rim.[1] In **PSi-AcIN** sample a component due to carboxylic carbon can be added at 289.2 eV but it is too close to the more intense component at 288.4 eV to single out its contribution.

O1s signal observed in **PSi** substrates consists of a single component at 532.1 eV, which is due to a partial oxidation of the substrates. The O1s band of functionalized **PSi** (Figure 3.4.3) consists instead of two components. The first at 532.1eV is due

to Si surface partial oxidation,[32a] similarly to **PSi** sample. The second is centered at 533.5 eV and represent the Ph-O-C arrangement in cavitands.[32b]

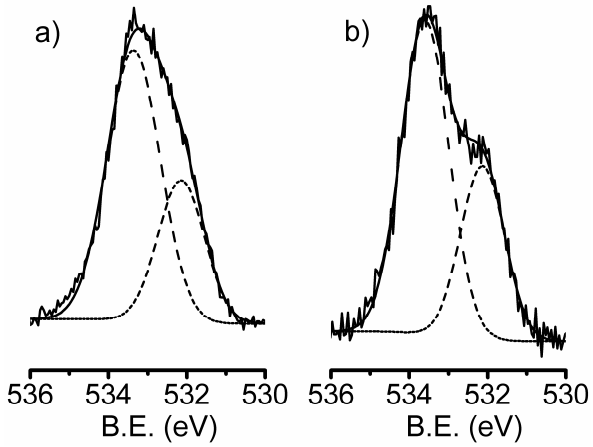

Figure 3.4.3: High-resolution O 1s XPS spectra (takeoff angle 45°) of a) **PSi-MeCav** and b) **PSi-AcIN**.

3.4.3 DMMP complexation: XPS, FTIR and thermal desorption study

Before the complexation tests, methyl-protected carboxylic functionalities of **PSi**-grafted **AcIN** and **AcOUT** cavitands were deprotected by hydrolysis of the methyl ester following a published procedure.[43,69] For complexation experiments, samples were placed for 20 min in a closed chamber saturated with DMMP vapors. The saturated DMMP vapor was obtained placing a beaker with DMMP (2 mL), in the closed chamber at 20°C for 1 h thus allowing vapor saturation. In this condition, the vapor pressures of DMMP is 0.3 Torr estimated from thermodynamic data taking into account the relative humidity.[70]

DMMP uptake was, evaluated by a surface sensitive technique (XPS) and by transmission FTIR, taking advantage of the high surface area of the porous samples.

Figure 3.4.4 shows FTIR difference spectra (before and after DMMP exposure) of **PSi-AcIN**, **PSi-AcOUT** and **PSi-MeCav** in the 1380-780 cm^{-1} region, where the main DMMP features are present.[62,71] Spectra of **PSi-AcIN** and **PSi-AcOUT** show a characteristic strong doublet at 1035 cm^{-1} and 1058 cm^{-1} due to the stretching *ν*(C-O-P) and a band at 1202 cm^{-1} assigned to the stretching of P=O group. Other bands at 787 cm^{-1} and 828 cm^{-1} due to the stretching in O-P-O group ($\nu(PO_2)$) and at 918 cm^{-1} and 1314 cm^{-1} respectively, assigned to rocking of CH_3P group ($\rho(CH_3P)$) and the antisymmetric deformation of CH_3P group ($\delta(CH_3P)$)[59] can be observed in the spectra. By contrast, much lower signals were detected on **PSi-MeCav**. It is worthy of note that in all spectra the *ν*(P=O) is significantly shifted at lower wavenumber compared to the frequencies of free gaseous DMMP (1240 cm^{-1}), likely due to the formation of hydrogen bonds during DMMP complexation.[72] This results suggests that DMMP up-take occurs only on **PSi-AcIN** and **PSi-AcOUT** in which the acid COOH moiety allows the formation of an H-bond with P=O. On **PSi-MeCav**, a negligible DMMP uptake occurs due to the presence of residual acid OH groups[13] on the **PSi** oxidized surface.

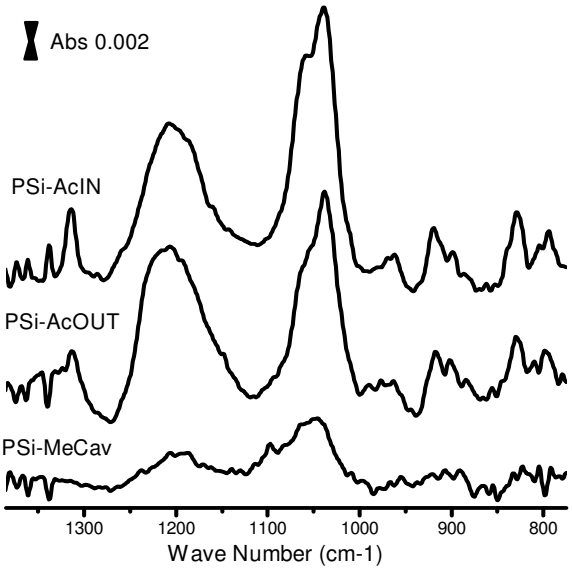

Figure 3.4.4: Difference FTIR spectra (between spectrum after DMMP exposure minus spectrum before DMMP exposure) of **PSi-AcIN**, **PSi-AcOUT** and **PSi-MeCav** samples in the 1380-780cm^{-1} region.

The complexation process on the active surfaces has been also demonstrated by XPS. Figure 3.4.5 compares the P 2p spectral regions of **PSi-AcIN**, **PSi-AcOUT** and **PSi-MeCav** after exposure to DMMP vapours. In both active surfaces, the presence of P(2p) band centered at 134.8 eV indicates, according to FTIR experiments, the presence of molecular DMMP on the surface.[73] No P 2p signals are evident in **PSi-MeCav**.

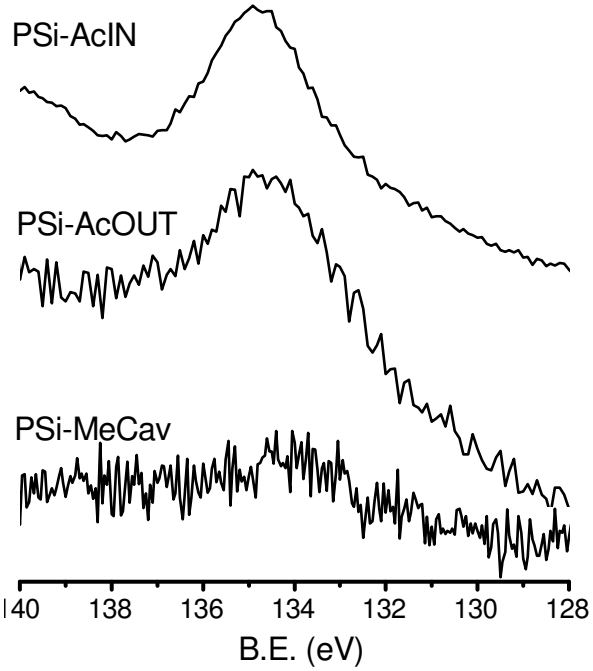

Figure 3.4.5: P 2p spectral region of **PSi-AcIN** (above), **PSi-AcOUT** (middle) and **PSi-MeCav** (bottom) after exposure to DMMP vapors.

Since onsite field monitoring demands a repeatable uptake/release of organophosphorous vapors, process reversibility has been investigated by FTIR monitoring of complexation/decomplexation cycles. A strong decrease of *ν*(C-O-P) and ν(P=O) bands in the FTIR spectra of DMMP-exposed **PSi-AcIN** and **PSi-AcOUT** samples is observed after heating (60°C) or N_2 rinsing for 15 min, thus indicating that decomplexation can be obtained either by thermal or by rinsing treatments. Figure 3.4.6 shows the evolution of the intensity of the ν(P=O) band in the FTIR spectra of **PSi-AcIN** (or **PSi-AcOUT**) samples undergoing various complexation/decomplexation cycles of DMMP- exposure (0.3Torr) followed by heating at 60°C for 15 min.

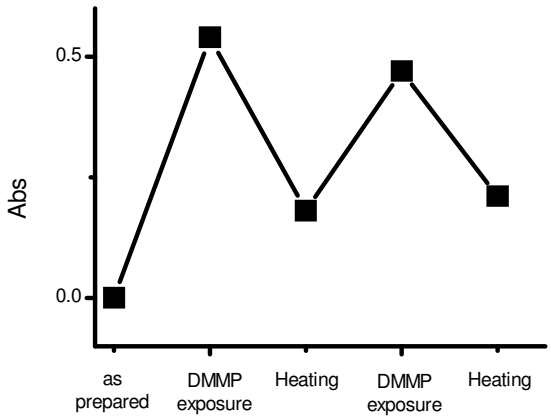

Figure 3.4.6: DMMP Complexation/Decomplexation cycles on **PSi-AcIN**.

Thermal desorption of DMMP molecules from **PSi-AcIN, PSi-AcOUT** and **PSi-MeCav** samples was also monitored by in situ Mass Spectroscopy. Various typical ions associated to fragmentation of DMMP[74] in the mass spectrometer were observed during the heating ramp (Figure 3.4.7).

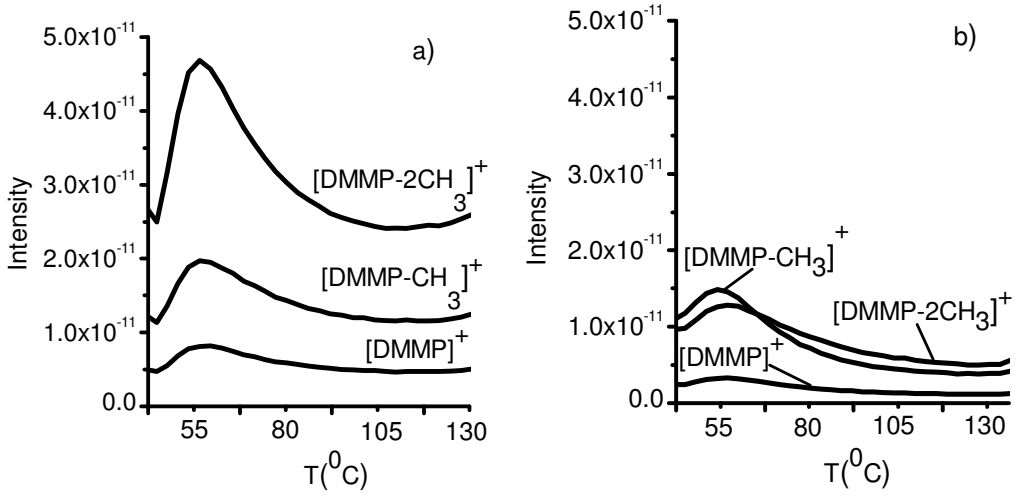

Figure 3.4.7: Ion intensity during thermal desorption from a) **PSi-AcIN** and from b) **PSi-MeCav** samples exposed to DMMP vapors. Thermal desorption from **PSi-AcOUT** is found comparable to **PSi-AcIN.**

In particular, the parent DMMP ion (124 amu) and the other intense cracking fragments, such as 79 (PO_3), 94 (CH_3PO_3) and 109 ($(CH_3)_2PO_3$) amu were observed with similar temperature profiles, thus suggesting the desorption of intact DMMP from the surface. A similar desorption experiment, carried out on **PSi-MeCav** after exposure to DMMP, showed a much lower amount of desorbed molecules from the surface (Figure 3.4.7 b), further confirming the poor DMMP uptake on **PSi-MeCav** surfaces.

3.4.4 Organophosphours vapor complexation: theoretical modeling

DFT modeling was performed to investigate the nature of the interaction involved in the DMMP uptake in the cavitands. The analysis allowed to explain the observed

similar behavior of **AcIN** and **AcOUT** receptors and to estimate energetic differences between these receptors and the reference **MeCav**.

Charge analysis (Table 3.4.1) shows that the interaction between DMMP and **AcOUT** in the host-guest adduct involves a general displacement of the electron density distribution in the DMMP molecules.

In particular, the negative charge centered on the O1 atom of the DMMP increases (Δ = 0.67) as a consequence of the H-bonding formation with the cavitand H_{Ac} atom (Figure 3.4.8). The O1-H_{Ac} distance (1.73 Å) and the O-H_{Ac}···O1 angle (172.1°) confirm the presence of the H-bond between DMMP and the cavitand.

	DMMP free	**DMMP-**AcOUT
P	2.167	**2.235**
O1	-1.003	**-1.070**
O2	-0.792	**-0.799**
O3	**-0.792**	**-0.808**

[a] Label refers to Figure 3.4.8.

Table 3.4.1: NBO atomic charge assignment on the DMMP guest free and in the DMMP-**AcOUT** adduct[a]

Lower increasing in the negative charge (Δ = 0.02) is also observed on O2 and O3 oxygen atoms of the DMMP on passing from free to the DMMP-**AcOUT** adduct. Also in this case, the oxygen atoms O2 and O3 point toward the C-H bond of the cavitand methylene groups (O···H-C ~ 167°). A tenuous interaction with the methylene H atoms (weakly acid in character) of the cavitand upper rim can explain the adduct charge distribution and the geometrical arrangement. Finally, the methyl group directly bonded to the P atom of the DMMP is involved in a threefold

CH-π interaction with the benzene fragments of the cavitand. These interactions are pointed out by the distance between methyl H atoms of the DMMP and the benzene centroid (2.38-2.58 Å) and by the C-H···Be_{centr} angles (141-157.0°). Geometrical constrains do not allow optimized CH-π interactions of all methyl C-H bonds with the cavitand benzene fragments.

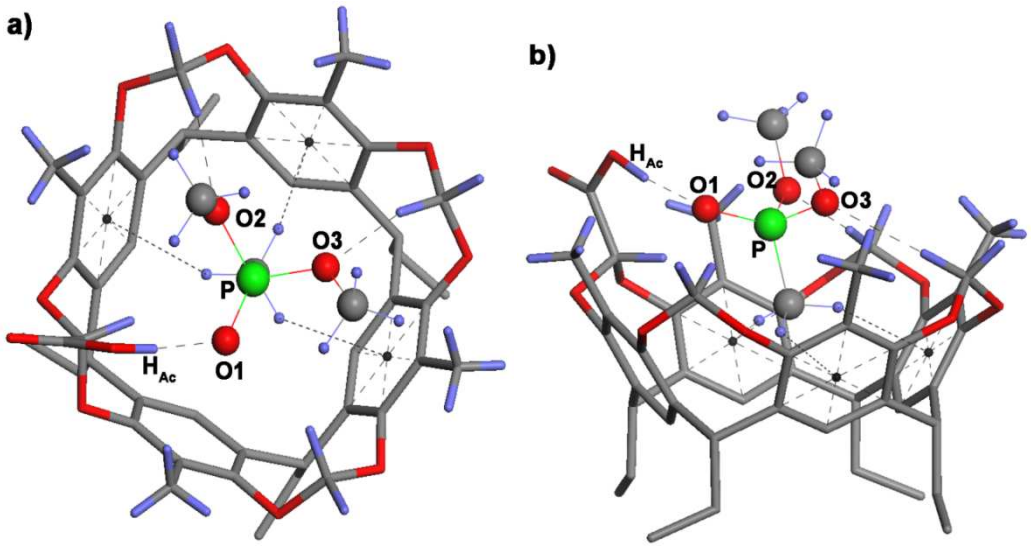

Figure 3.4.8: Host-guest adduct between DMMP and **AcOUT**. a) Top view and b) side view. Ethyl groups replace the alkyl chains in the bottom side of the cavitand. Hydrogen atoms in the bottom side are hidden for clarity.

From a dynamical point of view this arrangement can be explained by the geometrical availability of all cavitand benzene fragments with respect to the CH-π interactions due to both the mean distance of the DMMP methyl group with the inside cavitand walls and the possibility for the methyl group to turn around the P-C(Me) single bond. All these interactions yield to an overall stabilization of 35.5 kcal/mol in the adduct formation between DMMP and **AcOUT**. Similar

interactions are observed in the case of **AcIN**. The computed stabilization associated to the adduct formation is also comparable (36.3 kcal/mol).

The computational data are in agreement with both the SPR[17] and present porous silicon sensing experiments, indicating that **AcIN** and **AcOUT** are comparable as receptors, i.e. the orientation of the COOH group with respect to the cavity does not affect DMMP binding.

Vibrational analysis has been computed to acquire information about the effect of the H-bonding on the P=O stretching of the DMMP in the host-guest adduct. FTIR spectroscopic measurements revealed an evident frequency shift (Δ = -40 cm^{-1}) passing from 1242 cm^{-1} for the liquid DMMP to 1202 cm^{-1} for DMMP-**AcOUT** (or **AcIN**) adduct. A similar shift (Δ = -56.2 cm^{-1}) of the P=O stretching vibrational frequency on passing from free DMMP ($\nu_{P=O}$ = 1253.6 cm^{-1}) to the DMMP hosted in the cavitand ($\nu_{P=O}$ = 1197.4 cm^{-1}) is computed as consequence of the H-bonding interaction.

Similar adduct has been computed with the **MeCav** host as inactive reference in the perspective to confirm the role of the acid group in the recognition of the DMMP molecule. In this case, similar interactions of the O2 and O3 DMMP atoms with the acid methylene C-H groups of the cavitand as well as the CH-π interactions are active. The computed energy stabilization of the DMMP-**MeCav** adduct is, however, much lower (26.3 kcal/mol) than DMMP-**AcOUT** (or **AcIN**) adduct. The difference (Δ ~ 10 kcal/mol) is ascribable to the H-bond promoted by the acid functionality on the upper rim of the active cavitands. The acid functionality is, hence, responsible of the observed affinity of the **AcOUT** and **AcIN** cavitands for the DMMP guest.

Finally, in order to verify the performance of these receptors with respect to real nerve gases (experimentally very dangerous), the adduct formation between **AcIN** (or **AcOUT**) and a sarin molecule has been modeled.

In this case, a slightly greater stabilization (38.1 kcal/mol) with respect to the DMMP-**AcIN** adduct has been computed as a consequence of a greater affinity between sarin and **AcIN** (or **AcOUT**) cavitands. This result let us confident regarding the correct usage of the DMMP as suited and harmless model for the study of nerve gas agents sensing.

3.4.5 Conclusions

In this paragraph, I described the synthesis, characterization and complexation properties of functional materials consisting of high area substrates modified with cavitand receptors. The recognition properties of both **AcIN** and **AcOUT**, firstly proved on gold substrates for SPR detection,[17] have been successfully transferred to a silicon-based material relevant for device integration. Material characterization showed the success of the grafting on a porous substrate, thus obtaining a new active surface which combines typical robustness of Si-C covalent bonds[75] with the high surface area of **PSi**. Reversible host-guest complexation of DMMP on functionalized porous surface has been showed by XPS, FTIR and desorption experiments, while DMMP/surface nonspecific physisorption is proven negligible by blank experiments adopting a non-active methyl-bridged cavitand. Theoretical modeling has investigated the nature of the involved interactions and pointed out the efficiency of the cavitand recognition properties towards a real nerve gas (sarin).

The developed cavitand decorated surfaces retain the peculiar features of the supramolecular host guest interactions such as complexation properties and reversibility observed for bulk cavitands. In addition, sensing on monolayers on an high surface area material reduces nonspecific interactions with respect to thin films or bulk materials and allows simpler detection tools (i.e. Transmission IR techniques) compared to monolayers on flat surface which requires more expensive

surface sensitive techniques. Finally, the transfer of the cavitand recognition properties into a silicon framework can be considered a starting point towards the development of an integrated sensing devices for the recognition of organophosphorus toxic agents.

3.5 References

[1] G.G. Condorelli, A. Motta, M. Favazza, I.L. Fragalà, M. Busi, E. Menozzi, E. Dalcanale, L. Cristofolini, Langmuir 2006, 22, 11126-11133.

[2] a) Y. L. Bunimovich, Y. S. Shin, W.-S. Yeo, M. Amori, G. Kwong, J. R. Heath, J. Am. Chem. Soc. 2006, 128, 16323-16331. b) D. Narducci, P. Bernardinello M. Oldani, Appl. Surf. Sci. 2003, 212-213, 491-496.

[3] S. Zampolli, I. Elmi, F. Mancarella, P. Betti, E. Dalcanale, G. C. Cardinali M. Severi, Sens. Actuators B 2009, 141, 322-328.

[4] M. Dubey, S. L. Bernasek, J. Schwartz, J. Am. Chem. Soc. 2007, 129, 6980–6981.

[5] A. Motta, C. Tudisco, G. G. Condorelli, Sci. Adv. Mater. 2011, 3, 362-377.

[6] N. Elfström, E.A. Karlström, J. Linnros, Nano Lett., 2008, 8, 945-949.

[7] M. Yue, J. C. Stachowiak, H. Lin, R. Datar, R. Cote, A. Majumdar, Nano Lett. 2008, 8, 520-524.

[8] Yang, Y.; Ji, H-F.; Thundat T. J. Am. Chem.. Soc. 2003, 125, 1124-1125.

[9] M. Delalande, S. Clavaguera, M. Toure, A. Carella, S. Lenfant, D. Deresmes, D. Vuillaumeb, J.-P. Simonato, Chem. Commun. 2011, 47, 6048-6050.

[10] S.Jang, Y. Koh, J. Kim, J. Park, C. Park, S. J. Kim, S. Cho, Y. C. Ko, H. Sohn Materials Letters 2008, 62, 552–555.

[11] B. Chen, S. Xiang, G. Qian, Acc. Chem. Res. 2010, 43, 2115-2124.

[12] a) J. M. Buriak, Phil. Trans. R. Soc. A 2006, 364, 217-225. b) J. M. Buriak, M. P. Stewart, T. W. Geders, M. J. Allen, H. C. Choi, J. Smith, D. Raftery, L. T. Canham, J. Am. Chem. Soc. 1999, 121, 11491-11502.

[13] C. Tudisco, G. Trusso Sfrazzetto, A. Pappalardo, A. Motta, G. A. Tomaselli, I. L. Fragalà, F. P. Ballistreri, G. G. Condorelli, Eur. J. Inorg. Chem. 2011, 13, 2124–2131.

[14] S. Sam, L. Touahir, J. Salvador Andresa, P. Allongue, J.-N. Chazalviel, A. C. Gouget-Laemmel, C. Henry de Villeneuve, A. Moraillon, F. Ozanam, N. Gabouze, S. Djebbar, Langmuir 2010, 26, 809–814.

[15] a) D. K. Shenoy, E. B. Feresenbet, R. Pinalli, E. Dalcanale, Langmuir 2003, 19, 10454-10456. b) C. Di Natale, R. Paolesse, A. Macagnano, S. Nardis, E. Martinelli, E. Dalcanale, M. Costa, A. D'Amico, J. Mater. Chem. 2004, 14, 1281-1287.

[16] a) A. G. Cullis, L. T. Canham, Nature, 1991, 353, 335-338. b) J. M. Buriak Phil. Trans. R. Soc. A 2006, 364, 217–225

[17] S. M. Daly, M. Grassi, D. K. Shenoy, F. Ugozzoli, E. Dalcanale, J. Mater. Chem., 2007, 17, 1809–1818

[18] A. B. Sieval, A. L. Demirel, J. M. Nissink, M. R. Linford, J. H. van der Maas, W. H. de Jeu, H. Zuilhof, E. J. R. Sudhölter, Langmuir 1998, 14, 1759-1768.

[19] T.E.U van Velzen, J. F. J. Engbersen, D. N. Reinhoudt, Synthesis 1995, 8, 989-997.

[20] C. Chartier, S. Bastide, C. Lèvy-Clèment, Electrochimica Acta 2008, 53, 5509–5516.

[21] a) I. L. Swift, Surf. Interface Anal. 1982, 4, 47–51. b) D. Briggs, G. Beamson, Anal. Chem. 1992, 64, 1729–1736.

[22] J. Vande Vondele, M. Krack, F. Mohamed, M. Parrinello, T. Chassaing, J. Hutter, Comput. Phys. Commun. 2005, 114, 145.

[23] The CP2K developers group. http://cp2k.berlios.de/

[24] S. Goedecker, M. Teter, J. Hutter, J. Phys. Rev. B 1996, 54, 1703.

[25] J. P. Perdew, K. Burke, M. Ernzerhof, Phys. Rev. Lett. 1997, 78, 1396 (E).

[26] L. Genovese, T. Deutsch, A. Neelov, S. Goedecker, G. Beylkin, J. Chem. Phys, 2006, 125, 074105/1-074105/5.

[27] S. Grimme, J. Comput. Chem. 2006, 27, 1787-1799.

[28] a) M. Digne, P. Sautet, P. Raybaud, P. Euzen, H. Toulhoat, J. Catal. 2004, 226, 54-68. b) P. Raybaud, M. Digne, R. Iftimie, W. Wellens, P. Euzen, H. Toulhoat, J. Catal. 2001, 201, 236.

[29] M. J. Frisch, G. W. Trucks, H. B. Schlegel, G. E. Scuseria, M. A. Robb, J. R. Cheeseman, J. A. Montgomery Jr., T. Vreven, K. N. Kudin, J. C. Burant, J. M. Millam, S. S. Iyengar, J. Tomasi, V. Barone, B. Mennucci, M. Cossi, G. Scalmani, N. Rega, G. A. Petersson, N. H. Hada, M. Ehara, K. Toyota, R. Fukuda, J. Hasegawa, M. Ishida, T. Nakajima, Y. Honda, O. Kitao, H. Nakai, M. Klene, X. Li, J. E. Knox, H. P. Hratchian, J. B. Cross, C. Adamo, J. Jaramillo, R. Gomperts, R. E. Stratmann, O. Yazyev, A. J. Austin, R. Cammi, C. Pomelli, J. W. Ochterski, P.

Y. Ayala, K. Morokuma, G. A. Voth, P. Salvador, J. J. Dannenberg, V. G. Zakrzewski, S. Dapprich, A. D. Daniels, M. C. Strain, O. Farkas, D. K. Malick, A. D. Rabuck, K. Raghavachari, J. B. Foresman, J. V. Ortiz, Q. Cui, A. G. Baboul, S. Clifford, J. Cioslowski, B. B. Stefanov, G. Liu, A. Liashenko, P. Piskorz, I. Komaromi, R. L. Martin, D. J. Fox, T. Keith, M. A. Al-Laham, C. Y. Peng, A. Nanayakkara, M. Challacombe, P. M. W. Gill, B. Johnson, W. Chen, M. W. Wong, C. Gonzalez, J. A. Pople, Gaussian 09, Revision B.1; Gaussian, Inc., Pittsburgh PA, 2003.

[30] a) A. Bansal, X. Li, S. I. Yi, W. H Weinberg, N. S. Lewis, J. Phys. Chem. B, 2001, 105, 10266-10277. b) G.F. Cerofolini, C. Galati, S. Lorenti, L. Renna, O. Viscuso, C. Bongiorno, V. Raineri, C. Spinella, G.G. Condorelli, I.L. Fragalà, A. Terrasi, Appl. Phys. A: Mater. Sci. Process. 2003, 77, 403-409.

[31] a) F. J. Himpsel, F. R. McFeely, A. Taleb-Ibrahimi, J. A. Yarmoff, and G. Hollinger, Phys. Rev. B 1988, 38, 6084. b) A. Gulino, F. Lupo, G.G. Condorelli, P. Mineo, I. L.Fragalà, Chem. Mater., 2007, 19, 5102-5109.

[32] a) D. Briggs, In Practical Surfaces Analysis, D. Briggs, M. P. Seah, Wiley-VCH, Weinheim, Germany, 2nd ed., 1995, Vol. 1, p 444. b) G. Beamson, D. Briggs, High-Resolution XPS of Organic Polymers. The Scienta ESCA300 Database, Wiley & Sons, New York, 1992.

[33] a) G. G. Condorelli, A. Motta, I. L. Fragalà, F. Giannazzo, V. Raineri, A. Caneschi, D. Gatteschi, Angew. Chem. Int. Ed. 2004, 43, 4081–4084. b) M. Mannini, F. Pineider, P. Sainctavit, C. Danieli, E. Otero, C. Sciancalepore, A. M. Talarico, M.-A. Arrio, A. Cornia, D. Gatteschi, R. Sessoli, Nat. Mater. 2009, 8, 194–197

[34] a) G. F. Cerofolini, C. Galati, S. Reina, L. Renna, O. Viscuso, G.G. Condorelli, I.L. Fragalà, Mater. Sci. Eng., C, 2003, 23, 989-994. b) G. F. Cerofolini, C. Galati, S. Reina, L. Renna, Mater. Sci. Eng., C 2003, 23, 253-257.

[35] a) A. Vesel, M. Mozetic, A. Zalar, Vacuum 2008, 82, 248-251. b) A. P.Pijpers, R. J. Meier, Chem. Soc. Rev., 1999, 28, 233–238

[36] In order to confirm N1s assignment, reference spectra of salen powders have been recorded. N1s band of pure salen was observed at 398.8 eV consisting with the above assignment.

[37] a) S. J. Kerber, J. J. Bruckner, K. Wozniak, S. Seal, S. Hardcastle, T. L. Barr, J.Vac. Sci. Technol. A, 1996, 14, 1314-1320. b) J. N. O'Shea, J. Schnadt, P. A. Brühwiler, H. Hillesheimer, L. Patthey, J. Krempasky, C. Wang, Y. Luo, H. Agren, J. Phys. Chem B, 2001, 105, 1917-1920.

[38] a) S. W. Ong, X.L. Zhao, K.B. Eisenthal, Chem. Phys.Lett., 1992, 191, 327-335. b) Y. Duval, J. A. Mielczarski, O.S. Pokrovsky, E. Mielczarski, J. J. Ehrhardt, J. Phys. Chem. B 2002, 106, 2937-2945. c) K. Leung, I. M. B. Nielsen, L. J. Criscenti J. Am. Chem. Soc. 2009, 131, 18358-18365.

[39] a) H. C. Choi, J. M. Buriak, Chem. Mater., 2000, 12, 2151-2156. b) G. Mattei, V. Valentini, V. A. Yakovlev, Surf. Sci. 2002, 502–503, 58–62. c) S. A. Alekseev,V. Lysenko, V. N. Zaitsev, D. Barbier J. Phys. Chem. C 2007, 111, 15217-15222.

[40] a) F. Ozanam, J. N. Chazalviel, J. Electroanal. Chem., 1989, 269, 251. b) D. B. Mawhinney, J. A. Glass, J. T. Yates, J. Phys. Chem. B, 1997, 101, 1202-1206. c) W. Haiss, P. Raisch, D. J. Schiffrin, L. Bitsch, R. J. Nichols Faraday Discuss., 2002, 121, 167–180.

[41] a) R. Hofman, J. G. F. Westheim, I. Pouwel, T. Fransen, P. J. Gellings Surf. Inter. Anal. 1996, 24, 1-6. b) F. Massines, N. Gherardi, A. Fornelli, S. Martin Surf. Coat. Technol. 2005, 200, 1855-1861. c) B. B. Burton, S. W. Kang, S. W. Rhee, S. M. George J. Phys. Chem. C, 2009, 113, 8249–8257.

[42] X. N. Xie, H. J. Chung, C. H. Sow, A. T. S. Wee, Mater. Sci. Eng., R, 2006, 54, 1–48.

[43] G. G. Condorelli, C. Tudisco, A. Motta, A. Di Mauro, F. Lupo, A. Gulino, I. L. Fragalà, Eur. J. Inorg. Chem. 2010, 26, 4121-4129.

[44] D. M.Singer, F. Farges, G.E. Brown Jr, Geochimica et Cosmochimica Acta, 2009, 73, 3593–3611.

[45] D. Chadwick, Chem. Phys. Lett., 1973, 21, 291-294.

[46] Organophosphates: Chemistry, Fate, and Effects, Academic Press, San Diego, CA, 1992.

[47] J. Huang, J. Miragliotta, A. Becknell, H. E. Katz, J. Am. Chem. Soc. 2007, 129, 9366-9376.

[48] H. J. Lee, K. K. Park, Ö. Oralkan, M. Kupnik B. T. Khuri-Yakub, IEEE 2008, 434-439.

[49] I. Levitsky, S. G. Krivoshlykov, Anal. Chem. 2001, 73, 3441-3448.

[50] S. Jang, Y. Koh, J. Kim, J. Park, C. Park, S. J. Kim, S. Cho, Y. C. Ko, H. Sohn Materials Letters 2008, 62, 552–555.

[51] X. Du, Z. Ying, Y. Jiang, Z. Liu, T. Yang, G. Xie, Sensors and Actuators B 2008 134, 409-413.

[52] W. Hea, Z. Liua, X. Dua, Y. Jianga, D. Xiao, Talanta 2008, 76, 698–702.

[53] Y. Zhao, J. Hea, M. Yanga, S. Gaoa, G. Zuoa, C. Yana, Z. Chenga, Analytica Chimica Acta, 2009, 654, 120–126.

[54] K-L. Yang, K. Cadwell, N. L. Abbott, Sensors and Actuators B 2005,104, 50-56.

[55] Y. Yang, H-F. Ji, T. Thundat, J.Am. Chem.. Soc., 2003, 125, 1124-1125.

[56] S. M. Kanan, C. P. Tripp, Langmuir, 2001, 17, 2213-2218.

[57] X. Du, Z. Wang, J. Huang, S. Tao, X. Tang, Y. Jiang, J Mater Sci 2009, 44, 5872-5876.

[58] J. Huang, Y. Jiang, X. Du, J. Bi, Sensors and Actuators B 2010, 146, 388–394.

[59] M. K. Ferguson-McPherson, E. R. Low, A. R. Esker, J. R. Morris, J. Phys. Chem. B 2005, 109, 18914-18920.

[60] C. Y. Lee, R. Sharma, A. D. Radadia, R. I. Masel, M. S. Strano, Angew. Chem. Int. Ed. 2008, 47, 5018 –5021.

[61] L. Kong, J. Wang, X. Fu, Y. Zhong, F. Meng, T. Luo, J. Liu, Carbon 2010, 48, 1262-1270.

[62] L. Bertilsson, I. Engquist, B. J. Liedberg, Phys. Chem. B 1997, 101, 6021-6027.

[63] a) R. Zou, R. Zhong, S. Han, H. Xu, A. K. Burrell, N. Henson, J. L. Cape, D. D. Hickmott, T. V. Timofeeva, T. E. Larson, Y. Zhao, J. Am. Chem. Soc. 2010, 132, 17996–17999. b) C. Montoro, F. Linares, E. Q. Procopio, I. Senkovska, S. Kaskel, S. Galli, N. Masciocchi, E. Barea, J. A. R. Navarro, J. Am. Chem. Soc. 2011, 133, 11888-11891.

[64] T. M. Tesfai, V. N. Sheinker, M. B. Mitchell, J. Phys. Chem. B 1998, 102, 7299-7302.

[65] V. M. Bermudez Langmuir 2010, 26, 18144-18154.

[66] A. Friggeri, F. C. J. M. van Veggel, D. N Reinhoudt, Langmuir 1998, 14, 5457-5463.

[67] a) H. C. Choi, J. M. Buriak, Chem. Mater. 2000, 12, 2151– 2156. b) G. Mattei, V. Valentini, V. A. Yakovlev, Surf. Sci. 2002, 502–503, 58–62.

[68] S. A. Alekseev, V. Lysenko, V. N. Zaitsev, D. Barbier, J. Phys. Chem. C 2007, 111, 15217–15222.

[69] G. G. Condorelli, A. Motta, C. Bedoya, A. Di Mauro, G. Pellegrino, E. Smecca, Inorganica chimica acta 2007, 360, 170-178.

[70] a) D. E. Tevault, J. H. Buchanan, L. C. Buettner, International Journal of Thermophysics 2006, 27, 486-493. b) A. B. Butrow, J. H. Buchanan, D. E. Teveault, J. Chem. Eng. Data 2009, 54, 1876-1883.

[71] D. A. Panayotov, J. R. Morris, Langmuir 2009, 25, 3652-3658.

[72] S. M. Kanan, A. Waghe, B. L. Jensen, C. P. Tripp, Talanta 2007,72, 401–407.

[73] J. S. Ratliff, S. A. Tenney, X. Hu, S. F. Conner, S. Ma, D. A. Chen, Langmuir 2009, 25, 216-225.

[74] D. A. Chen, J. S. Ratliff, X. Hu, W. O. Gordon, S. D. Senanayake, D. R. Mullins, Surface Science 2010, 604, 574–587.

[75] X. Wang, E. C. Landis, R. Franking, R. J. Hamers, Acc. Chem. Res. 2010, 43, 1205-1215.

Chapter 4

Concluding Remark

This thesis described some strategies to introduce specific properties onto the silicon surface through the covalent anchoring of organic and inorganic molecules. The great interest of these grafting strategies is motivated by the huge availability of molecular systems with different functional properties and by the continuous effort of organic and inorganic synthetic chemists toward the preparation of new and more efficient systems. A key point in the evaluation of the developed strategies is the precise characterization of the resulting hybrid material which has been achieved by combining different complementary techniques such as XPS which is the ideal tool for chemical characterization of surface layers, FTIR spectroscopy which give molecular information on molecules grafted on porous Si AFM and AFM lithography methodologies which can give morphological and structural information of the monolayers and optical high sensitive technique as fluorescence spectroscopy. The combination of the previous mentioned techniques with the evaluation of the functional properties of the grafted monolayers demonstrate the efficiency of the presented anchoring strategies. In particular, the reported methodologies allowed not only to anchor intact molecules on the silicon surface but also to control of their surface orientation which is often an important requirement to maintain their functionalities. In addition, a strong support to the characterization analysis and to the validation of the investigated functional properties has been given by the design of “ad hoc” marked-guests, which allow an

efficient characterization, and by the preparation of inactive surfaces, structurally analogues to the functional ones, which allow control experiments.

Finally, the presented cavitand-based functionalization strategies allowed to introduce specific molecular recognition properties on silicon surfaces (flat and porous). The obtained hybrid organic-inorganic materials showed interesting potentialities in specific sensing applications in which selectivity and, hence, molecular recognition is a critical point. An example is the detection of the methylated-aminoacid sarcosine in biological fluids, therefore in the presence of overwhelming amounts other aminoacids. Also for the gas phase sensing of dmmp the specific role of the cavity in the recognition process improved the detection process of this analyte compared to other systems based onll on the less specific H interaction. However, sensing is not the only application field of these materials. The introduction of molecular recognition properties on Si plays an important role in the controlled nanoengineering of its surface via specific and reversible self-assembling processes of functional complexes. The presented hierarchical self-assembly of luminescent lanthanide complexes is an example of this particular synthetic approach.

Acknowledgments

This thesis is dedicated to my daughter which has always been with me during this period.

This hard work would have been incomplete without this page and that is why, at the end of this path, I feel to thank some people.

Thanks to my Tutor , Prof. G.G. Condorelli, who gave me the opportunity to work with him as PhD student, driving me and allowing me to be independent in any situation.

The total devotion to his work and especially his love for the research have been for me a model to follow.

Thanks to Prof. E. Dalcanale; our conversations always have been for me inspirational source.

Thanks to the Prof. E. Dalcanale group and a special thanks to Dr. E. Biavardi and Dr. K. Misztal: to working with you has been a pleasure.

Thanks to Prof. F. Ballistreri and his research group for the hard work done.

Thanks to Dr. Nicola Armaroli e Dr. J. Malicka for the fluorescence measures.

Thanks to my colleagues, Dr. A. Motta, Dr. F. Lupo and Dr. M.R. Catalano for the moments dedicated to science but especially for all the breaks we spent together.

And last , but not least, I want to give thanks to my husband and my family who have encouraged and supported me in all the choices I made; without you I would not have ever become the woman I am now. I love you all.